12-2019

# A Comparative Study on the Stability and Degradation of Perovskite Solar Cells

Jyotiska Chakraborty
*Grand Valley State University*

# A COMPARATIVE STUDY ON THE STABILITY AND DEGRADATION OF PEROVSKITE SOLAR CELLS

Jyotiska Chakraborty

A Thesis Submitted to the Graduate Faculty of

GRAND VALLEY STATE UNIVERSITY

In

Partial Fulfillment of the Requirements

For the Degree of

Masters of Science in Engineering

School of Engineering

December 2019

**Acknowledgments**

First, I would like to express my gratitude to God for helping me complete the work. The next in line would be my thesis advisor Dr. Heidi Jiao, whose office was always open for me whenever I ran into trouble or had a question about my research or writing. She consistently steered me towards the right direction whenever she thought I needed it.

I wish to express my gratitude to my thesis committee members Dr. Bruce Dunne and Dr. Nabeeh Kandalaft for their valuable feedback and attention during the whole process.

Special thanks go to my academic advisor, Dr. Shabbir Choudhuri for crucial guidance and support during the different phases of the work.

I want to extend sincere gratitude to all associated administrative personnel of Padnos College of Engineering and Computing, and Grand Valley State University who helped me at various stages.

I must express my profound gratitude to my parents for providing me with unfailing support and continuous encouragement throughout my years of study and through the process of researching and writing this thesis.

Thank you.

Jyotiska Chakraborty

**Abstract**

This study aims to investigate the environmental factors that affect the performance and long-term stability of the perovskite solar cells (PSCs). PSCs are based on organo-metallic halides (perovskites) that act as a light-sensitive compound that produces excitons when placed under the light. However, PSCs have a limited operating lifetime due to the degradation of the perovskite layer. There are many factors like moisture, UV light, and temperature that lead to the degradation of the perovskite layer. From the literature review, it was found that the PSCs do not degrade with the presence of oxygen in a dry and dark environment. However, the presence of moisture along with oxygen causes an irreversible degradation of the perovskite layer.

This study aims at fabricating perovskite solar cells using two different techniques. The first technique is the spin coating technique, and the second technique is the blade coating technique. The performance and the long-term stability of the solar cells were investigated, and improved perovskite solar cells were fabricated. The improved solar cells were then tested under different environments to study the stability of these solar cells. The structure of the PSC used in this study contains the Transparent Conductive Oxide (TCO), electron transport layer ($TiO_2$), perovskite absorber, hole transport layer, and the conductive metallic silver layer. Blade coating and spin coating methods were used to fabricate the perovskite solar cells. These solar cells were investigated under various environmental conditions like controlled humidity (30% to 38% RH), high humidity (>50% RH), nitrogen under room temperature of 22°C, and nitrogen under elevated temperature at 80°C.

The properties of solar cells studied are the optical absorption of the perovskite absorber, the open-circuit voltage ($V_{OC}$), short circuit current ($I_{SC}$), fill factor (FF), and efficiency of the PSCs.

The solar cells were stored under both dark and light (sunlight during the day, and room light at night) with controlled humidity (30% to 38% RH), high humidity (>50% RH), nitrogen under room temperature of 22°C and elevated temperature of 80°C. Each solar cell under different environments was tested as a function of time. It was found that high humidity, elevated temperature, and presumably the UV part of the white light caused the solar cell to degrade rapidly. It was seen that the nitrogen atmosphere with a room temperature of 22°C had the best environment for storing the perovskite solar cell. Further, the introduction of $Al_2O_3$ as a buffer layer and an epoxy resin increased the stability of the solar cell.

## Table of Contents

## List of Figures

## List of Tables

## Abbreviations

DI: Deionized water

DMM: Digital Multimeter

ETL: Electron Transport Layer

FF: Fill Factor

FTO: Fluorine doped Tin Oxide

HTL: Hole Transport Layer

IPA: Isopropyl Alcohol

MAI: Methylammonium Iodide

PCE: Power Conversion Efficiency

PSC: Perovskite Solar Cell

RH: Relative Humidity

SEM: Scanning Electron Microscope

TCO: Transparent Conducting Oxide

# 1 – Introduction

## 1.1 Introduction

The most abundant renewable source of energy that can be harnessed is solar energy. This energy is harnessed by using technologies like solar heating, photovoltaics, solar architecture, and many more. The technologies are classified into two types; active solar and passive solar. Passive techniques involve materials with favorable thermal mass or light dispersing properties like orienting a building facing towards the sun for abundance of light, while active techniques involve solar electric energy conversion, which converts sunlight into electricity (photovoltaics) [1].

A photovoltaic system converts sunlight into electricity through the photovoltaic effect. The core of a photovoltaic system is solar panels which consist of solar cells. Different solar cell technologies have been developed. These include monocrystalline, polycrystalline silicon, thin films, organic, dye-sensitized, and perovskite-based solar cell technologies. Among these, perovskite-based solar cell technology represents one of the fast-growing photovoltaic technologies. Perovskites are organo-metallic halides that have light absorptive qualities and can be used as the absorption layer of solar cells. This quality was first reported by Kojima et al. 2009[2]. Rapid progress has been made to develop efficient perovskite solar cells since 2009[3].

Perovskite is a group of compounds characterized by the general formula $ABX_3$, which has the crystalline structure of Calcium Titanate ($CaTiO_3$) [4]. The most commonly explored perovskite is an organic-inorganic metal halide $CH_3NH_3PbI_3$. This is composed of a large organic cation ($CH_3NH_3^+$), a small inorganic divalent cation ($Pb_2^+$), and a halogen anion (mainly $I^-$). Figure 1 represents the crystalline structure of the perovskite compound [5].

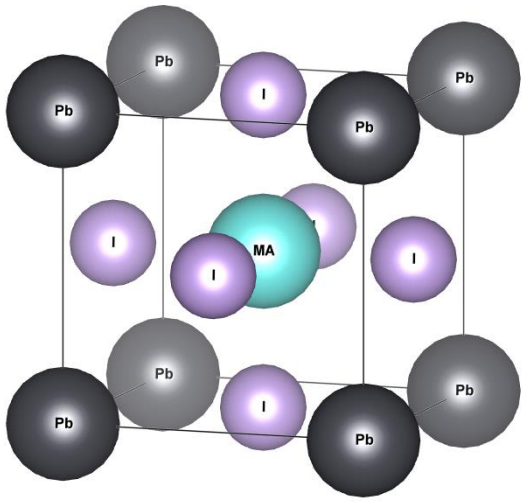


*Figure 1: Crystalline Structure of Perovskite compound*

Perovskite solar cells have low production costs, easy laboratory fabrication techniques like blade coating and spin coating as compared to fabricating silicon solar cells [6].

Figure 2 shows the structure of the perovskite solar cells (PSCs):

1. The first layer is the transparent conductive oxide (TCO) layer on a glass substrate that acts as an active electrode (photo-anode),
2. The second layer comprises an electron transport layer (ETL),
3. The third layer consists of the perovskite layer,
4. The fourth layer consists of a hole transport layer (HTL),
5. The fourth layer is followed by a metal back contact, mainly Au or Ag, which acts as a counter electrode (photo-cathode).

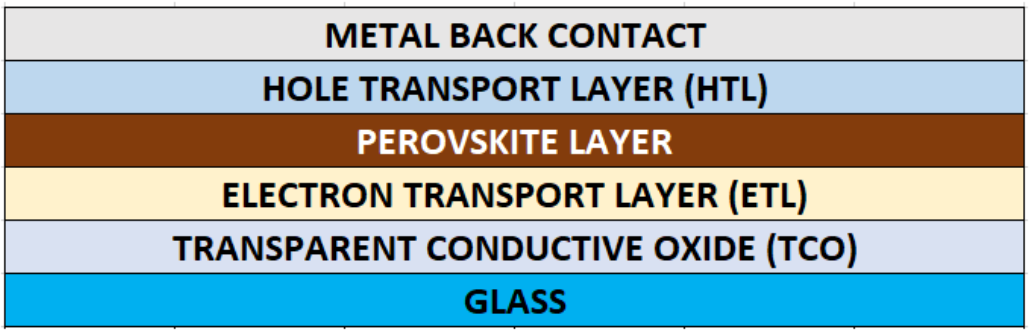


*Figure 2: Basic Perovskite Solar Call Structure*

As sunlight enters through the glass, it gets absorbed by the perovskite layer and produces excitons. An exciton is a bound state of electron and hole that forms when a material absorbs a photon of higher energy than the bandgap that material. The electrons are then transported to the conduction band of the ETL, while the holes are transported to the valence band of the HTL [7].

The efficiency of a solar cell is defined as the ratio of electric power generated to the incoming solar power. The efficiency of the cell is related to short circuit current, open-circuit voltage, and the fill factor of the solar cell. Fill factor, and solar cell efficiency are defined by the points $V_{MPP}$ and $I_{MPP}$. $V_{MPP}$ and $I_{MPP}$ are the solar cell's maximum power point voltage and maximum power point current. They can be obtained from an I-V characteristic curve of the solar cell shown in Figure 3. The short-circuit current ($I_{SC}$) is the current through the solar cell when the voltage across the solar cell is zero. The open circuit voltage ($V_{OC}$) is the maximum voltage available from a solar cell when there is zero current flowing through the solar cell.

Fill factor (FF) is defined as the ratio of the maximum power of the solar cell to the product of $V_{OC}$ and $I_{SC}$. From Figure 3, FF is the ratio of the green area of the solar cell to the area of the

largest rectangle (product of $V_{OC}$ and $I_{SC}$) in the I-V curve. Higher FF corresponds to higher efficiency given $V_{OC}$ and $I_{SC}$.

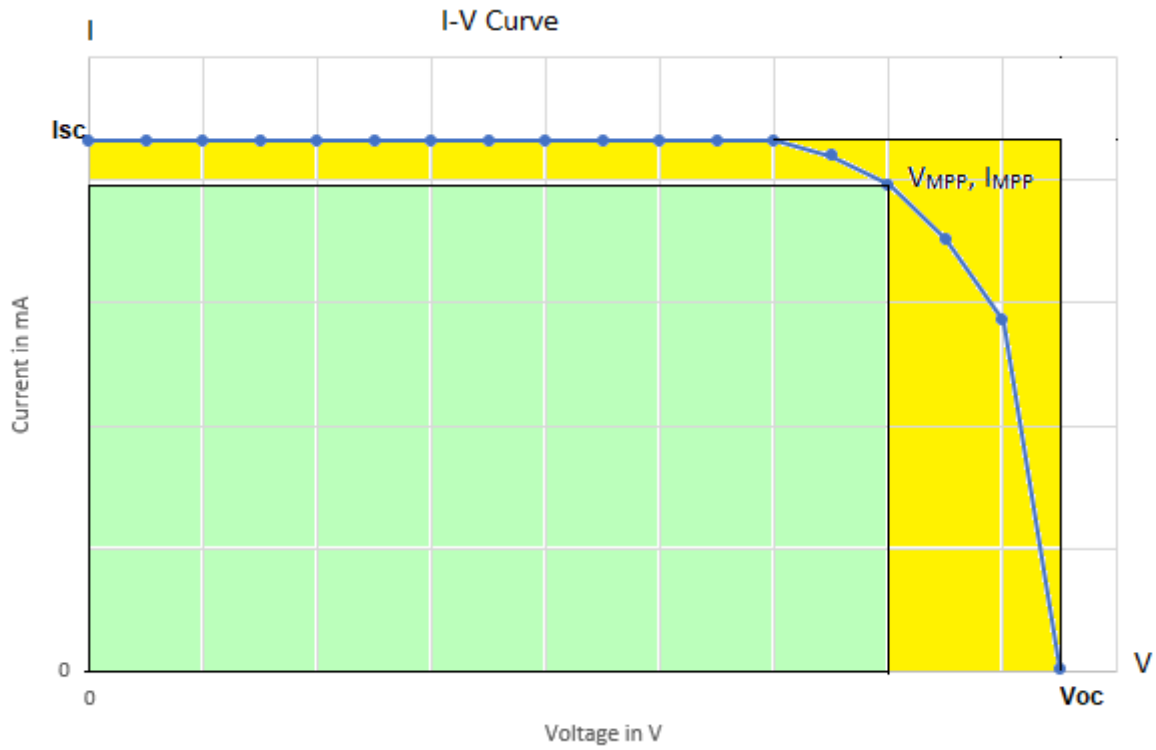


*Figure 3: I-V Characteristic Curve example*

Typically, $P_{in}$ is expressed as the power per unit area that the solar cell receives from sunlight AM1.5. $P_{MPP}$ is the maximum power achieved by a solar cell. Equations (1) and (2) represent the calculation of Fill factor and efficiency respectively.

$$FF = \frac{V_{MPP}.I_{MPP}}{V_{OC}.I_{SC}} \quad (1)$$

$$\eta = \frac{P_{MPP}}{P_{in}} = \frac{FF.I_{SC}.V_{OC}}{P_{in}} \quad (2)$$

The solar cell can be modeled as an equivalent circuit shown in Figure 4. In the model, $I_L$ is the generated photocurrent from the solar cell. The $I_D$ is the dark current that is generated due to

the thermal generation of electrons and holes within the depletion region. The dark current is a relatively small electric current that flows through solar cells even when no photons are entering the device. $R_{SH}$ is the shunt resistance, and $R_S$ is the series resistance present in the solar cell. I and V are the resulting current and the voltage of the solar cell. The current I can be calculated by subtracting the dark current, $I_D$, and shunt resistance current $I_{SH}$ from the photogenerated current, $I_L$. Hence if there is a high recombination rate or if the shunt resistance is low, the current $I_D$ and $I_{SH}$ will increase, leading to an overall decrease in the total current. This will lead to a decrease in the efficiency. Correspondingly, a high series resistance will lead to a low output voltage resulting in diminished solar cell efficiency.

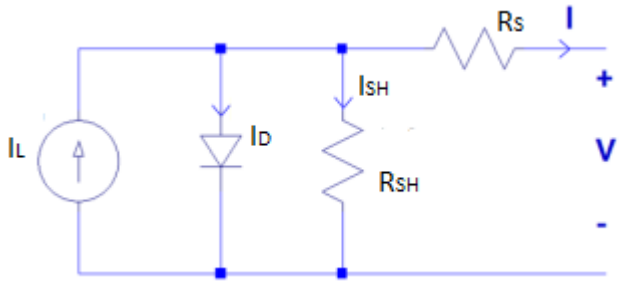


*Figure 4: Solar cell equivalent circuit model*

As new photosensitive materials and their properties are discovered, their applications in photovoltaic systems are explored. In recent years, there has been an increased focus on the perovskite compound for the fabrication of solar cells. Perovskite is an absorber material in solar cells and possesses desirable traits useful for photovoltaic applications. The fabrication of perovskite solar cells involves a low-cost technique, which makes it cost-effective [30]. There has been rapid progress in developing highly efficient and long-term stable perovskite solar cells from 3% in 2006 to 25.2% in 2019 [38]. However, there has been a hindrance in its

practical use due to its lack of stability. Moisture, temperature, and UV radiation play a key role in perovskite decomposition [31]. Several methods have been implemented to increase the stability of the perovskite layer [32]. Pistor et al., Phillipe et al. have performed tests under various environments like controlled humidity of 30% and high humidity of 60% along with an elevated temperature of 100°C [34] [35]. Nitrogen atmosphere is used for the fabrication of the solar cell. There have not been studies to evaluate the stability of the perovskite solar cells stored under ideal conditions like nitrogen environment with and without elevated temperatures which can give rise to understanding the stability of perovskite solar cells under nitrogen. Similarly, analyzing the solar cells stored under controlled humidity (30% to 38% RH) and high humidity (>50% RH) can provide us with clear information on how the different levels of humidity degrade the perovskite layer.

## 1.2 Motivation

The purpose of the study is to understand the stability of the different fabricated perovskite solar cells stored under various environments. The various environmental conditions include keeping the solar cells in $N_2$ environment at room temperature of 22°C, $N_2$ environment at elevated temperature of 80°C, controlled humidity (30% to 38% RH) and high humidity (Humidity above 50% RH). All the fabricated solar cells under the atmospheres are stored in both light (sunlight during the day, and room light at night) and dark conditions. The I-V characteristic curve of individual solar cells under each environment are studied with respect to time and the degradation of efficiency is examined. The best possible environment is taken into consideration, and correspondingly, improvements are made to the solar cell. The I-V

characteristics are studied after storing them under the selected environments, and the best solar cell is compared to a similar fabricated solar cell from the literature review under the same conditions. Finally, the I-V characteristics curve and the efficiency of the best solar cell is studied.

## 1.3 Scope

The focus of the present work is to understand the stability of the two different fabricated PSCs when placed in different environmental conditions after fabrication. There are various factors that lead to the degradation of solar cells. This study focuses primarily on a few factors

- High humidity, where the humidity is more than 50% RH,
- Controlled humidity, where humidity in between 30% RH and 38% RH,
- $N_2$ at room temperature of 22°C,
- $N_2$, at elevated temperatures of 80°C for a prolonged period of time.

The individual layers of the perovskite solar cells were characterized by scanning electron microscope (SEM). The I-V characteristics of the solar cells were studied with a power supply and a digital multimeter. The FF and PCE are calculated and compared with each other to find out the best possible results for the least degraded PSC. A new buffer layer is introduced to increase the stability of the PSC under different environments, and then the characteristics of the solar cells were analyzed and compared with a similar fabricated perovskite solar cell reported and stored under the same environment.

## 1.4 Assumptions

The assumption in the analysis of data is that none of the components of the solar cell were contaminated in their development. Additionally, any leakage of gas from the glove box while fabricating the PSC is not taken into consideration.

## 1.5 Hypothesis

This study examines how moisture, light, and temperature affect the degradation of the perovskite layer in the perovskite solar cell. It is expected that under sunlight, the UV degrades the perovskite. Oxygen alone does not degrade the perovskite; the effect of moisture with oxygen degrades perovskite the most. Thermal decomposition also plays a key role in the degradation of the perovskite layer.

## 2 - Literature Review

Perovskite mineral was discovered in the Ural Mountains of Russia by Gustav Rose in 1839 and was named after the Russian mineralogist L.A. Perovski [7]. This mineral has a specific crystal structure with $ABX_3$ as the main formula. '$A^{+}$' being a larger monovalent cation, '$B^{2+}$' being a relatively smaller divalent cation, and '$X^{-}$' being either oxygen or halogen ions. The perovskite has a cubic-octahedral structure with Space group P m -3 m, which is like that of Calcium Titanate ($CaTiO_3$) [35]. In a cubic-octahedral lattice structure, the large 'A' cation surrounded by twelve 'X' anions while the relatively smaller 'B' cation is surrounded by six 'X' anions. The oxide-based perovskite is studied due to its electrical properties of ferroelectricity and superconductivity. The halide-based perovskite exhibit semiconductor like properties and has good semiconductor to metal transition characteristics [8]. Additionally, they have a bandgap of 1.5eV and 2.3 eV depending on the amount of halogen ions and is favorable for solar cell applications. The earliest demonstrated PCE of basic PSC was reported by Park et al. 2011 to be around 6.5% [9]. The perovskite showed an absorption coefficient that was 10 times more than that of regular dyes like ruthenium amphiphilic dye Z-907, organic dyes based on porphyrin, and other naturally occurring dyes. Park et al. 2012 reported the PCE of relatively long-term stable perovskite solar cells to be around 9.7% [36]. Rapid progress was made over the years, and the PCEs exceeding more than 15% were achieved and reported [10]. Perovskite solar cell technology was selected as one of the biggest scientific breakthroughs by Science and Nature article in the year 2013.

The basic solid-state perovskite solar cell is composed of layered structures. The first layer is the transparent conductive oxide layer which is present in the glass substrate (FTO: Fluorine doped

Tin Oxide). The second layer is the $TiO_2$ layer, which is the Electron Transport Layer (ETL). It is composed of a compact $TiO_2$ layer and a mesoporous $TiO_2$ layer. The function of the compact $TiO_2$ layer is to develop the electron transport properties being an n-type material. The addition of mesoporous $TiO_2$ makes the surface of the compact $TiO_2$ smooth, thus enabling a better contact with the next layer. The third layer comprises of the solid perovskite layer, which acts as a light absorber. The fourth layer is made of a common hole transport material of spiro-OMeTAD which is then followed by a metal back contact, either silver or gold (Ag or Au). Figure 5 represents the side view structural schematics of the perovskite solar cell.

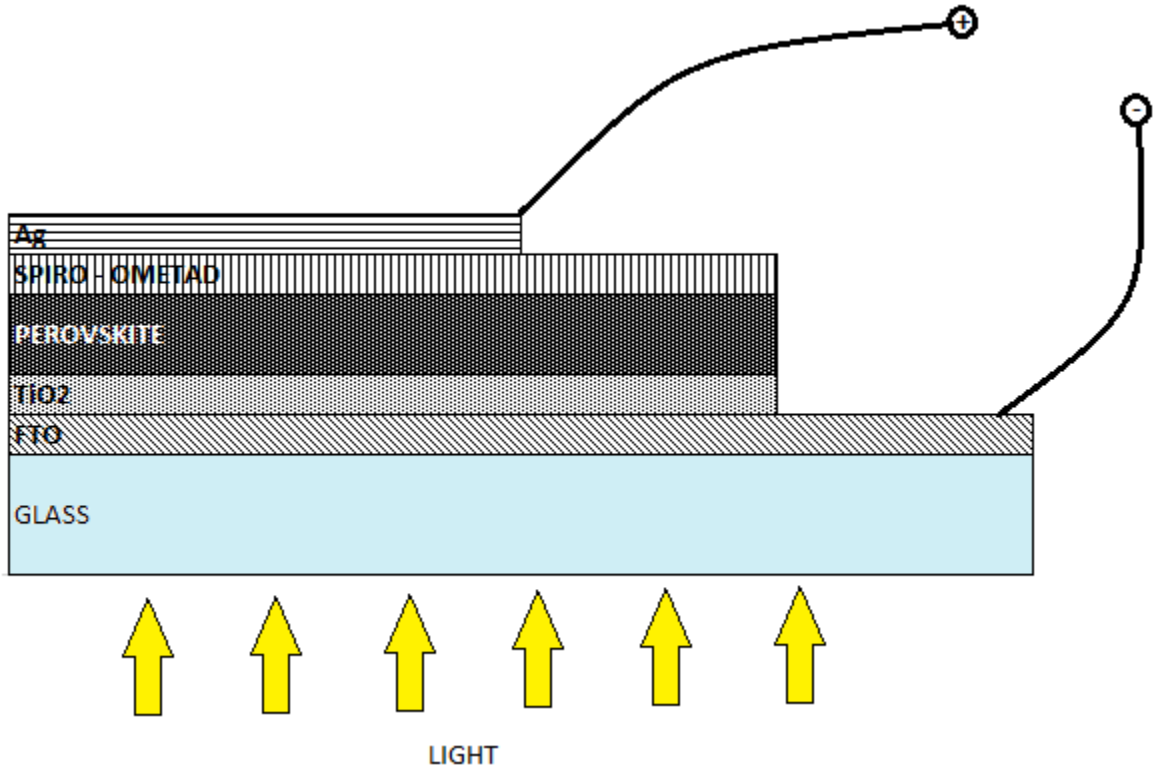


*Figure 5: Schematics of the PSC*

When light falls on the perovskite solar cell, the perovskite layer, represented in Figure 5, produces excitons. Excitons are electron-hole pairs that form when any material absorbs

photons of higher energy than its Bandgap. The bandgap is referred to as the energy differences between the conduction band and the valence band of a material. The valence band is located below the fermi level, and the conduction band is located above the Fermi level in an electronic band structure of a material [11].

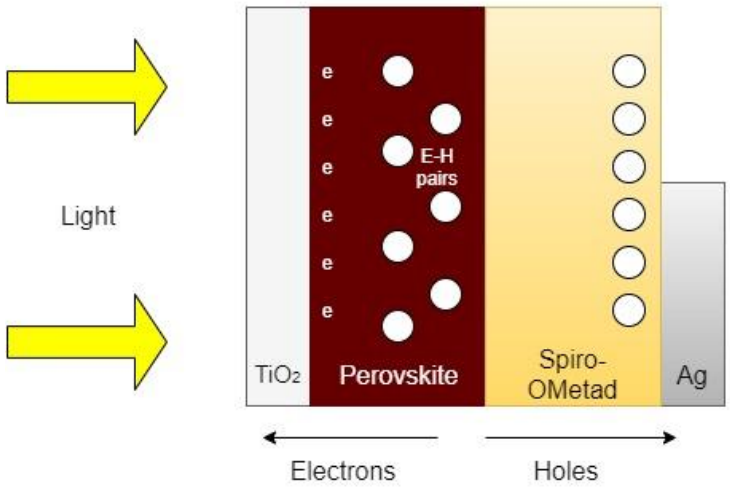


*Figure 6: Electron transfer process in perovskite solar cell*

When the perovskite creates excitons, as shown in Figure 6, the electrons are then transferred to the conduction band of the $TiO_2$ layer, and the holes are then transferred to the valence band of the spiro-OMeTAD layer. The conduction band minimum and the valence band maximum of the $TiO_2$ layer are -4.0 eV and -7.0 eV, respectively. The conduction band minimum and the valence band maximum of the perovskite layer are -3.93 eV and -5.43 eV, respectively. Similarly, the conduction band minimum and the valence band maximum of the spiro-OMeTAD layer are -2.12 eV and -5.22 eV, respectively [12]. The electron transfer process in the schematic energy level of the perovskite solar cell is given in Figure 7 [33].

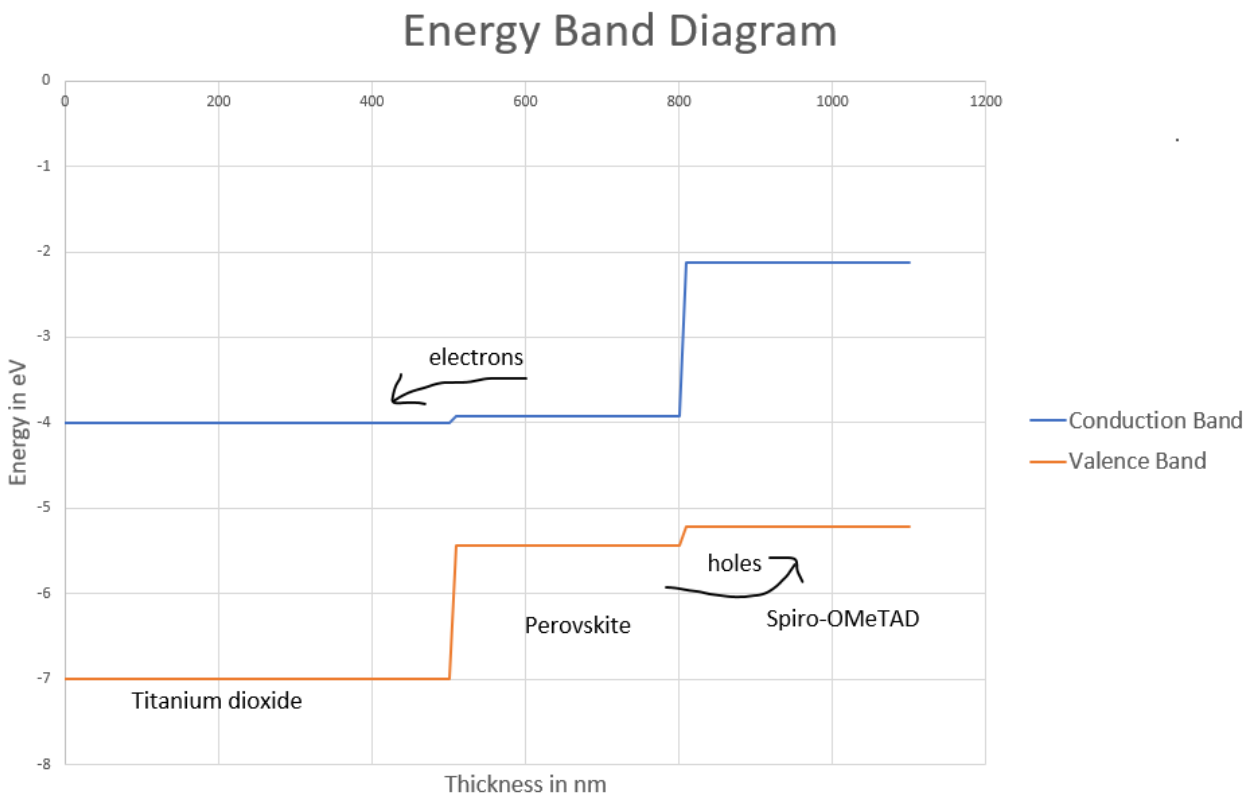


*Figure 7: Energy band diagram and Transfer of electrons and holes in between the layers*

The design of the perovskite solar cells was procured from dye-sensitized solar cell (DSSC) technology. $CH_3NH_3PbI_3$ and other perovskite minerals were used as an alternative dye material with a mesoporous $TiO_2$ layer. The efficiency of the perovskite solar cell is high and is achieved due to the ambipolar charge transport of the perovskite layer. It can transport both positive and negative charges simultaneously. Though perovskite has high efficiency, the key problem is its long-term stability. One of the key factors of the decomposition of the perovskite layer is its exposure to moisture. Niu et al. [13] reviewed the chemical processes that caused the degradation of the perovskite film. They identify three key factors causing the degradation of the film.

- Moisture ($H_2O$ and $O_2$),
- UV part of the white light,
- Temperature.

The amine component present in the compound gets easily decomposed in contact with moisture ($H_2O$ and $O_2$). The equations (3), (4), and (5) suggest the series of reactions that leads to the degradation of the perovskite layer placed in a high moisture environment:

$CH_3NH_3PbI_3$ <-> $CH_3NH_3I$ (aq) + $PbI_2$ (s) (presence of moisture) (3)

$CH_3NH_3I$ (aq) <-> $CH_3NH_2$ (aq) + HI (aq) (presence of moisture) (4)

4HI (aq) + $O_2$ -> $2I_2$ (s) + $2H_2O$ (l) (presence of oxygen) (5)

The equation (3) and (4) corresponds to the degradation of the perovskite layer to HI and aqueous methyl ammonia. Equations (3) and (4) suggests the reversible reaction of the perovskite layer when in contact with water. The methyl- ammonium lead iodide turns into methyl ammonia and hydrogen iodide. Equation (5) suggests the further irreversible degradation of HI to solid iodine and water when in contact with oxygen. The irreversible degradation of the perovskite layer is a hindrance to the stability of the solar cells. Hence, the perovskite solar cells are always fabricated in an inert gas-filled glove box to achieve high performance. Leguy et al. investigated that after being exposed to humidity more than 70% for 60 h, the bandgap of $CH_3NH_3PbI_3$ single crystal was found to increase from 1.5 eV to 3.1 eV [14]. That confirmed the complete, irreversible reaction from perovskite to lead iodide ($PbI_2$), leaving solid iodine as a substrate. Christians et al. (2015) have investigated the interaction of controlled humidity with perovskite while fabricating the perovskite layer [15]. The perovskite

film made under 0% to 25% humidity (RH) at room temperature of 22°C became a complex perovskite crystal $(MA)_4PbI_6.2H_2O$. The complex crystal had a decreased light absorption coefficient leading to lower efficiencies and faster degradation compared to fabricating under nitrogen atmosphere. The degradation due to moisture was reduced by encapsulation of the sole cell with epoxy.

Illumination with UV light can also lead to the degradation of the perovskite film in the solar cell [39]. High efficient solar cells were obtained by applying $TiO_2$ as the electron transport layer. $TiO_2$ layer is susceptible to UV-induced degradation and was first shown by Leijtens et al. in 2013 [16]. Schoonman et al. 2015 investigated the mechanisms of photodecomposition of the perovskite layer and the formation of metallic lead under UV light exposure [17]. The degradation from UV light is mainly due to the UV absorptive properties of the $TiO_2$ scaffold. Three methods were proposed by Ito et al. to circumvent the problem [18].

- Avoid UV from reaching the $TiO_2$ layer,
- Replace $TiO_2$ scaffold with a different material, and
- Replace $TiO_2$ with other ETL material.

To reduce the UV induced degradation of the $TiO_2$ layer, Leitjens et al. introduced a UV filter that blocked UV from entering the $TiO_2$ layer [16]. This led to the fact that the degradation of the perovskite layer is presumably due to the UV range of the white light bandwidth.

To replace the $TiO_2$ scaffold, Ito et al. introduced a buffer layer of $Sb_2S_3$ at the $TiO_2/CH_3NH_3PbI_3$ interface that improved the stability from other perovskite solar cells without the buffer [18]. This indicated that the decomposition of the perovskite under illumination might be driven by

the reaction at the $TiO_2/CH_3NH_3PbI_3$ junction. The authors propose that the $Sb_2S_3$ layer inserted at the interface blocks the UV induced degradation in the perovskite layer.

Exposure of the solar cells to elevated temperatures causes degradation of the perovskite layer. While annealing the perovskite layer, the cell is kept at 100°C for 10 minutes. Phillipe et al. investigated the effects of elevated temperature on both regular and hybrid perovskite films [19]. The perovskite layer turns to lead iodide. They observed that the perovskite layer, when annealed at 140°C and 160°C, caused severe degradation of the layer to $PbI_2$.

The following reaction shown in equation (6) indicates degradation due to prolonged exposure to high temperatures. The prolonged exposure caused the perovskite to sublime, leading to lead iodide as a substrate, while the methyl ammonia and hydrogen iodide to evaporate.

$$CH_3NH_3PbI_3 \rightarrow PbI_2(s) + CH_3NH_2(g)\uparrow + HI(g)\uparrow \quad (6)$$

The first layer that to study the stability of the perovskite solar cell is the $TiO_2$ layer, which is the electron transport layer. Titanium crystals and oxygen vacancies create non-stoichiometric defects, which can reduce the performance of the solar cell. Pathak et al. demonstrated that doping Al into $TiO_2$ led to a decrease of the defects and, thus, an increase in the performance of the solar cell [20]. Yang et al. investigated a heat-treated ZnO layer instead of the $TiO_2$ layer. The heat treatment of the ZnO layer removes the surface hydroxyl groups, which leads to an accelerated thermal decomposition [21].

Song et al. replaced $TiO_2$ with $SnO_2$ as the electron sensitive contact. The layer was formed by spin coating $SnO_2$ nanoparticles and annealing at 200°C for 1 hour [22]. The non-encapsulated devices stored in ambient conditions were stable for 700 hours. This was significantly more

stable than $TiO_2$ based devices. However on exposure to high temperatures of 100°C for a prolonged period of time, the perovskite solar cells degraded rapidly.

The next layer is the hole transport layer. The most common HTL material used in this case is spiro-OMeTAD. The material requires 4-tert-butyl pyridine (TBP) or bis(trifluoromethane)sulfonimide lithium salt (Li-TFSI) to improve the conductivity. These additives in the spiro-OMeTAD layer, however, degrades the perovskite layer and reduces the stability. Han et al. showed that using spiro-OMeTAD as HTL increased the series resistance of the solar cells that were tested under a constant temperature of 55°C and a relative humidity RH of 50% at AM1.5 [23]. Habisreutinger et al. studied thermal and moisture-induced degradation in the hole transport layer [24]. They studied three HTLs that yielded the highest efficiency results,

- Spiro -OMeTAD,
- Poly 3-hexylthiophene commonly known as P3HT,
- Poly bis(4-phenyl)(2,4,6-trimethylphenyl) also known as PTAA.

They observed that for all HTLs, there was a rapid degradation of the Perovskite film. To increase the stability of the HTL layer, Polycarbonate (PC), acting as an insulator, was combined with single-wall carbon nanotubes (SWNT) to increase the conductivity. The devices that were fabricated with SWNT was then wrapped with a monolayer of P3HT to increase the hydrophobic nature [24]. This showed extreme stability towards moisture, and the solar cell was exposed to running water for 60 seconds, and the efficiency value changed from 12.9% to 12.7%.

Many scientists have used organic HTL for perovskite solar cells. Kim et al. incorporated inorganic HTL, $NiO_x$ [25]. The inorganic oxide showed better environmental stability but a decrease in efficiency than organic HTLs. To increase efficiency, Kim et al. doped copper with NiOx to form a Cu-NiOx film. This achieved a maximum efficiency of 15.4%.

The most common organic HTL, Spiro-OMeTAD displays low conductivity, and hence it is mostly with a p-type dopant. Spiro-OMeTAD is usually doped with Li-bis(trifluoromethanesulfonyl) imide (Li-TFSI) to allow for high performance with increased conductivity. A separate dopant free HTL material, a tetrathiafulvalene derivative (TTF-1), is added to reduce the degradation. Liu et al. demonstrated this technique, where they annealed the layer at 65°C in an argon environment for 24hours. The devices were measured under a relative humidity of 40% and were stable for 360 hours [26].

The next layer is the counter electrode. Gold is the most common electrode for developing high efficient perovskite solar cells. Gold is expensive, and hence silver paste is used as an alternative material. Kato et al. detected an issue while using silver that displayed the formation of silver iodide (AgI) on exposure to relative humidity (RH) more than 40% RH[27]. The formation of silver iodide (AgI) is indicated in Figure 8.

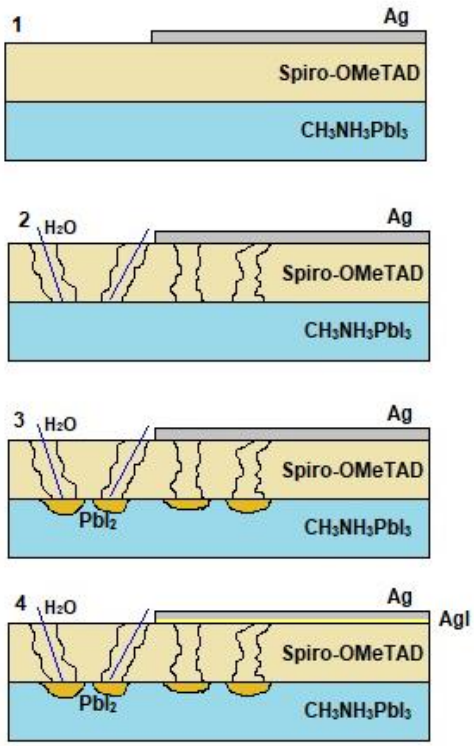


*Figure 8: Formation of AgI in the perovskite solar cell*

The formation of silver iodide begins from diffusion of water to the perovskite layer through the spiro-OMeTAD layer creating lead iodide and hydrogen iodide. The hydrogen iodide migrates through the spiro-OMeTAD layer to the Ag electrode giving rise to the development of AgI. The AgI leads to the tarnish of the reflective silver to a yellowish color, as shown in Figure 8.

Guarnera et al. incorporated a buffer layer consisting of $Al_2O_3$ nanoparticles in between the perovskite layer and the HTL [28]. The addition of $Al_2O_3$ as a buffer layer stopped the effect of moisture on the solar cell tarnishing silver. They also incorporated the encapsulation technique in a nitrogen-filled glove box using an epoxy resin cured in sunlight for 30 minutes. This stopped the moisture contact altogether, and the best device maintained 95% of its initial efficiency for

350 hours. They proposed that the degradation was not because of moisture or by UV radiation, but by the migration of the metal from the top contact to the perovskite layer.

The addition of $Al_2O_3$ and epoxy has shown to increase the stability of the perovskite solar cells. This has made the perovskite layer more stable towards moisture and migration of metal to the perovskite layer. However, the study of the improved solar cell under an ideal environment of $N_2$, elevated temperatures of 80°C and controlled humidity (30% to 38% RH) still needs to be understood.

## 3 – Methodology

### 3.1 Constructing the Glovebox and preparing the working station

#### 3.1.1 Materials

The materials required to prepare the working glove box are as follows

- Empty glove box,
- Nitrogen gas cylinder,
- Vacuum pump,
- Purity Nitrogen gas regulator,
- Ball valves,
- Polyethylene tube [0.25 inch diameter],
- 1 inch diameter polyethylene pipe,
- 0.5 inch diameter polyethylene pipe.

#### 3.1.2 Process

The glove box contains two chambers, the big (primary) chamber and the small (secondary) chamber, separated by a small door that can be opened to transfer materials to and from the main chamber. When the glove box is closed, the connection between the two chambers was maintained by using a 0.5 inch polyethylene pipe and ball valves that maintained proper pressure and environment inside the main chamber. The dimension of the main chamber is 48'' x 32'' x 36'', with a total volume of 55296 cubic inches or 32 cubic feet. The dimension of the secondary chamber is 17'' x 7'' x 10'', with a total volume of 1190 cubic inches or 0.68 cubic feet. A picture of the glovebox with dimension is given in Figure 9.

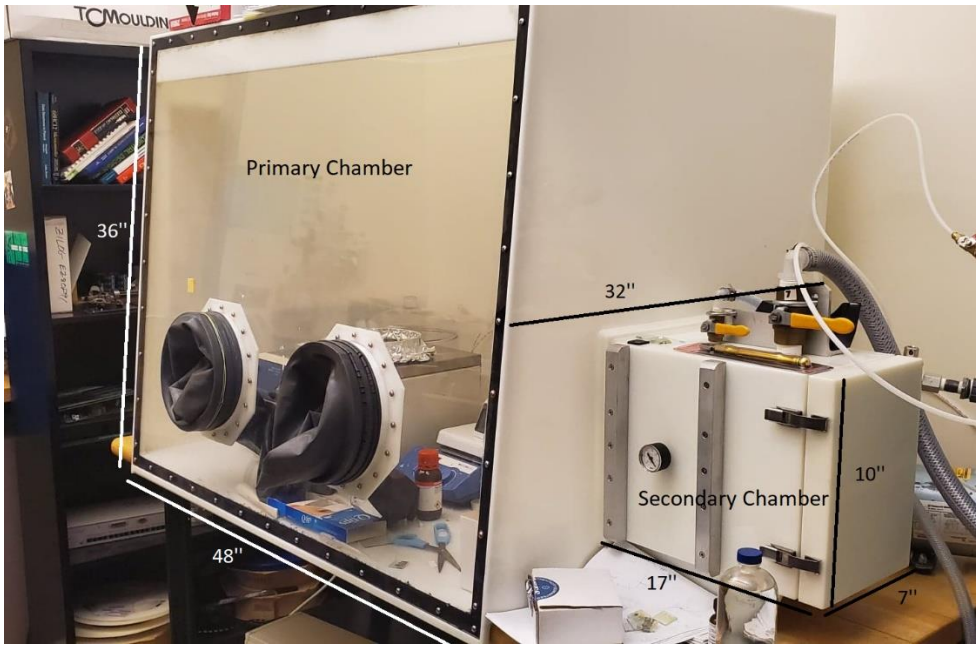


*Figure 9: Glove box with dimensions*

The environment used in this case was $N_2$. $N_2$ gas cylinder was connected using a pressure valve and then was split into two directions. One was attached directly to the connection of the spin coater, and the other line was connected to a point leading directly into the secondary chamber of the glove box, which was then connected to the main chamber using the 0.5 inch polyethylene pipe. A vacuum pump was used to remove the air from inside the glovebox, and $N_2$ gas was introduced inside the glovebox. Figure 9 and Figure 10 shows the proper connection of the $N_2$ gas cylinder and the vacuum pump to the glove box.

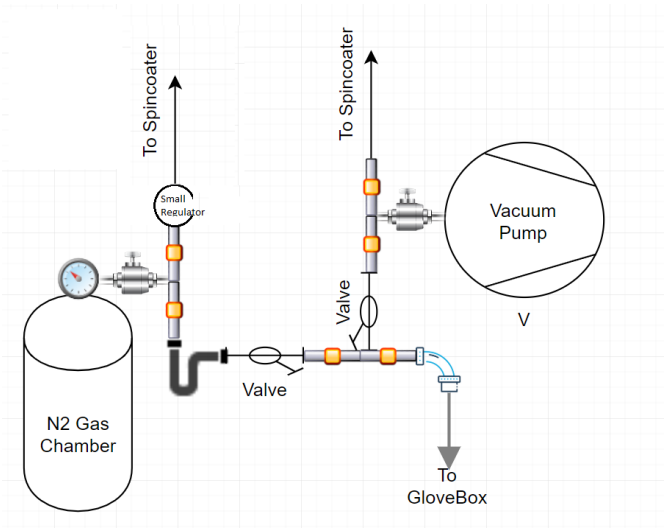


*Figure 10: Schematic diagram of connection to the glovebox*

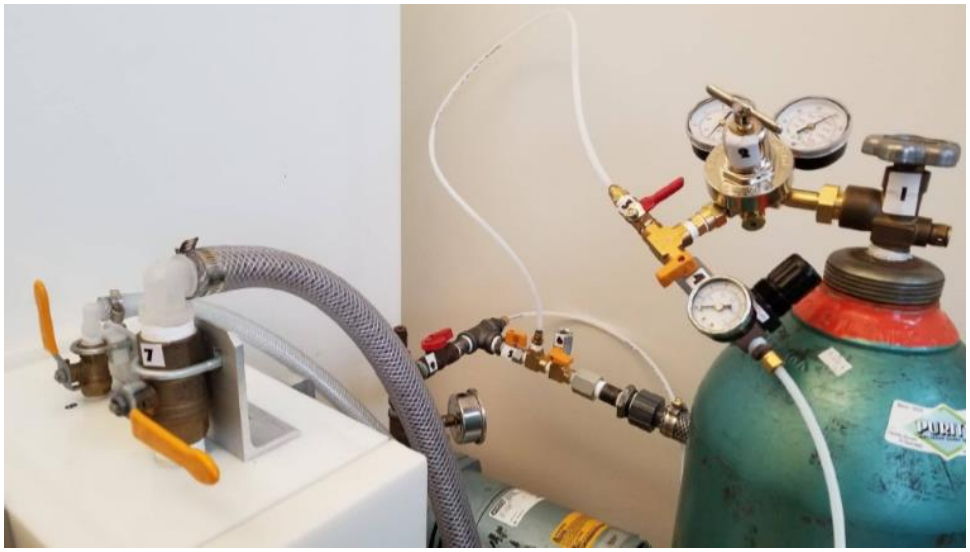

*Figure 11: Actual connection of nitrogen and vacuum to the glovebox*

The labels of the valves are numbered and are used for a specific function.

#1: N2 from the cylinder,

#2: N2 pressure valve can handle >2000 psi,

#3: Valve for N2 to go into the glove box (secondary chamber),

#4: Valve for N2 to go into the spin coater,

#5: Valve for Vacuum to go into the glove box (secondary chamber),

#6: Valve for Air inlet into the glove box (secondary chamber),

#7: Valve for either Vacuum or N2 or Air into the glove box (secondary chamber),

#8: Valve to connect the small chamber to the primary chamber of the glove Box,

#9: Valve of the main vacuum pump.

The manual to use the glove box is included in Appendix A.

### 3.2 Making the $TiO_2$ paste outside the glove box

#### 3.2.1 Materials

- P25 $TiO_2$,
- 1M Acetic Acid ($CH_3COOH$),
- Mortar and Pestle,
- Measuring cylinder,
- Pipette.

#### 3.2.2 Compact $TiO_2$ Process

20g of P25 $TiO_2$ powder was taken into a mortar, and pestle and 6ml of 1M acetic acid ($CH_3COOH$) were added into it. The contents were then mixed to form a lump-free paste, as shown in Figure 12.

*Figure 12: Titanium dioxide paste in dilute acetic acid*

### 3.2.3 Mesoporous $TiO_2$ Process

2 grams of P25 $TiO_2$ powder was taken out from the storage vessel and weighed using a weighing scale and then poured into the dark glass bottle. 5ml of 1M acetic acid was taken out using a pipette and then measured using a measuring cylinder. The 1M acetic acid was poured into the glass bottle containing 2g of $TiO_2$. The entire mixture was then stirred till it became a colloidal solution of 40% weight ready to be used for solar cell application.

## 3.3 Making basic perovskite solution inside the glove box

### 3.3.1 Materials

- Methyl Ammonium Iodide ($CH_3NH_3I$),
- Lead Iodide ($PbI_2$),
- Di-Methyl Formamide (DMF),
- Weighing scale,
- Hot Plate,
- Dark glass bottle,

- Pipette,
- Measuring cylinder,
- Small spatula.

### 3.3.2 Process

0.80g of methylammonium iodide and 2.30g of lead iodide was added into a dark glass container using a weighing scale and spatula. 5ml of DMF was added to the container to make 1M of perovskite solution. The mixture was made by stirring the solution at 80°C until it forms a complete homogenous solution. Figure 13 and 14 shows the process of making the basic perovskite solution.


*Figure 13: Weighing the precursors on the weighing scale*


*Figure 14: Heating the perovskite solution at 80°C for proper homogenous solution*

### 3.4 Making hybrid perovskite solution inside the glove box

#### 3.4.1 Materials

- Methyl Ammonium Iodide ($CH_3NH_3I$),
- Lead Chloride,
- Di-Methyl Formamide (DMF).

#### 3.4.2 Process

2.39g of methylammonium iodide and 1.39g of lead chloride was added into a dark glass container using a weighing scale and spatula. 5ml of DMF was added to the container to make

1M of hybrid perovskite ($CH_3NH_3PbI_2Cl$) solution. The mixture was made by heating the solution to 80°C and stirring until it forms a complete homogenous solution.

### 3.5 Making Spiro-OMeTAD solution outside the glove box

#### 3.5.1 Materials

- Methyl Ammonium Iodide ($CH_3NH_3I$),
- Spiro-OMeTAD,
- Chlorobenzene,
- Weighing scale,
- Dark glass bottle,
- Pipette,
- Measuring cylinder,
- Spatula.

#### 3.5.2 Process

80mg of spiro-OMeTAD was added into a dark glass container using a weighing scale and spatula. 1ml of chlorobenzene was added to the container and stirred at room temperature of 22°C to make a homogenous spiro-OMeTAD solution.

### 3.6 Counter Electrode

#### 3.6.1 Materials

- Conductive silver paste from Ted Pella in Figure 15.


*Figure 15: Ted Pella conductive silver paste*

### 3.7 Making of the $Al_2O_3$ buffer solution and Epoxy Resin outside the glove box

#### 3.7.1 Materials

- $Al_2O_3$ powder,
- Chlorobenzene,
- Dark glass bottle,
- Measuring cylinder,
- Pipette,
- Spatula,
- Weighing scale, and
- Epoxy Resin.

### 3.7.2 Process

2 grams of $Al_2O_3$ powder was taken out from the storage vessel and weighed using a weighing scale and then poured into the dark glass bottle. 5ml of chlorobenzene was taken out using a pipette and then measured using a measuring cylinder. The chlorobenzene was poured into the glass bottle containing 2g of $Al_2O_3$. The entire mixture was then stirred till it became a colloidal solution of 40% weight ready to be used for solar cell application.

Epoxy resin was bought from Ossila. The chemical composition of the epoxy resin was 7-oxabicyclo[4.1.0]hedtan-3-ylmethyl 7-oxabicyclo[4 1 0]hedtane-3-carboxylate.

### 3.8 Fabricating perovskite solar cell structure

The perovskite solar cell has a layered structure. The first layer is the FTO coated glass. The second layer is the $TiO_2$ layer. The FTO glass was prepared by agitating them in isopropyl alcohol and letting them dry by blowing $N_2$ gas on it. Once the FTO glass was dry, the opposite ends were covered with scotch tape such that 4mm was covered from each side, and compact $TiO_2$ paste was applied on to the open area of the FTO glass, and then the paste was uniformly spread with the help of a glass rod. The purpose of scotch tape was to avoid leakage of the $TiO_2$ into the covered ends of the FTO glass. The scotch tape was removed, and the wet $TiO_2$ layer was then annealed to 400°C for 30 minutes and then kept at rest for 3 hours till it reached room temperature of 22°C and the scotch tape was applied on two opposite sides before starting on the third layer.

### 3.8.1 Spin Coating Fabrication of perovskite solar cell in the glove box

The third layer was a mesoporous $TiO_2$ layer where the previous layered compact $TiO_2$ was then scotch taped on the sides and placed in a Spin coater (Specialty Coating Systems Model P-6708D) inside a glove box, and then three to four drops of $TiO_2$ (0.075 mL to 0.1mL) were added on it and then the sample was placed at 4000rpm for 1 minute. The scotch tape was removed. The mesoporous $TiO_2$ layer was then annealed to 400°C for 30 minutes and rested for 3 hours until it reached room temperature of 22°C. The annealing process can be seen in Figure 16.

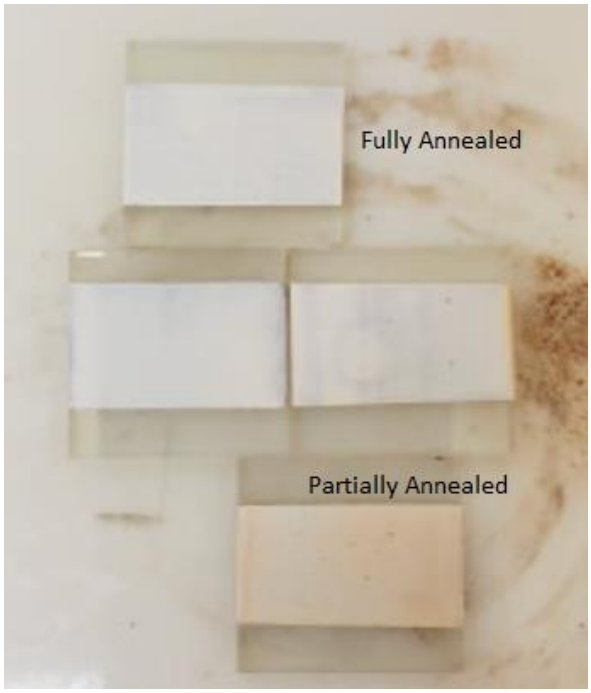


*Figure 16: Annealing of titanium dioxide layer*

The next layer is the perovskite layer. The sample FTO glass with $TiO_2$ was scotch-taped to the sides again for the perovskite solution to not leak into the sides covered with scotch tape, the sample was then placed in the spin coater, and then three to four drops (0.075 mL to 0.1mL) of perovskite solution were added and then spin-coated for 4000rpm for 1 minute. Some leaked

perovskite solution that reached the sides were then wiped with a Q-tip dipped in chlorobenzene to remove the perovskite solution. The scotch tape was removed and then annealed for 10 minutes at 100°C. By doing this step, the sample turns from bright yellow to dark brown, as mentioned in Figure17.

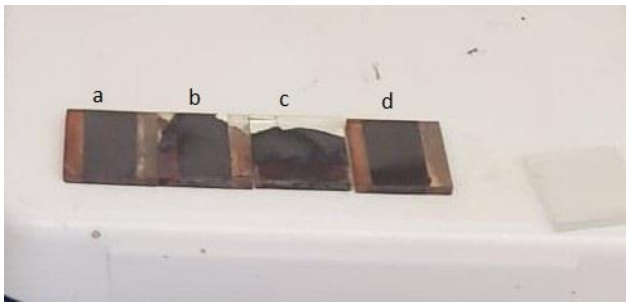


*Figure 17: Annealing of the perovskite layer*

Figure 17 shows the annealed perovskite layers in the glove box containing $N_2$ at 100°C for 10 mins. Sample a, and sample d represent the annealed spin coated perovskite layer, while sample b, and sample c represent the annealed blade coated perovskite layer. Annealing the perovskite for more than 20 minutes leads to degradation of the perovskite layer.

The next layer is the hole transport layer (HTL), the Spiro-OMeTAD layer. Scotch tape was added to the two opposite sides of the annealed perovskite sample so as to stop the leakage of the perovskite solution into the active electrode. The sample was placed in the spin coater again. Three to four drops (0.075 mL to 0.1mL) of spiro-OMeTAD solution were added and spin-coated at 4000rpm for 1 minute. The final sample was then annealed at 100°C for 10 minutes.

The last step was to add the conductive silver layer inside the glove box, where the silver paste was added on to the areas as droplets (0.025mL) so as not to disturb the spiro-OMeTAD layer in any way, as shown in Figure 18. Figure 19 shows sample perovskite solar cells. Sample A, and sample C are fabricated using spin coated technique, while sample B, and sample C are fabricated using blade coating technique.

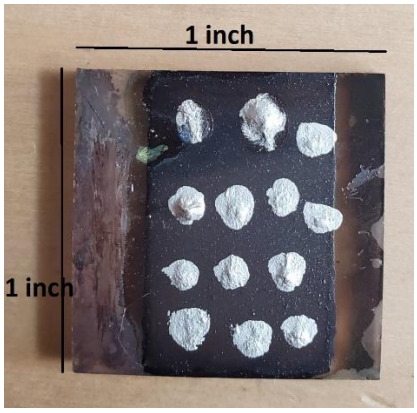


*Figure 18: Droplets of silver paste on top of the spiro-OMeTAD layer*

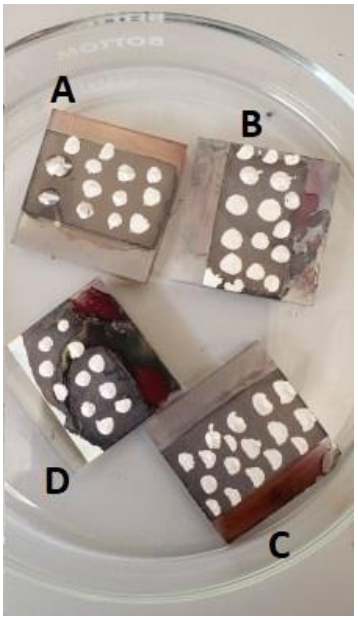


*Figure 19: Sample Perovskite Solar Cells*

### 3.8.2 Blade Coating Fabrication of perovskite solar cell in the glove box

The third layer was a mesoporous $TiO_2$ layer, and then three to four drops (0.075 mL to 0.1mL) of $TiO_2$ were added, and then the solution was uniformly spread with a glass rod. The scotch tape was removed. The mesoporous $TiO_2$ layer was then annealed to 400°C for 30 minutes and rested for 3 hours until it reached room temperature of 22°C.

The next layer is the perovskite layer. The sample FTO glass with $TiO_2$ was scotch taped to the sides again for the perovskite solution to not leak into the sides covered with scotch tape. Three to four drops (0.075 mL to 0.1mL) of perovskite solution were added and spread with the help of a glass rod and annealed at 100°C for 10 minutes. Three to four drops (0.075 mL to 0.1mL) of spiro-OMeTAD was then added on top of the perovskite layer, and the excess solution was removed with a Q-tip. The final sample was annealed at 100°C for 10 minutes. Glass rod was not utilized in this layer as it would disturb the perovskite layer. Solutions of 0.075 mL to 0.1 mL was enough to cover the entire top layer of the solar cell structure.

### 3.8.3 Fabrication of improved perovskite solar cell inside the glove box

Sixteen PSCs were fabricated and then were tested under light at AM1.5 to get the initial results, and then the solar cells were placed at different environmental conditions being controlled humidity (30% to 38% Moisture), high humidity (>50% Moisture), $N_2$ at room temperature of 22°C, and N2 at elevated temperature of 80°C.

After the fabrication and analysis of the twelve PSCs, two new sets of solar cells were fabricated by adding a buffer layer (0.1mL) of $Al_2O_3$ in between the perovskite layer and the spiro-

OMeTAD layer. The buffer layer was spin-coated to reduce any human error from the blade-coating technique. The buffer layer was then annealed at 40°C for 10 minutes. Chlorobenzene vapour was important to assist in the fabrication of the perovskite solar cell [37]. The first set comprised of the buffer layer and the second set comprised of the buffer layer and encapsulation with epoxy resin. Two drops (0.05 mL) of epoxy resin were dropped on top of the spiro-OMeTAD layer to avoid any moisture contact to any of the layers of the solar cell. The epoxy resin was then set for 5 minutes under sunlight for the solar cell to get ready for testing under different environments.

### 3.8.4 Testing environment and storing structure of the perovskite solar cells

Initially, eight perovskite solar cells were fabricated using two different perovskite solutions (regular and hybrid perovskite) and two different fabricating techniques (blade coating and spin coating) that were placed in different environmental conditions under dark and light (sunlight during the day, and room light at night) using a desiccator. The various environments were as follows,

- Controlled Humidity (30% to 38% RH),
- High Humidity (>50% RH),
- Nitrogen (room temperature of 22°C),
- Nitrogen (elevated temperature of 80°C).

For each environment, there were eight different sets involved.

*Table 1: Solar cell fabricating and storing structure per environment*

| Layer Manufacturing | Perovskite Used | Stored In |
|---|---|---|
| Spin Coated | Regular | Light |
| Spin Coated | Regular | Dark |
| Spin Coated | Hybrid | Light |
| Spin Coated | Hybrid | Dark |
| Blade Coated | Regular | Light |
| Blade Coated | Regular | Dark |
| Blade Coated | Hybrid | Light |
| Blade Coated | Hybrid | Dark |

These eight cells indicated in Table 1 were repeated for the four environments and were analyzed in the dark chamber, also known as the solar simulator. A total of thirty-two solar cells were fabricated and tested. The efficiency and the fill factor decreased gradually, indicating degradation in the perovskite layer and correspondingly the spiro-OMeTAD layer.

### 3.9 Testing

#### 3.9.1 Materials

- Dark Chamber,
- Power supply (BK PRECISION MODEL – 1760A),
- Multimeter (FLUKE 289 TRUE RMS MULTIMETER).

#### 3.9.2 Process

The perovskite solar cell was placed in a dark chamber where the light was calibrated to supply 100mW/cm$^2$ at AM1.5.

Power supply and a multimeter were used to acquire the I-V characteristics of the solar cell. The proper connection diagram for the setup is given in Figure 20 and Figure 21.

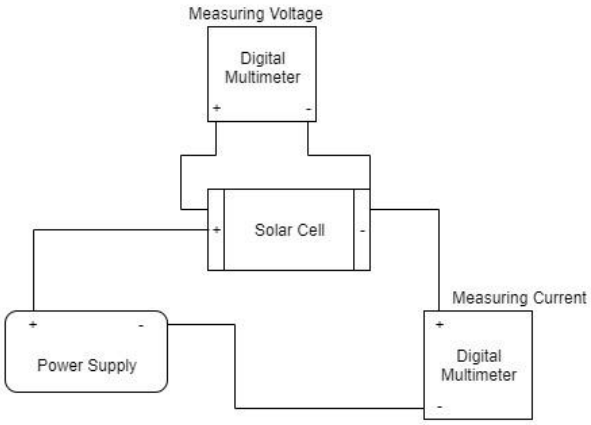


*Figure 20: Schematic diagram of solar cell testing*

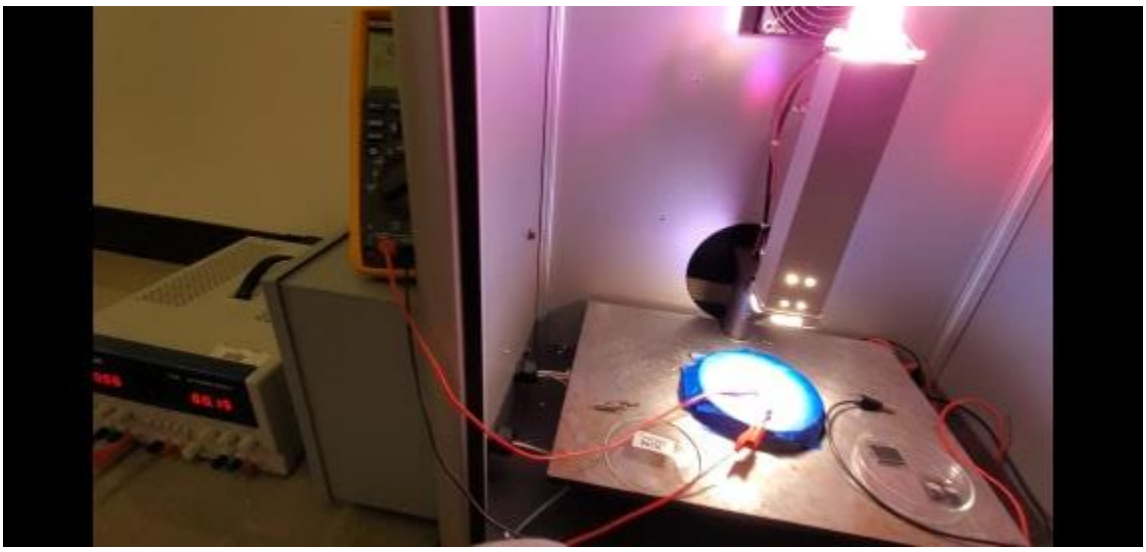

*Figure 21: Live solar cell testing*

As shown in Figure 20, the positive end of the solar cell was connected to the positive terminal of the power supply, the negative terminal of the solar cell was connected to the positive terminal of the multimeter to measure the current generated from the solar cell. The positive end of the solar cell was connected to the positive end of the multimeter and the negative end of the solar cell was connected to the negative terminal of the multimeter to measure the

voltage of the solar cell. Finally, the negative terminal of the power supply was connected to the negative terminal of the multimeter to complete the circuit. This setup was required to determine the open-circuit voltage ($V_{oc}$), short circuit current ($I_{sc}$), maximum power point voltage ($V_{MPP}$), and maximum power point current ($I_{MPP}$). The values of voltage and current were then noted down in an excel sheet where the I-V characteristic curve was plotted of each individual solar cell kept under different environmental conditions.

## 4 – Results

### 4.1 – Perovskite solution and annealed layer absorption

The absorption spectrum of perovskite solution and annealed perovskite were observed using a spectrophotometer (Cole Parmer Model – UV2100PU). The data obtained was the absorbance of light per wavelength by that solution.

Figure 22 and Figure 23 shows the absorption spectrum of the liquid perovskite solution and the annealed perovskite sample.

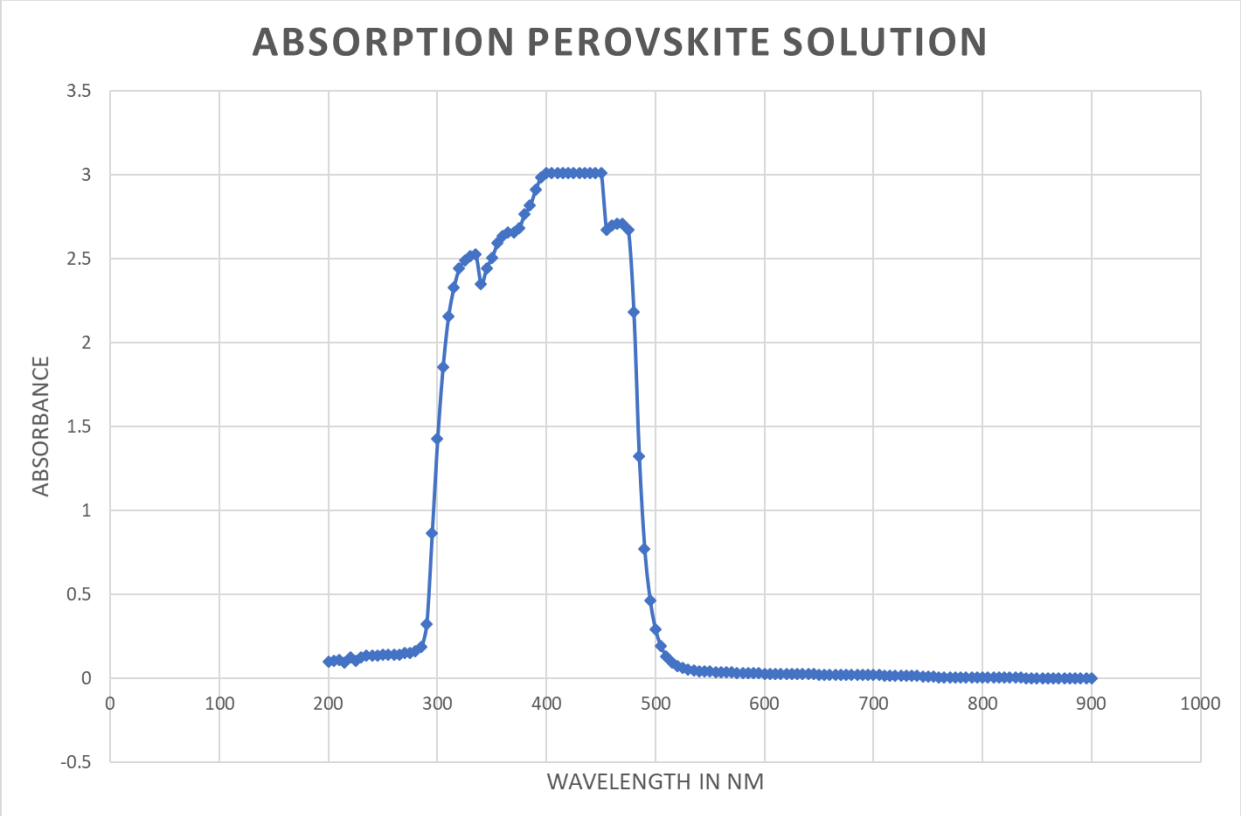


*Figure 22: Absorption spectrum of liquid perovskite solution*

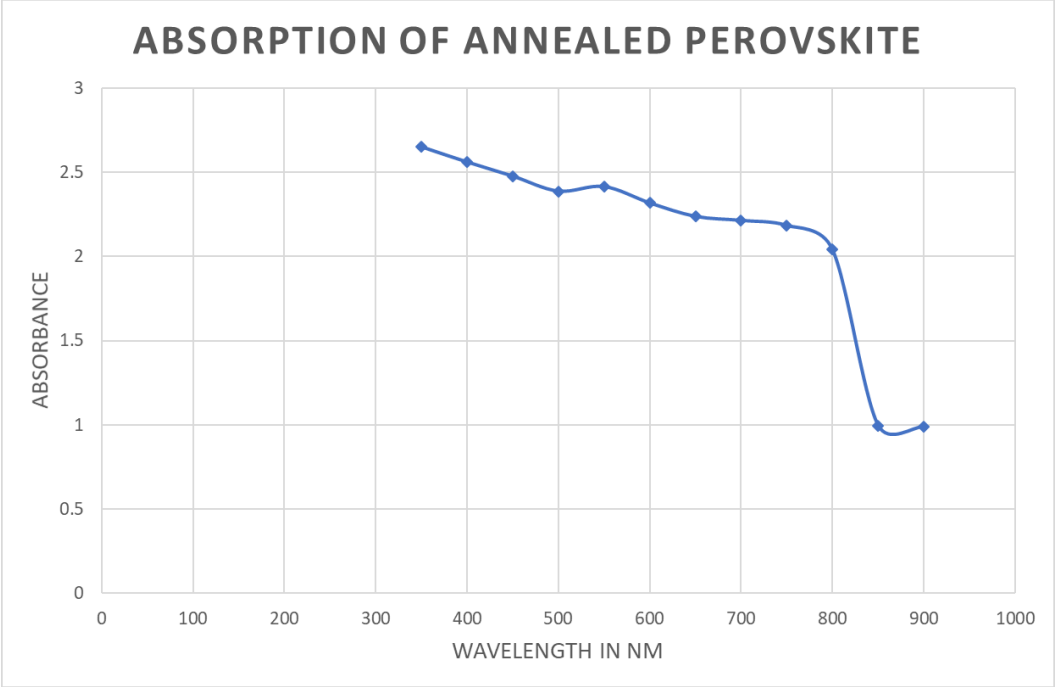


*Figure 23: Absorption spectrum of the annealed perovskite layer*

From Figure 22, the absorption of light by the perovskite solution is ranged from 300nm to 480nm, which signifies that the perovskite solution is highly absorptive of the ultraviolet region. The solution should be stored in a dark place to avoid degradation by UV. Similarly, from Figure 20, the annealed perovskite has good absorption from 380nm to 800nm. This also signifies that the annealed perovskite layer absorbs UV rays. The change in the absorption in Figure 22 is due to the change of the structure of the perovskite from solution to crystalline perovskite.

**4.2 – Perovskite solar cell structure**

As discussed in the literature review, a typical perovskite solar cell structure contains several layers

1. The first layer is the transparent conductive oxide (TCO) layer on a glass substrate that acts as an active electrode (photo-anode); in our case, fluorine doped tin oxide is used (FTO) as the TCO layer.
2. The second layer comprises an electron transport layer (ETL); titanium dioxide is used as ETL ($TiO_2$).
3. The third layer consists of the perovskite layer; basic perovskite 1M solution of $CH_3NH_3PbI_3$ in DMF is used.
4. The fourth layer consists of a hole transport layer (HTL); a 1M solution of spiro-OMeTAD in chlorobenzene is used as HTL.
5. The fifth layer is followed by a metal back contact, mainly Au or Ag, which acts as a counter electrode (photo-cathode).

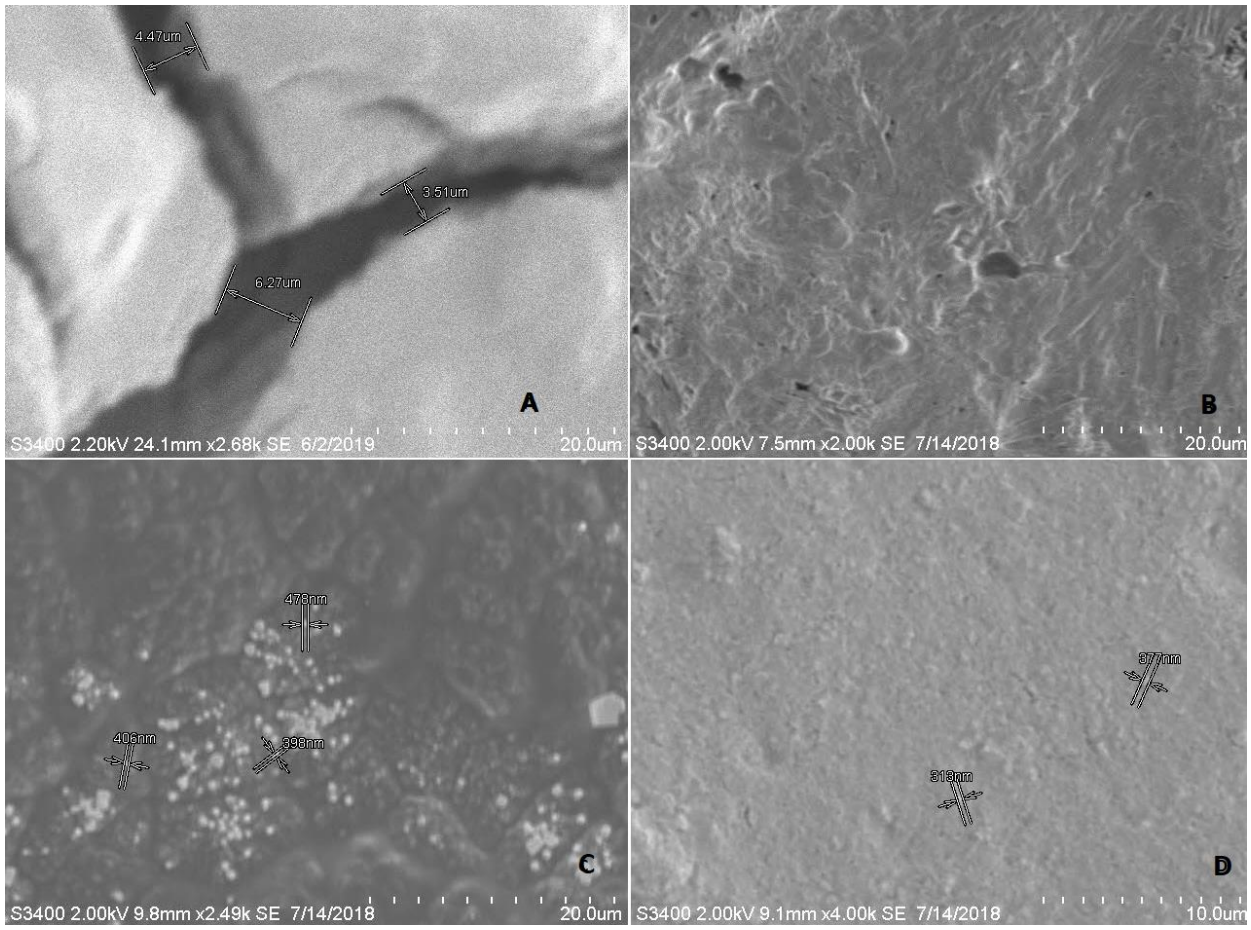


*Figure 24: Morphology of the different layers of the perovskite solar cell*

Figure 24 represents the morphology of the different layers in the perovskite solar cell. The scale of sample A, B, and C are 20µm, while the scale of sample D is 10µm. A voltage of 2.2kV was applied for sample A, while a voltage of 2.0kV was applied for samples B, C, and D. Sample 24A shows the titanium dioxide layer after annealing at 400°C for 30 minutes and cooling down to room temperature of 22°C for 3 hours. The function of the compact $TiO_2$ layer is to develop the electron transport properties being an n-type material. The cracks developed in the figure can get replenished with the addition of mesoporous $TiO_2$. The addition of mesoporous $TiO_2$ makes the surface of the compact $TiO_2$ smooth, thus enabling a better contact with the

perovskite layer. Sample 24B shows the perovskite layer after annealing at 100°C for 10 minutes. Sample 24C shows the spiro-OMeTAD layer after annealing at 100°C for 10 minutes. Finally, sample 24D shows the buffer layer of $Al_2O_3$ after annealing at 100°C for 10 minutes.

### 4.3 – I-V characteristics and efficiency of the regular perovskite structure

The hybrid solar cell with the blade coating technique was the best solar cell. Solar cells kept under nitrogen at room temperature of 22°C, and the dark atmosphere showed the lowest degradation and the best stability. It showed stability for 30 hours. Table 2 represents the initial efficiency of the different fabricated perovskite solar cells.

*Table 2: Initial efficiency of the different fabricated perovskite solar cell*

| Layer Manufacturing | Perovskite Used | Initial Efficiency Range |
|---|---|---|
| Spin Coated | Regular | 3.48 - 3.56 |
| Spin Coated | Hybrid | 3.48 - 3.56 |
| Blade Coated | Regular | 3.54 - 3.63 |
| Blade Coated | Hybrid | 3.56 - 3.74 |

Figure 25, and 26 represents the I-V characteristic curve of the hybrid perovskite solar cell and how it degrades over time under a controlled environment. The solar cells are stored in the dark. Figure 26 represents the I-V characteristic curve of a blade coated perovskite solar cell stored under dark in controlled humidity of 30% to 38% RH. Similarly, Figure 26 represents the I-V characteristic curve of a spin coated perovskite solar cell stored under the exact same conditions.

From Figures 25, and 26, it can be seen the degradation of the solar cells under controlled humidity with an interval of 10 hours. I-V characteristic curve of solar cells under other environments can be seen in Appendix B.

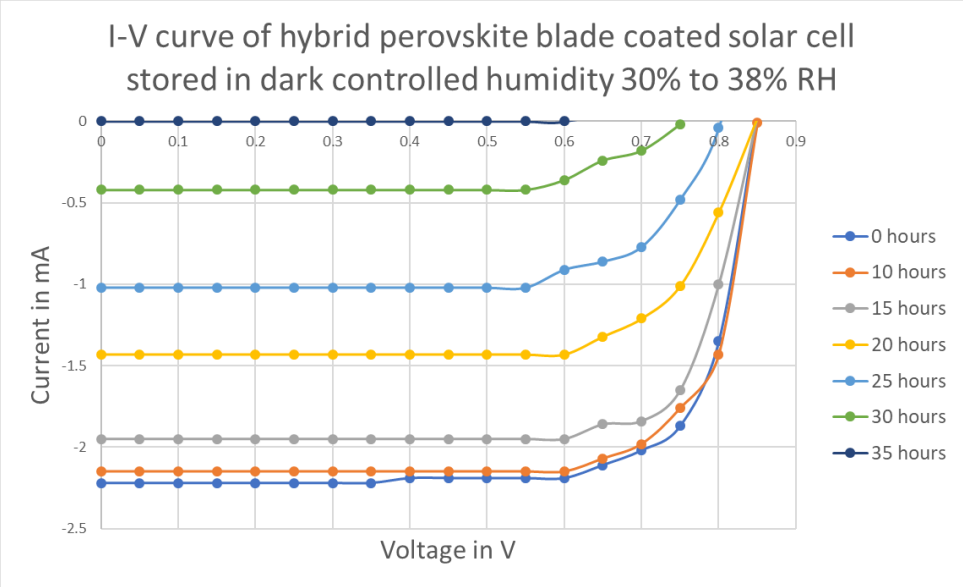


*Figure 25: I-V curve of hybrid blade coated perovskite solar cell stored in dark controlled humidity 30% to 38% RH*

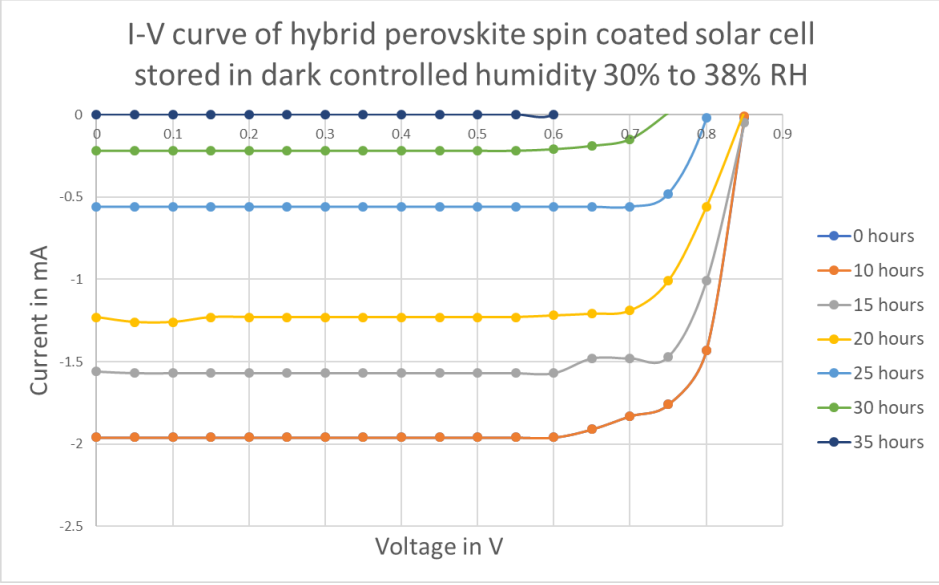


*Figure 26: I-V curve of hybrid spin coated perovskite solar cell stored in dark controlled humidity 30% to 38% RH*

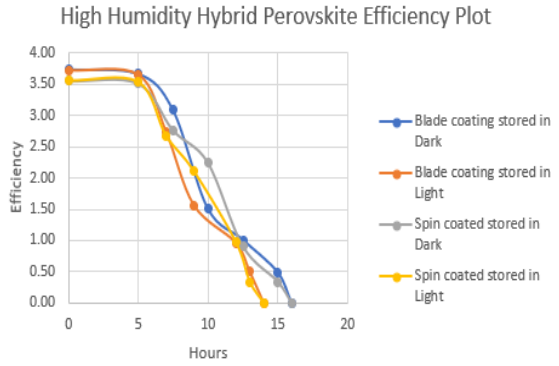


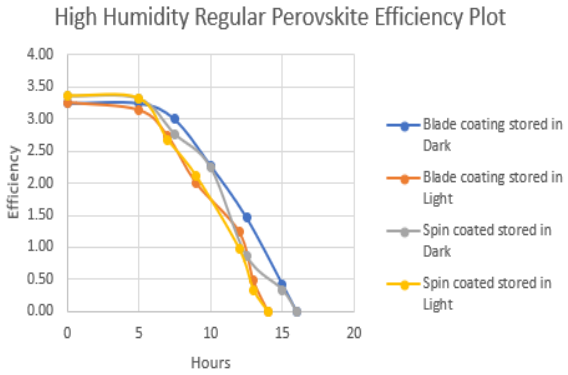


*Figure 27: Efficiency plot of hybrid and regular perovskite under high humidity of >50% RH*

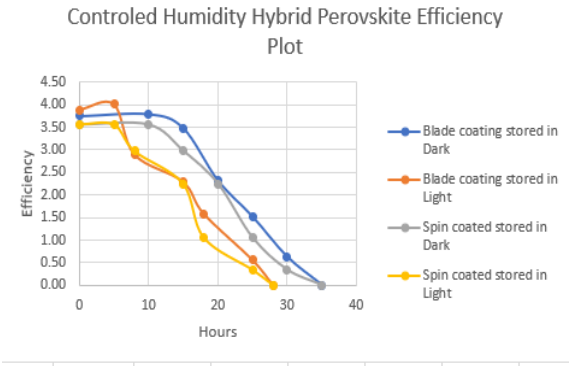


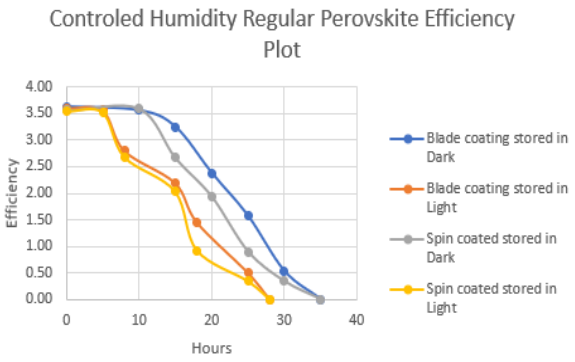


*Figure 28: Efficiency plot of hybrid and regular perovskite under controlled humidity of 30% to 38% RH*

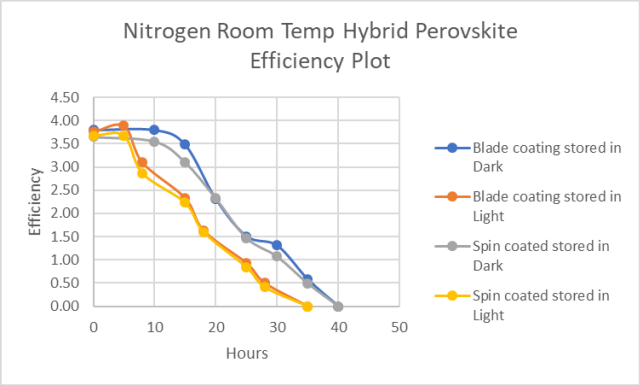


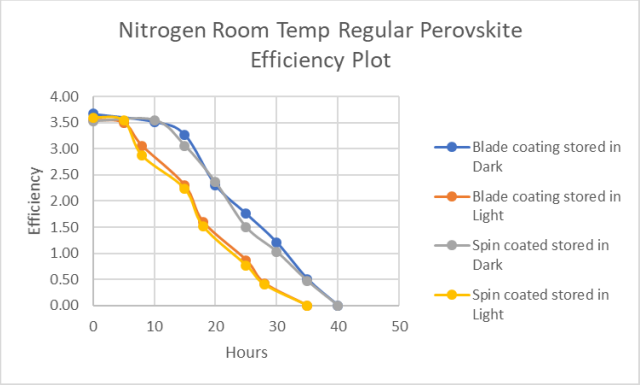


*Figure 29: Efficiency plot of hybrid and regular perovskite under nitrogen at room temperature of 22°C*

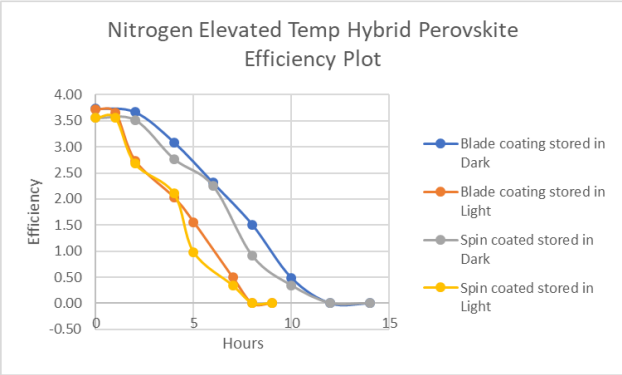


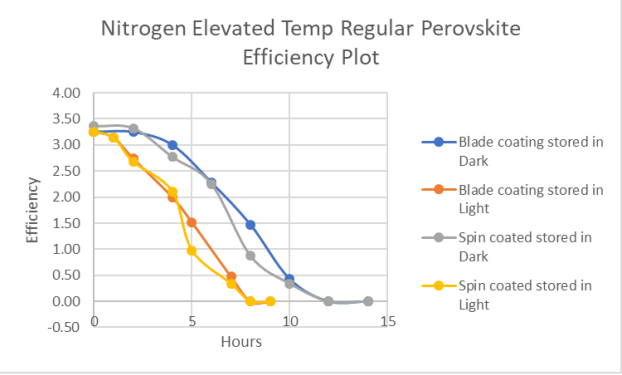


*Figure 30: Efficiency plot of hybrid and regular perovskite under nitrogen at an elevated temperature of 80°C*

The above Figures 27 to 30 represent the degradation of efficiency. From the above Figures 27 to 30, solar cells fabricated with blade coating technology were more efficient than the solar cells fabricated with spin coating technology. The solar cells stored under light was much prone to get degraded than that stored under dark conditions. Figure 27 represents solar cells fabricated by spin coating and blade coating and stored under high humidity conditions of >50% RH. The solar cells made from regular perovskite solution (spin coated, and blade coated) and

stored under light had degraded completely from 3.5% at 0 hours to 0% at 14 hours. The solar cells made from hybrid perovskite had a higher efficiency of 3.67% at 0 hours. The degradation however remained like that of regular perovskite to only 14 hours. Similarly, the solar cells made from regular perovskite solution (spin coated, and blade coated) and stored under dark had degraded completely from 3.5% at 0 hours to 0% at 16 hours, while the hybrid solar cell had a higher efficiency of 3.67%, but the degradation remained similar to that of 16 hours. The efficiency plot of Figure 27 is obtained from Figures 51 to 58 in Appendix B.

Figure 28 represents the different fabricated solar cells stored in a controlled humidity environment of 30% to 38% RH. The solar cells made from regular perovskite solution (spin coated, and blade coated) and stored under light had degraded completely from 3.5% at 0 hour to 0% at 28 hours. The solar cells made from hybrid perovskite had a higher efficiency of 3.67% at 0 hour. The degradation however remained like that of regular perovskite to only 28 hours. Similarly, the solar cells made from regular perovskite solution (spin coated, and blade coated) and stored under dark had degraded completely from 3.5% at 0 hour to 0% at 35 hours, while the hybrid solar cell had a higher efficiency of 3.67%, but the degradation remained similar to that of 35 hours. The efficiency plot of Figure 28 is obtained from Figures 37 to 42 in Appendix B.

Figure 29 represents the different fabricated solar cells stored in a nitrogen environment at room temperature of 22°C. The solar cells made from regular perovskite solution (spin coated, and blade coated) and stored under light had degraded completely from 3.5% at 0 hour to 0% at 35 hours. The solar cells made from hybrid perovskite had a higher efficiency of 3.67% at 0 hour. The degradation however remained like that of regular perovskite to only 35 hours.

Similarly, the solar cells made from regular perovskite solution (spin coated, and blade coated) and stored under dark had degraded completely from 3.5% at 0 hour to 0% at 40 hours, while the hybrid solar cell had a higher efficiency of 3.67%, but the degradation remained similar to that of 40 hours. The efficiency plot of Figure 29 is obtained from Figures 43 to 50 in Appendix B.

Figure 30 represents the different fabricated solar cells stored in a nitrogen environment at an elevated temperature of 80°C. The solar cells made from regular perovskite solution (spin coated, and blade coated) and stored under light had degraded completely from 3.5% at 0 hour to 0% at 8 hours. The solar cells made from hybrid perovskite had a higher efficiency of 3.67% at 0 hour. The degradation however remained like that of regular perovskite to only 8 hours. Similarly, the solar cells made from regular perovskite solution (spin coated, and blade coated) and stored under dark had degraded completely from 3.5% at 0 hour to 0% at 11 hours, while the hybrid solar cell had a higher efficiency of 3.67%, but the degradation remained similar to that of 11 hours. The efficiency plot of Figure 30 is obtained from Figures 59 to 66 in Appendix B.

The worst outcome was the solar cells that were stored under high humidity and elevated temperatures for a prolonged period. This was due to the fact of sublimation of the methylammonium particles from the perovskite layer, turning the perovskite solar cell from dark brown to yellow. This indicated the formation of lead iodide in the solar cell. The best possible environment to store the solar cell was the nitrogen atmosphere at a room temperature of 22°C.

### 4.4 – I-V characteristics and efficiency plot of the improved perovskite structure

The next stage was to improve the solar cell. This was done by introducing a buffer layer of aluminum dioxide ($Al_2O_3$) in between the layers of perovskite and spiro-OMeTAD. This enabled the cells to improve by 10 hours, and hence the solar cell was stable for 45 hours under a controlled humidity at dark storage. This is shown in Figure 30.

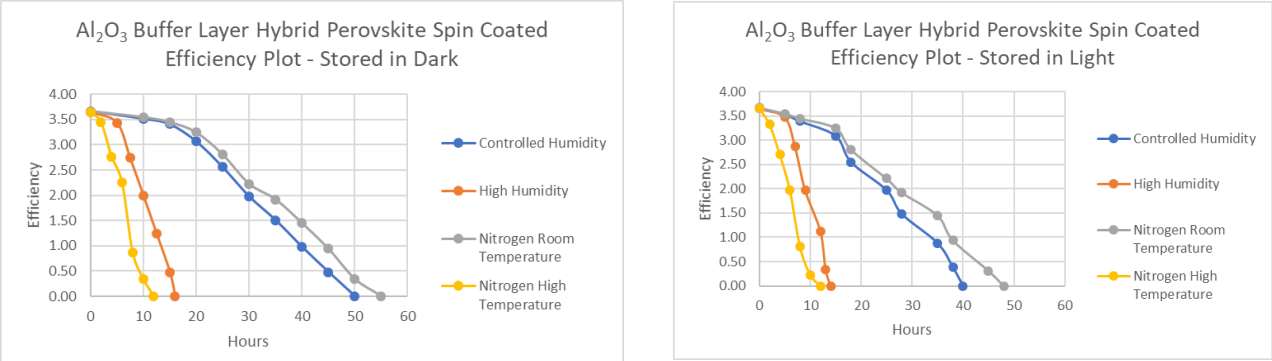


*Figure 31: Efficiency plot of the solar cell with aluminum oxide as the buffer layer under different environmental conditions*

From Figure 31, it can be concluded that adding $Al_2O_3$ increases the stability of the perovskite solar cell by stopping the back migration of the metal to the perovskite layer. However, adding the layer $Al_2O_3$ does not completely block moisture, and hence the degradation is caused mainly due to moisture, and the stability was only for 13 hours. The efficiency plot of Figure 31 is obtained from Figures 67 to 74 in Appendix B. Figure 32 displays the degradation of the solar cell with $Al_2O_3$ in a controlled humidity environment in the dark.

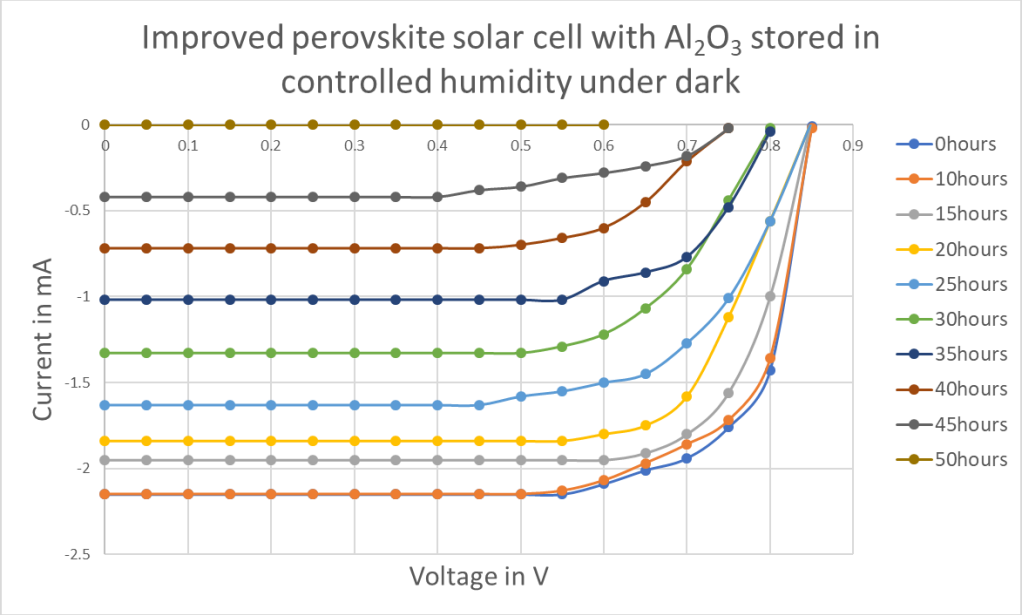


*Figure 32: I-V characteristic curve of hybrid perovskite solar cell with $Al_2O_3$ stored in dark controlled humidity 30% to 38% RH*

The final step was to introduce a layer of epoxy. Epoxy decreased the contact of moisture to the perovskite layer and hence increasing the stability to 85 hours under controlled humidity. All the solar cells were observed in their respective environments, and out of the four environments, a nitrogen room temperature of 22°C showed the best results, as shown in Figure 32. This indicated that the solar cells showed the best stability when the environment was nitrogen at room temperature of 22°C and was stored in the dark until testing. The stability lasted from 3.67% at 0 hour to 0% at 100 hours.

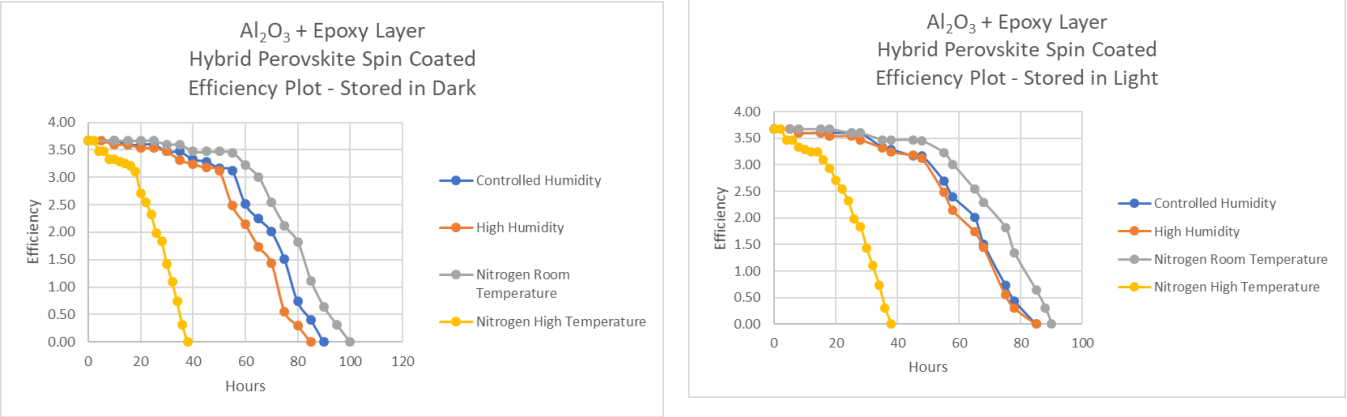


*Figure 33: Efficiency plot of the solar cell with aluminum oxide and epoxy under different environmental conditions*

From Figure 33, it can be concluded that adding epoxy increased stability when it came to moisture. The light and dark conditions are nearly equal since epoxy blocks the UV rays. The long-term stability of the solar cell towards high temperature is 36 hours. This explains that the epoxy did increase the stability of the solar cell compared to other fabricated solar cells. The efficiency plot of Figure 33 is obtained from Figures 75 to 82 in Appendix B.

Figure 34 displays the degradation of the solar cell with $Al_2O_3$ and epoxy in a controlled humidity environment in the dark. The I-V characteristic curve of solar cells under other environments can be seen in Appendix B.

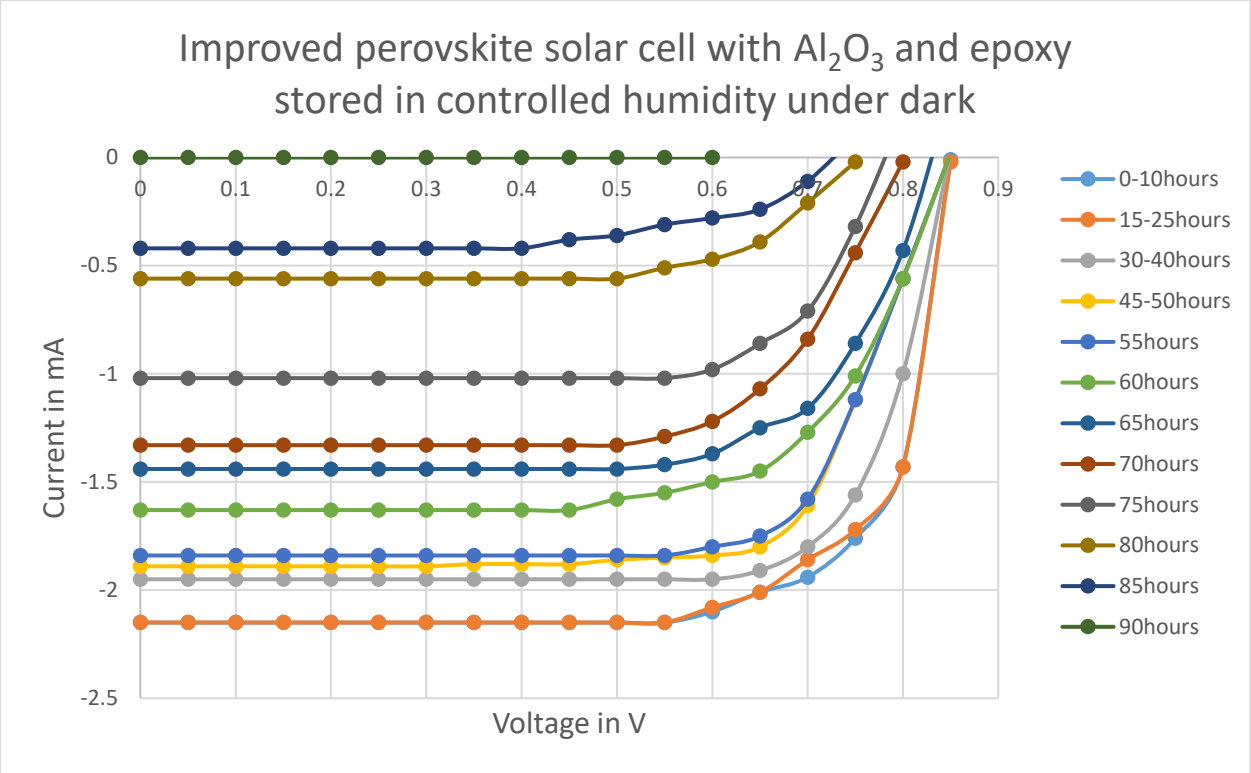


*Figure 34: I-V characteristic curve of hybrid perovskite solar cell with $Al_2O_3$ and epoxy stored in dark controlled humidity 30% to 38% RH - Degradation Plot*

## 5 – Discussion

The efficiency of the solar cells made with a hybrid perovskite solution was higher than that made with regular perovskite solution. Out of the four environments chosen, the nitrogen with a room temperature of 22°C showed the best stability. Perovskite solar cells must be fabricated very carefully and under proper nitrogen environment and must be annealed under proper temperature. For the first layer of titanium dioxide layer, the annealing must be done in such a way that there are no remains of acetic acid on the layer that can cause an adverse effect on the perovskite layer. The annealing of the titanium dioxide goes to 400°C for 30 minutes and then cooling the layer for 3 hours till room temperature of 22°C. This will have a color change of the layer initially from white to the transition stage of dark brown to the final stage of white. This means that titanium dioxide is ready for the next layer.

Annealing of the perovskite must be done at 100°C for 10 minutes. Annealing for less than 100°C would lead to the formation of smaller crystals, which would, in turn, have lower efficiency and faster degradation due to the trapped moisture in the cracks of the perovskite layer. Annealing for temperature more than 100°C for more than 10 minutes would lead to sublimation of the methylammonium particles from the perovskite layer and, in turn, have sediment of lead iodide remaining at the perovskite layer. This would mark a change in the layer from the dark brown color of the annealed perovskite to the bright yellow color of the lead iodide particle. The dark brown color of the layer is what was expected, which in turn means that the layer is ready for the hole transport material.

The hole transport material is spiro-OMeTAD in chlorobenzene. The reason chlorobenzene is added is that it acts as a solvent and does not disturb the annealed perovskite layer. Spiro-

OMeTAD layer is annealed at 100°C for 10 minutes. If the annealed temperature or the time of annealing is more, then the spiro-OMeTAD may sublimate, leading to the entire hole transport layer to get degraded. The buffer layer of $Al_2O_3$ is annealed at 100°C for 10 minutes. This leads to the chlorobenzene to evaporate, leaving behind the $Al_2O_3$ particles. This adds additional stability to the solar cell. Finally, the counter electrode of conductive silver paste was added with a brush and gently tapping onto the top layer instead of brushing. Brushing disturbs the spiro-OMeTAD layer, and hence there is no hole transport material to complete the circuit of a proper solar cell.

Perovskite solar cells are highly vulnerable to moisture, high temperature, and light. Hence it is important to enclose it in such a way that it becomes stable to these factors. Adding epoxy resin decreases the vulnerability of moisture into the perovskite layer, and an added stability towards light and $Al_2O_3$ in between the layer of spiro-OMeTAD and perovskite leads to the counter electrode in our case silver to remain as silver and not tarnish into silver iodide.

The final solar cell developed is FTO/c-$TiO_2$/m-$TiO_2$/$MAPBI_xCl_{3-x}$/$Al_2O_3$/Spiro-OMeTAD/Ag/Epoxy. This solar cell was fabricated under a nitrogen environment. A similar type of solar cell was fabricated by Dong et al. (2015) with Ag as the counter electrode and Guarnera et al. (2015) with Au as the counter electrode. All these solar cells were kept under a high humid environment and were analyzed. The compared results are displayed in Table 3.

*Table 3: Solar cells specification comparison under high humidity*

| Solar Cell | Sample Solar Cell | Dong et al. | Guarnera et al. |
|---|---|---|---|
| **Layers** | **Spiro + $Al_2O_3$ + Ag** | **Spiro + $Al_2O_3$ + Ag** | **Spiro + $Al_2O_3$ + Au** |
| **Fabrication Method** | One step spin coated | One step spin coated | One step spin coated |
| **Initial Efficiency 0hr** | 3.74 | 4.00 | 4.60 |
| **Fill Factor** | 78% | 76% | 78% |
| **Environment Tested** | High Humidity >50% RH | High Humidity 50% RH | High Humidity 60% RH |
| **Life Span** | 15hrs | 16hrs | 18hrs |
| **Degradation Factor** | Moisture | Moisture | Moisture |

All of the solar cells were fabricated by using a one-step spin-coated method. This was where the perovskite solution was fabricated earlier by using the precursor solutions and then was spin-coated at the time of fabrication and annealing. From Table 3, it can be concluded that the gold electrode has better conductivity and hence higher efficiency.

Smith et al. (2015) fabricated solar cells similar to Guarnera et al. with epoxy resin and had a stability of 250 hours with no degradation. The solar cell had an efficiency of 4.73% and was stored under room temperature of 22°C with a controlled humidity of 30%RH.

*Table 4: Solar cell comparison with epoxy under controlled humidity*

| Solar Cell | Sample Solar Cell with Epoxy | Smith et al. |
|---|---|---|
| **Layers** | **Spiro + $Al_2O_3$ + Ag + Epoxy** | **Spiro + $Al_2O_3$ + Au + Epoxy** |
| **Perovskite Material** | $MAPbI_2Cl$ | $MAPbBr_3$ |
| **Fabrication Method** | One step spin coated | One step spin coated |
| **Initial Efficiency 0hr** | 3.74 | 4.73 |
| **Fill Factor** | 78% | 79% |
| **Environment Tested** | Controlled 30%-38% RH | Controlled 30% RH |
| **Life Span** | 90hrs | 250hrs |
| **Degradation Factor** | Oxidation of Ag | Br more stable than I and Cl |

From Table 4, it can be seen that the stability of the perovskite also depends on the size of halogen ions. The stability of the solar cell fabricated by Smith et al. had a life span of 250

hours, whereas our sample solar cell had only 90 hours. This occurred due to the fact that there were some spaces left on the top layer where moisture penetrated into the solar cell and caused the degradation to both the perovskite layer and oxidizing the silver electrode. This caused the tarnish of the silver to silver iodide and silver oxide.

## 6 – Conclusion

Perovskite material has tremendous potential in the field of photovoltaics. However, it rapidly degrades mostly in the presence of moisture, temperature and UV light. Our study focused on the efficiency degradation of the solar cells when stored in four different environments. The environments included high humidity (>50% RH), controlled humidity (30% to 38% RH), nitrogen at room temperature of 22°C, and nitrogen at elevated temperature of 80°C. After analyzing the fabricated solar cells stored under these environments, it was found that the solar cells stored under a nitrogen atmosphere with a room temperature of 22°C showed the best stability. It was reported that storing perovskite solar cells at elevated temperatures of more than 100°C degraded the perovskite material [40]. From our study, it was seen that storing perovskite solar cells at a temperature of 80°C also degraded the perovskite. Even though, nitrogen had an ideal environment to store the perovskite solar cell, an elevated temperature of 80°C degraded the perovskite layer. This led to the fact that the thermal degradation of the perovskite is independent of other degradation factors like moisture and UV light. The basic solar cells stored under high humidity showed maximum degradation. It was concluded that the higher the humidity the faster is the degradation.

The solar cells fabricated without adding the buffer layer of $Al_2O_3$ and epoxy showed stability of 40 hours where the efficiency ranged from 3.5% at 0 hour to 0% at 40 hours when stored in a nitrogen atmosphere at room temperature of 22°C under dark. Adding the buffer layer and the epoxy increased the stability to 100 hours when stored in the dark and 85 hours when stored in light under the same environment.

Fabricating stable perovskite solar cells is a difficult task, and the entire solar cell should be considered as a single system instead of focusing on individual layers. The solar cells should be fabricated in a nitrogen environment. For increased stability, suitable encapsulation and UV filters must be used to decrease the degradation from moisture and UV light. Storing the solar cells under ideal environments also lead to an increased stability. This allows the solar cells to approach ideal lifetimes under controlled environments.

## 7 – Future Works

Since perovskite absorber is highly sensitive to moisture, testing under ambient conditions becomes cumbersome. Testing of the perovskite solar cells under various environmental conditions would help to understand the mechanisms that cause degradation and help to improve the stability of the devices. To further understand the perovskite solar cell stability, studies can be made as follows;

- To develop a hybrid perovskite absorber, which is hydrophobic and thermally stable,
- To replace the organic compounds of the perovskite with an inorganic compound while maintaining the light absorptive qualities,
- To understand the degradation of the solar cells under different intensities of UV light for a prolonged period of time in different environments.

**Appendix A – Glove box manual**

1. **Creating Vacuum inside the glove box**

Make sure all the valves are closed properly (perpendicular to the line of connection, and the $N_2$ gas tank is closed). Then follow the steps below,

i. Turn on the vacuum pump.

ii. Open valve #9 and #5, making sure that valve #6 and #3 is closed.

iii. Open the valve #7, making sure that valve #8 is closed, to let the vacuum inside the secondary chamber. You can watch as the pressure decreases below 0.

iv. Gently open valve #8 to let vacuum inside the primary chamber and monitor the vacuum inside through the reading from the secondary chamber, as opening the valve #8 makes the air pressure equal.

v. Once the required air pressure is achieved, close the valve #8, #7, and #3. The vacuum is used in running a spin coater. It is explained below.

2. **Turning on the spin coater**

Three things are required to make sure the spin coater is running and working,

- A continuous flow of $N_2$.
- A continuous flow of Vacuum and,
- Power supply.

For a continuous flow of $N_2$ into the spin coater follow the steps below,

i. Open the $N_2$ valve labeled #1.

ii. Gently open Valve #2 in such a way that the pressure does not exceed 50psi in the pressure valve.

iii. Put valve #4 in parallel with the line connection for it to open.

iv. Gently turn the second small pressure valve and set it to 5psi. (The spin coater can only handle 5psi)

v. The connection of $N_2$ is established to the spin coater.

For a continuous Flow of Vacuum into the spin coater follow the steps below,

i. Make sure that the valve #5, #6 and #9 are closed. i.e., Perpendicular to the line of connection.

ii. Turn on the vacuum pump connection.

iii. Put valve #9 in parallel with the line connection (open it).

iv. The connection of a vacuum is established to the spin coater.

**3. Filling $N_2$ inside the secondary chamber in the glovebox (100% $N_2$)**

Before putting the $N_2$ inside the secondary chamber, make sure that the secondary chamber is in a vacuum. Follow steps from i to iii in part 1 of how to use, to keep inside chamber vacuumed. Close all the valves that needed to be opened for the vacuuming section.

**REMEMBER $N_2$ and vacuum should be kept separately. Use $N_2$ carefully. Carefully monitor valves #5 and #6 in this scenario.**

Make sure that valves #5, #3, #6, #7 and #8 are closed and follow the steps below,

i. Open valve #3 and #7 sequentially to let the $N_2$ flow inside the vacuumed small chamber.

ii. The secondary chamber is now ~100% in a vacuum.

### 4. HOW TO TURN OFF EVERYTHING

Close all the valves one at a time and then finally close the valve #1 at the $N_2$ gas tank. Plug out the vacuum pump to shut it down. Before leaving for the day, make sure all the valves are closed.

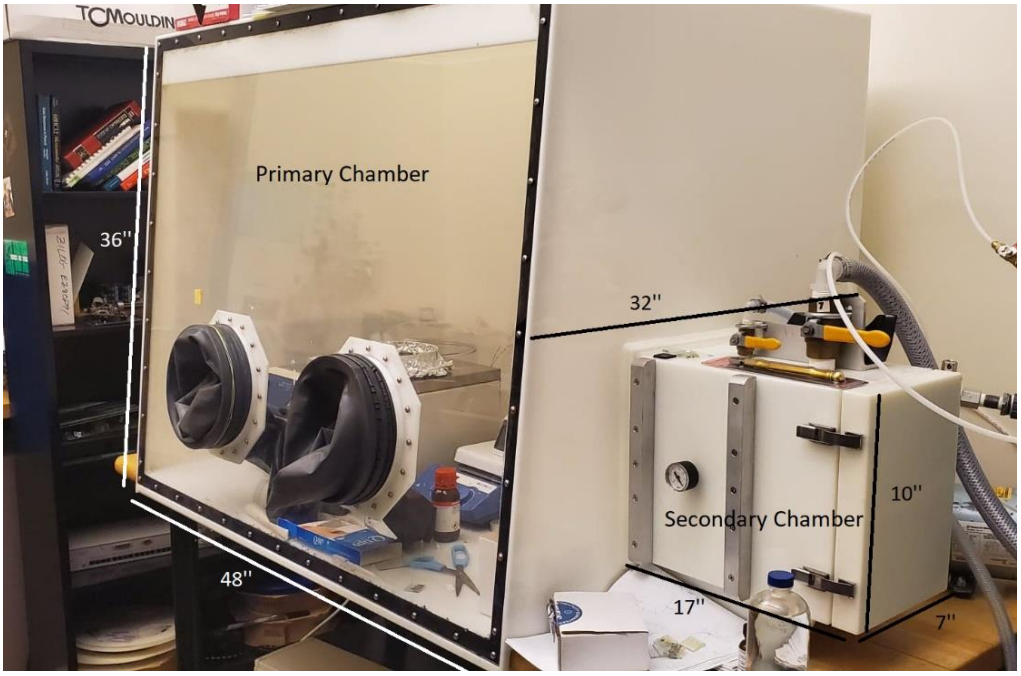


*Figure 35: Glove box with dimensions – User Manual*

*Figure 36: Connection to the Glove box – User Manual*

**Appendix B – I-V Characteristic Plots**

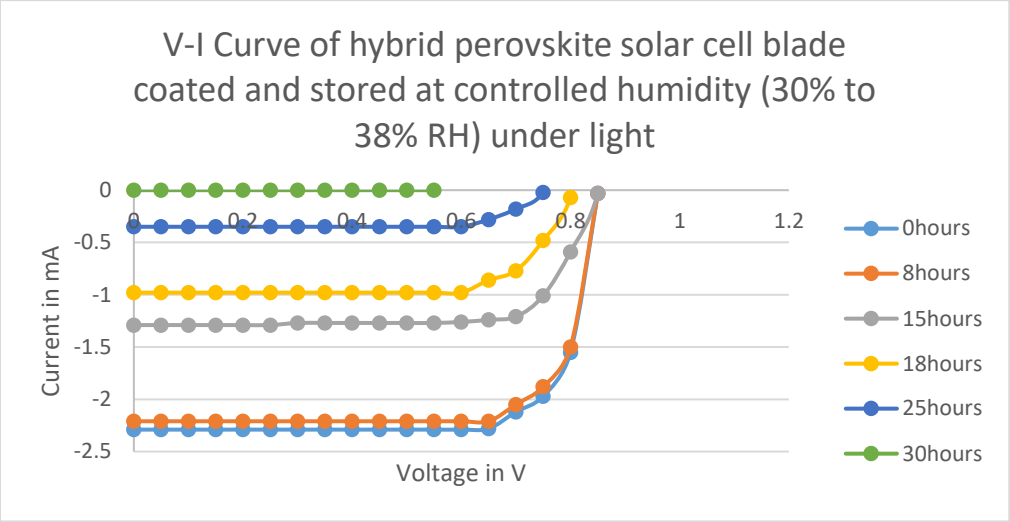


*Figure 37: I-V characteristic curve of hybrid perovskite solar cell blade coated and stored in sunlight under controlled humidity 30% to 38% RH - Degradation Plot*

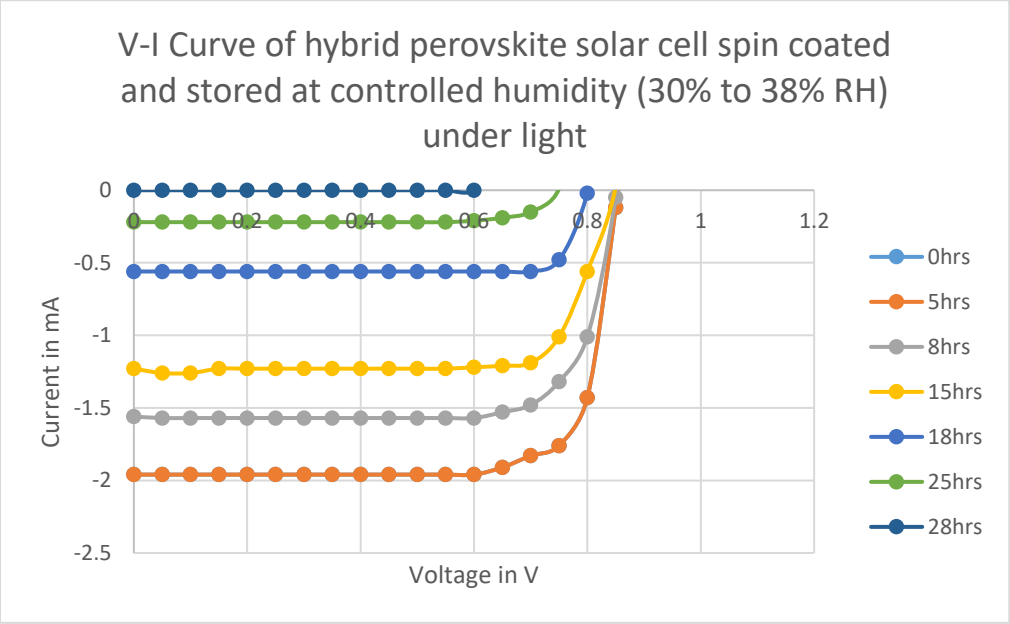


*Figure 38: I-V characteristic curve of hybrid perovskite solar cell spin coated and stored in sunlight under controlled humidity 30% to 38% RH - Degradation Plot*

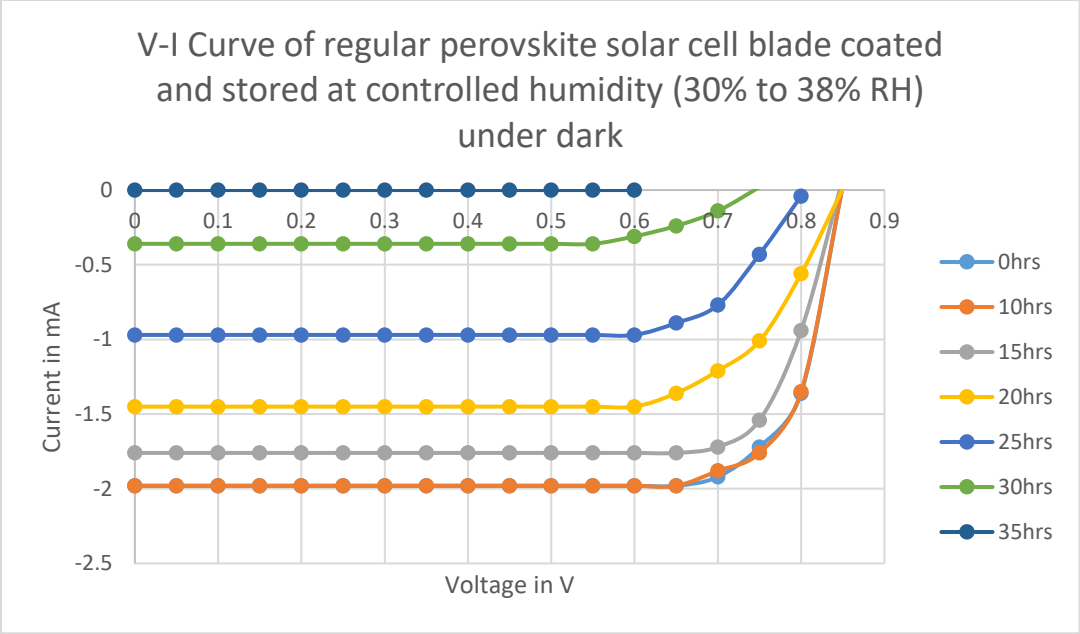


*Figure 39: I-V characteristic curve of regular perovskite solar cell blade coated and stored in dark under controlled humidity 30% to 38% RH - Degradation Plot*

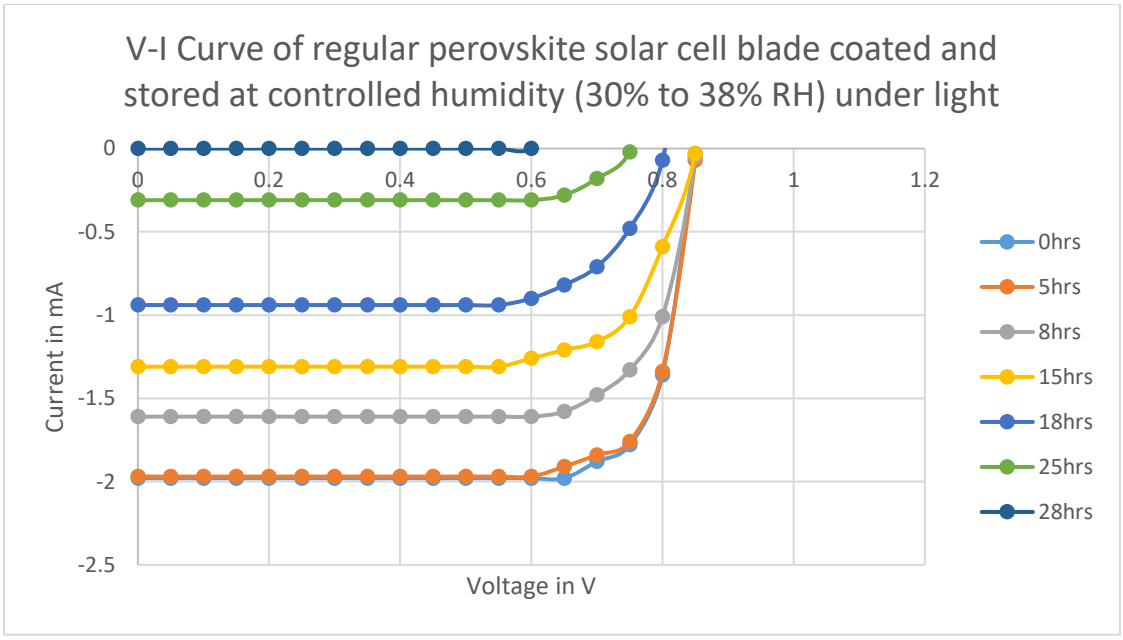


*Figure 40: I-V characteristic curve of regular perovskite solar cell blade coated and stored in light under controlled humidity 30% to 38% RH - Degradation Plot*

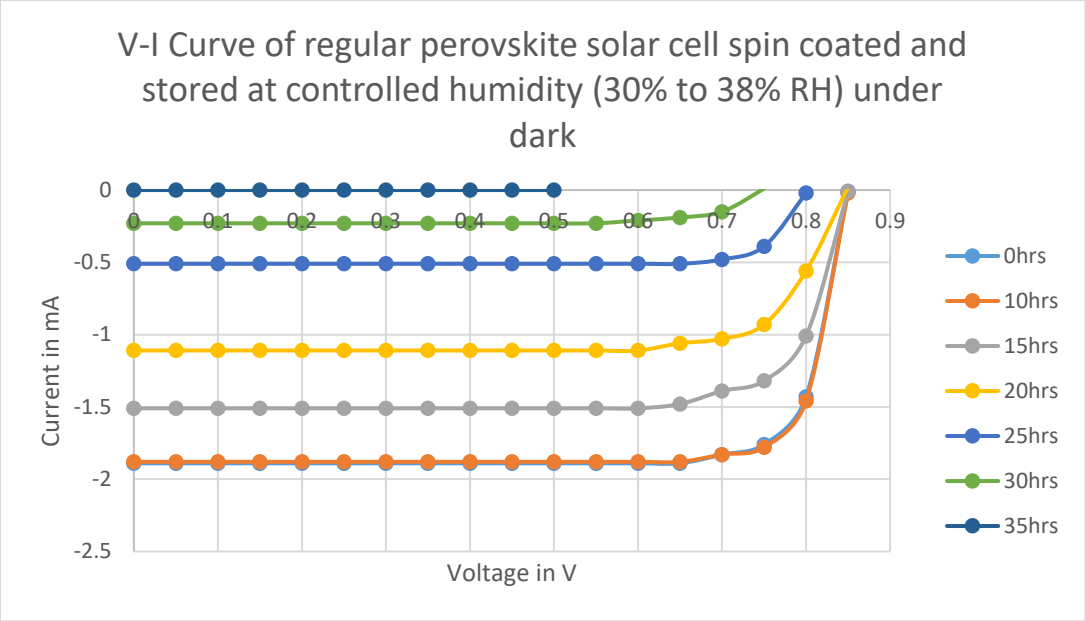


*Figure 41: I-V characteristic curve of regular perovskite solar cell spin coated and stored in dark under controlled humidity 30% to 38% RH - Degradation Plot*

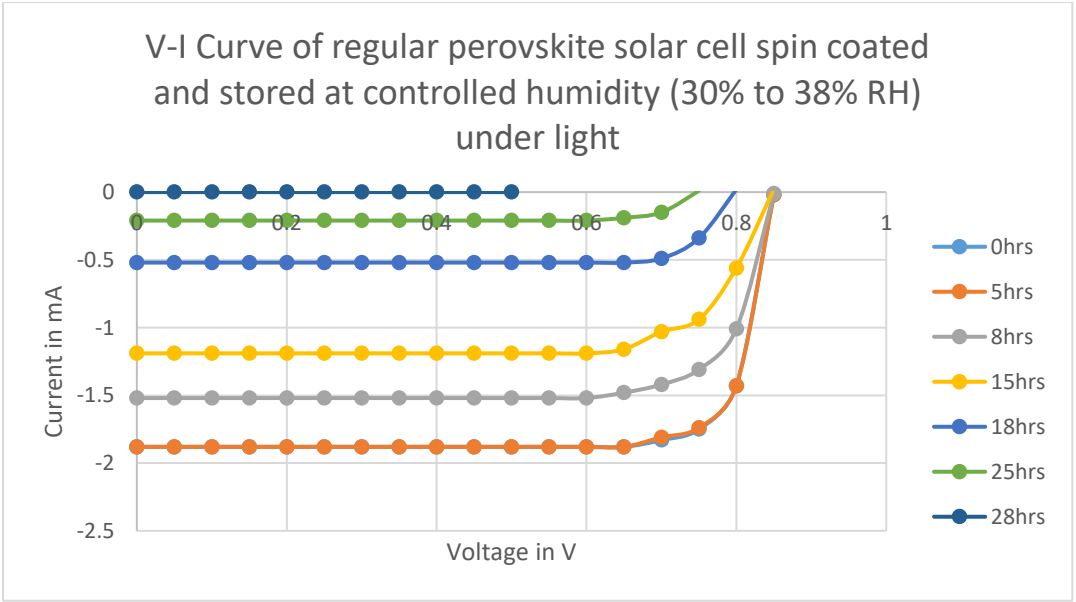


*Figure 42: I-V characteristic curve of regular perovskite solar cell spin coated and stored in light under controlled humidity 30% to 38% RH - Degradation Plot*

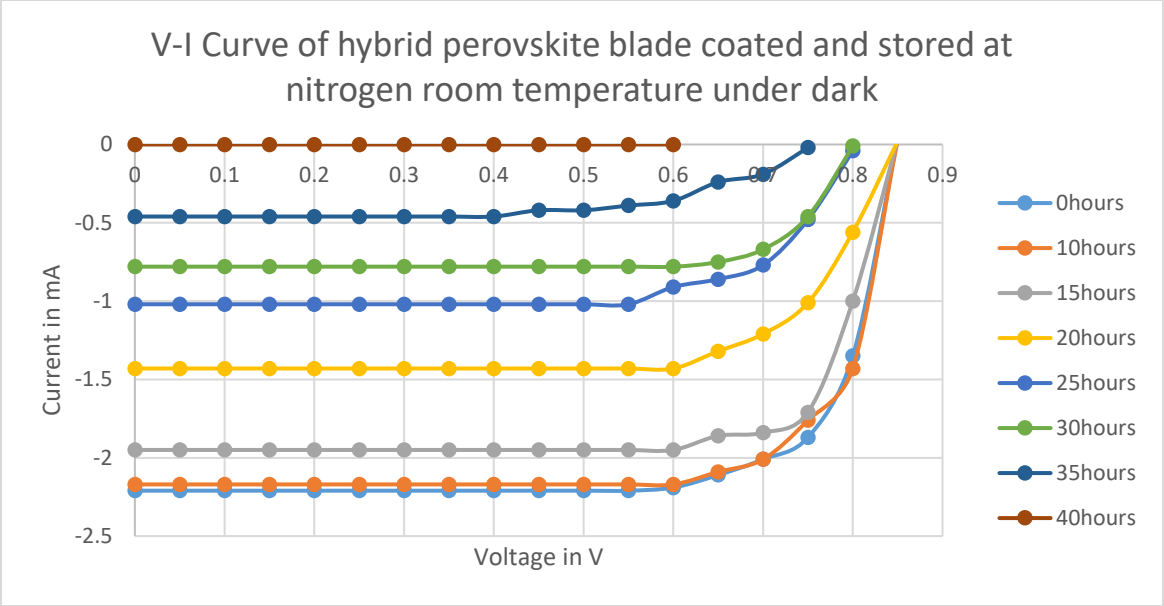


*Figure 43: I-V characteristic curve of hybrid perovskite solar cell blade coated and stored under dark in nitrogen at room temperature of 22°C - Degradation Plot*

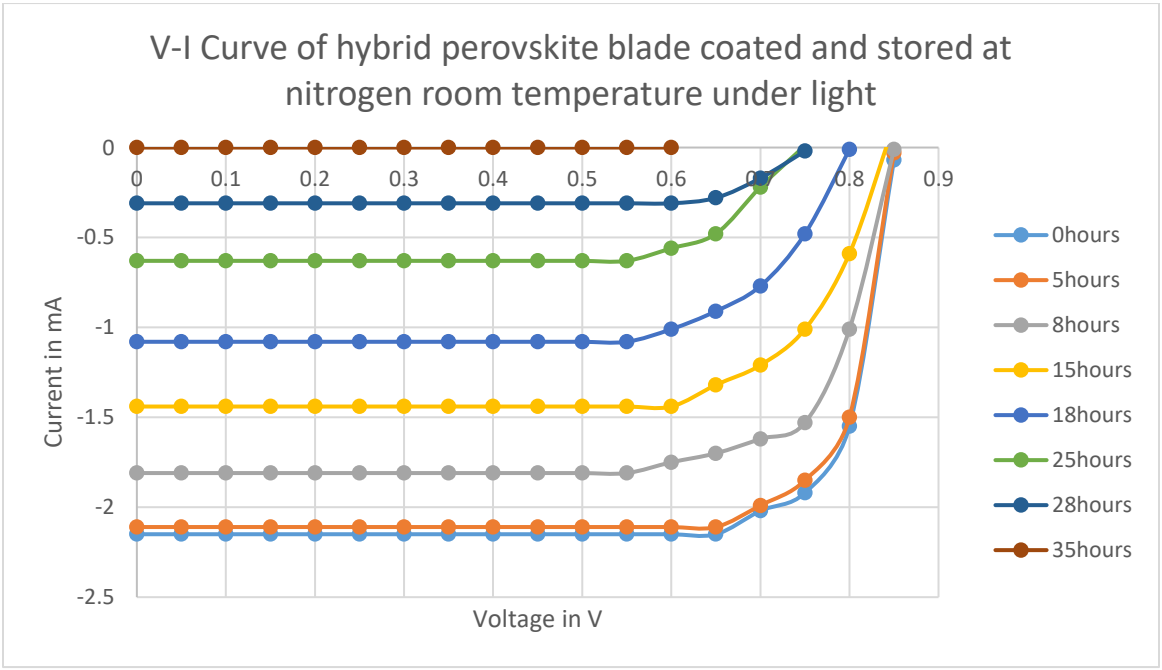


*Figure 44: I-V characteristic curve of hybrid perovskite solar cell blade coated and stored under light in nitrogen at room temperature of 22°C - Degradation Plot*

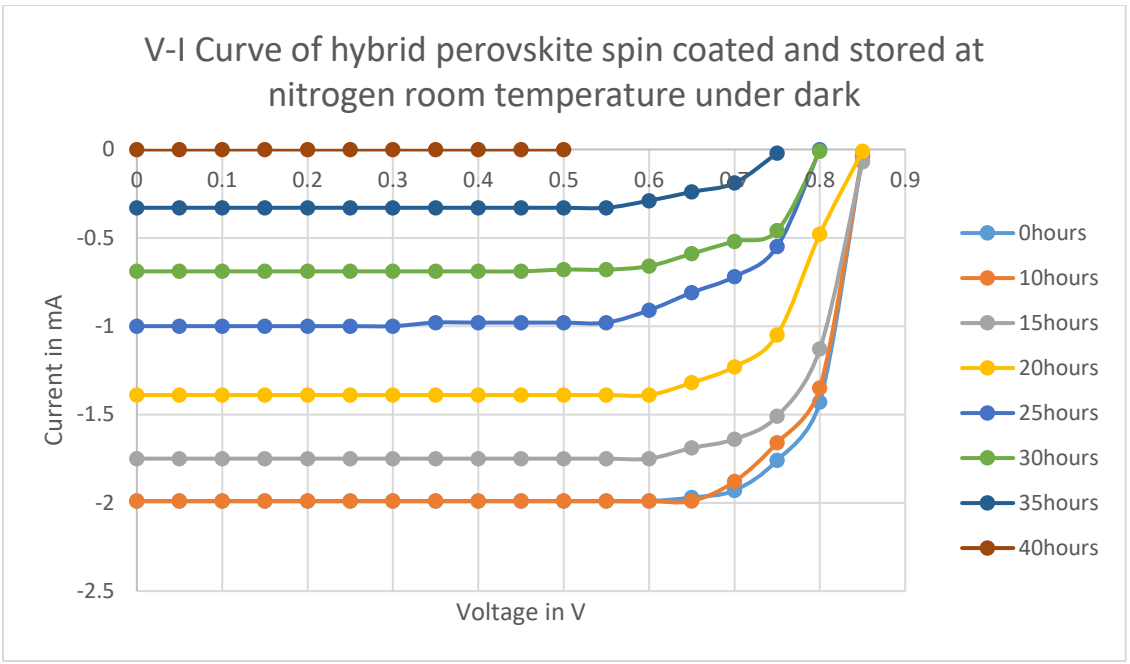


*Figure 45: I-V characteristic curve of hybrid perovskite solar cell spin coated and stored under dark in nitrogen at room temperature of 22°C - Degradation Plot*

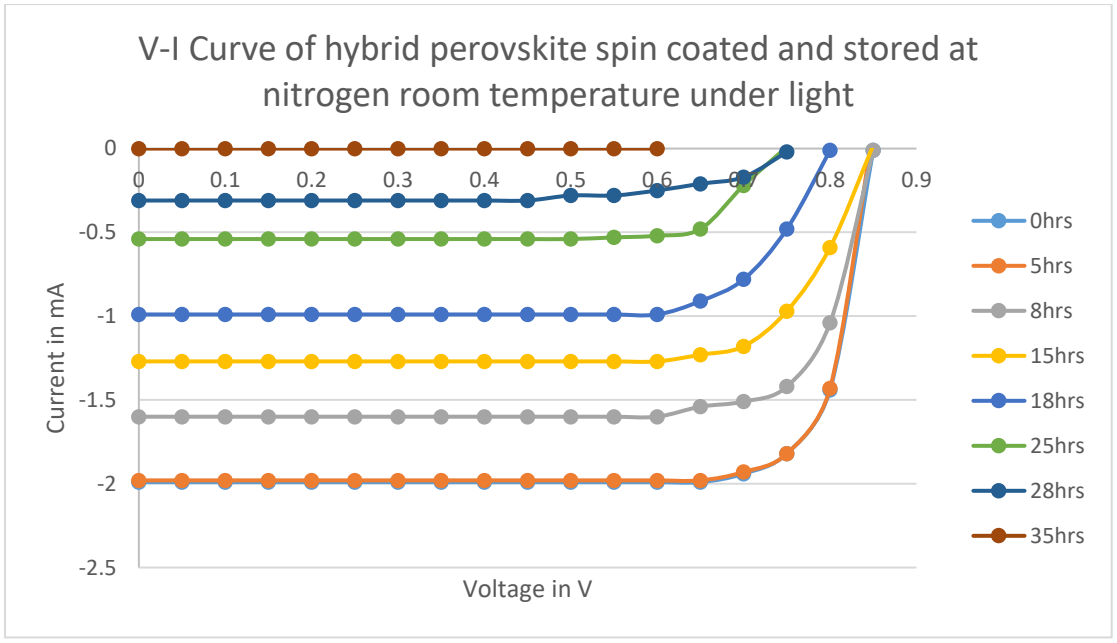


*Figure 46: I-V characteristic curve of hybrid perovskite solar cell spin coated and stored under light in nitrogen at room temperature of 22°C - Degradation Plot*

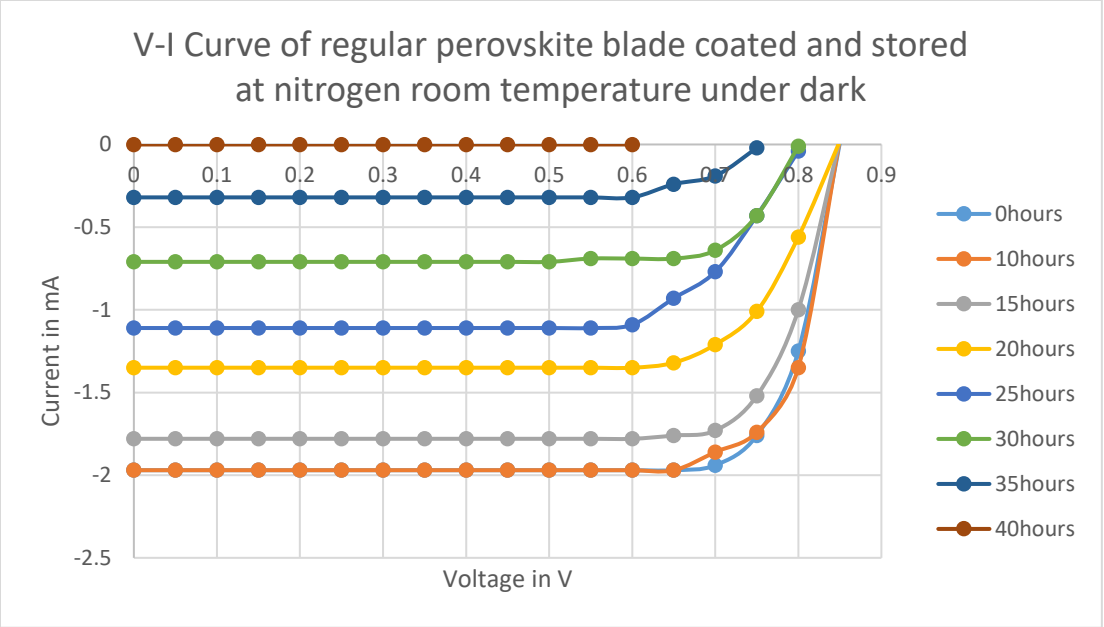


*Figure 47: I-V characteristic curve of hybrid perovskite solar cell blade coated and stored under dark in nitrogen at room temperature of 22°C - Degradation Plot*

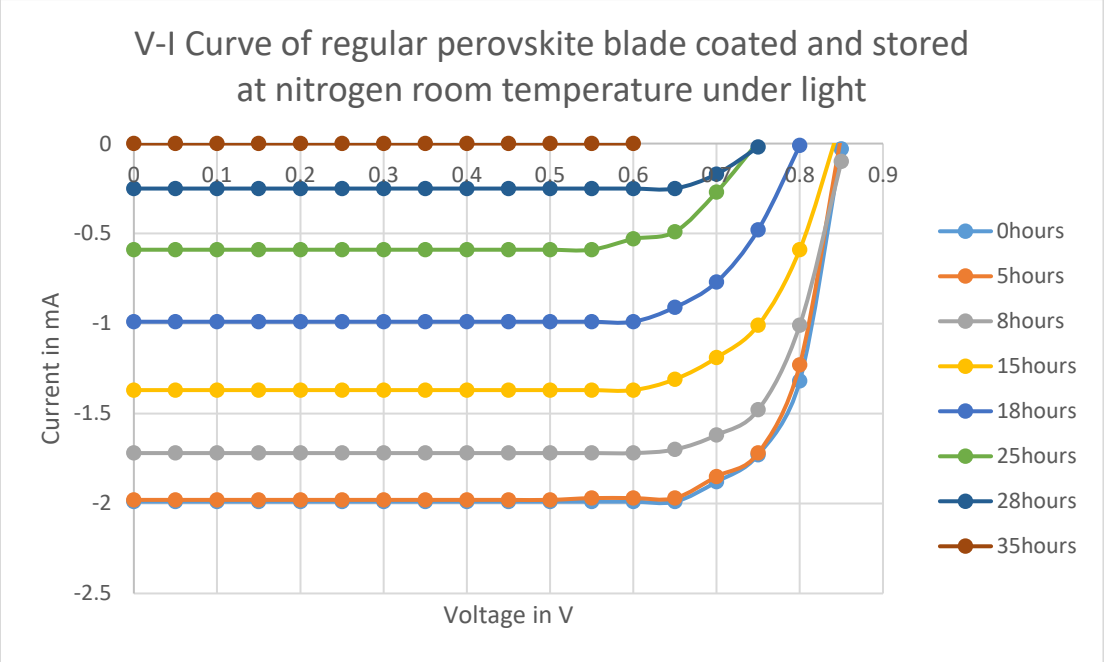


*Figure 48: I-V characteristic curve of hybrid perovskite solar cell blade coated and stored under light in nitrogen at room temperature of 22°C - Degradation Plot*

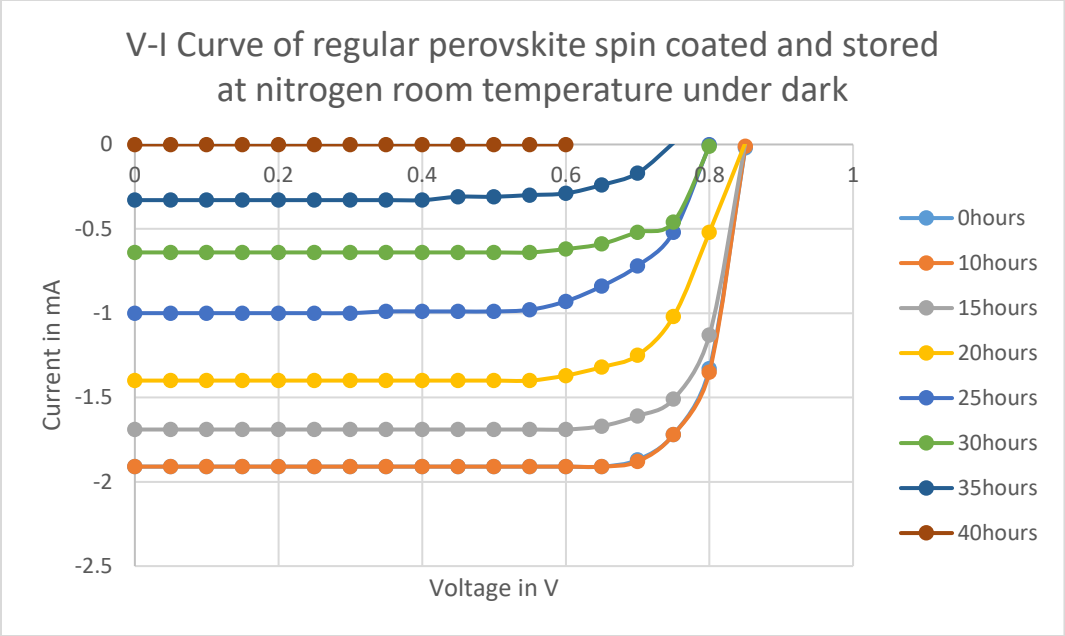


*Figure 49: I-V characteristic curve of hybrid perovskite solar cell spin coated and stored under dark in nitrogen at room temperature of 22°C - Degradation Plot*

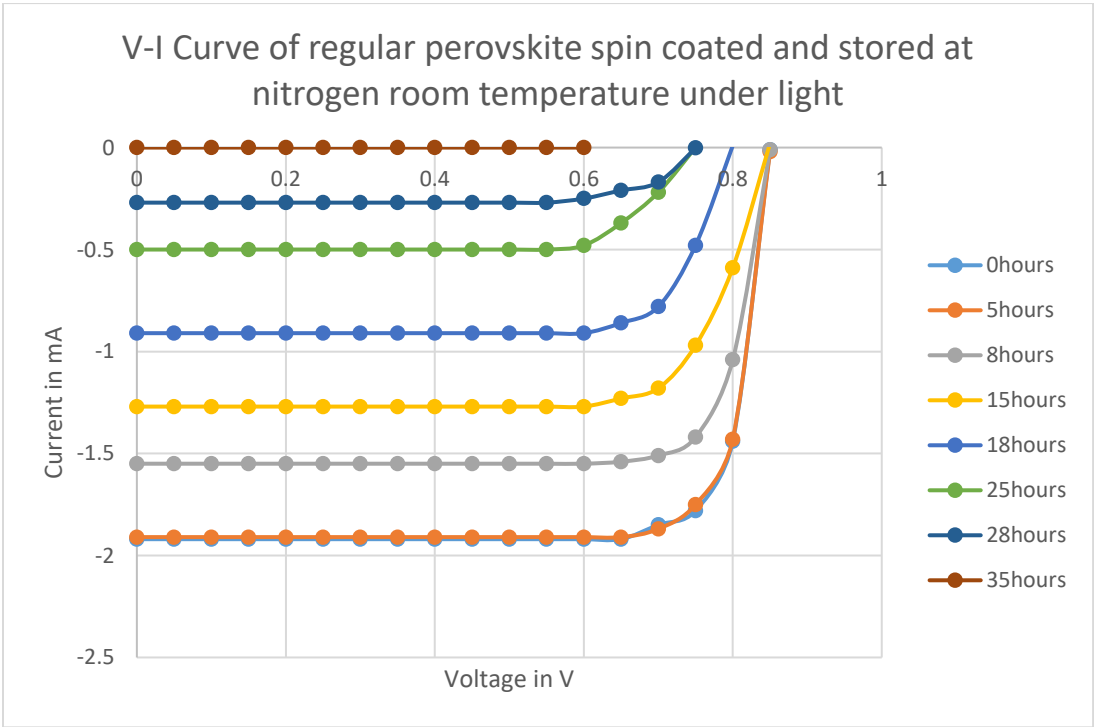


*Figure 50: I-V characteristic curve of hybrid perovskite solar cell spin coated and stored under light in nitrogen at room temperature of 22°C - Degradation Plot*

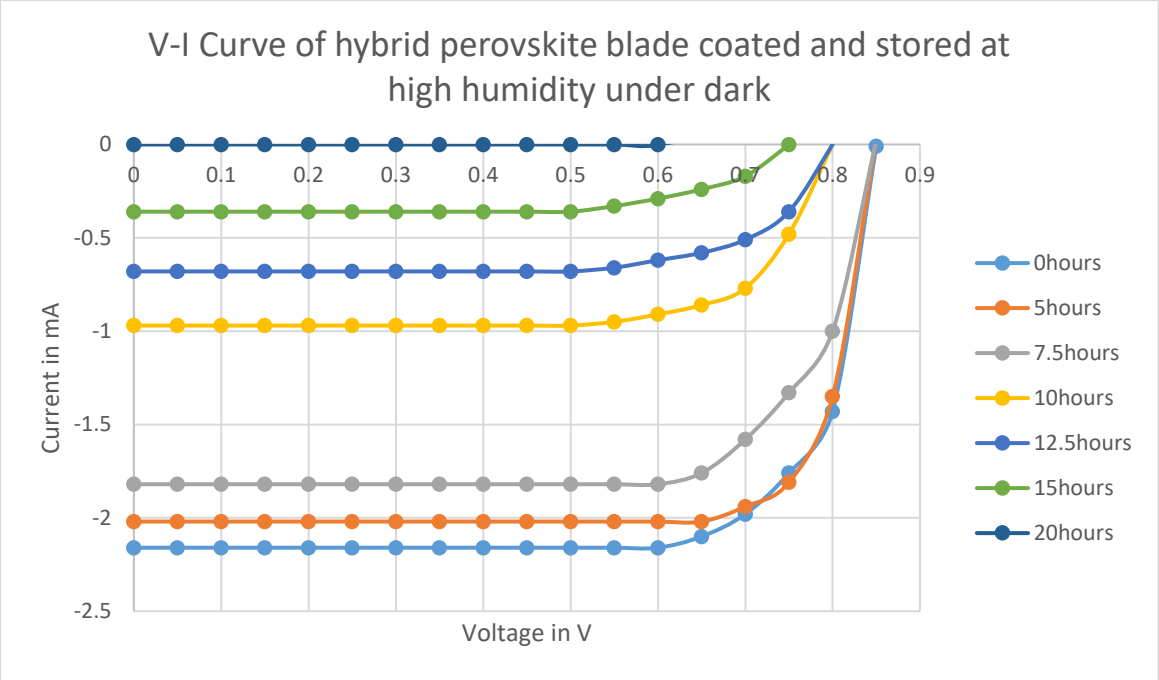


*Figure 51: I-V characteristic curve of hybrid perovskite solar cell blade coated and stored under dark in high humidity - Degradation Plot*

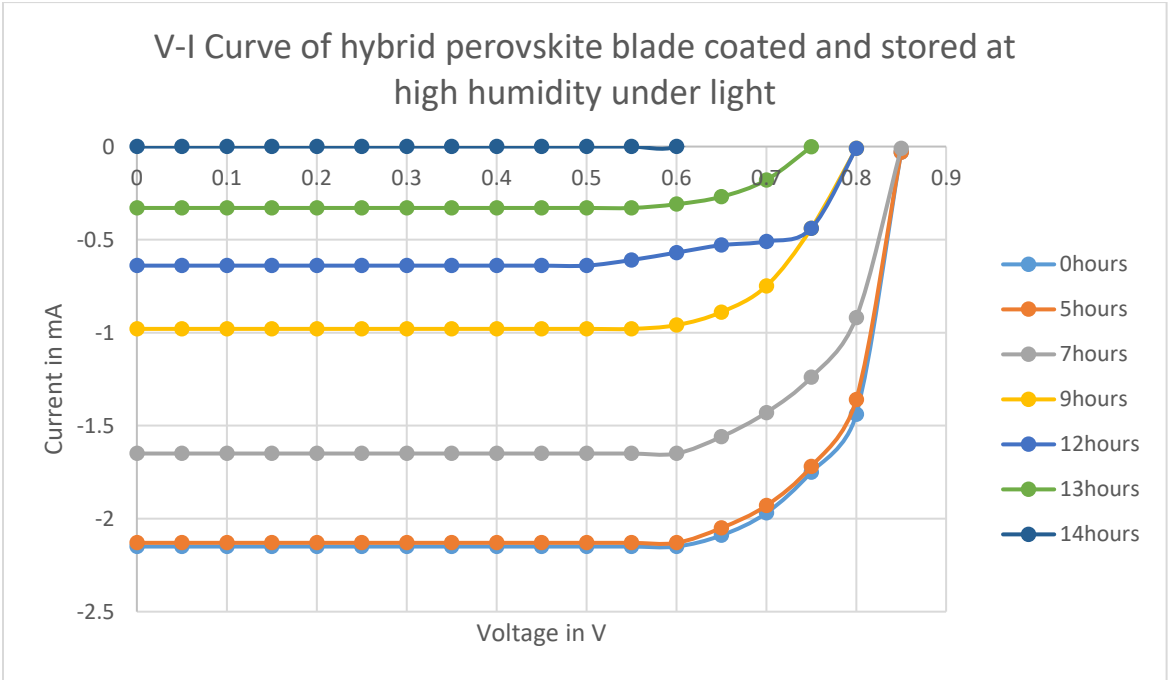


*Figure 52: I-V characteristic curve of hybrid perovskite solar cell blade coated and stored under light in high humidity - Degradation Plot*

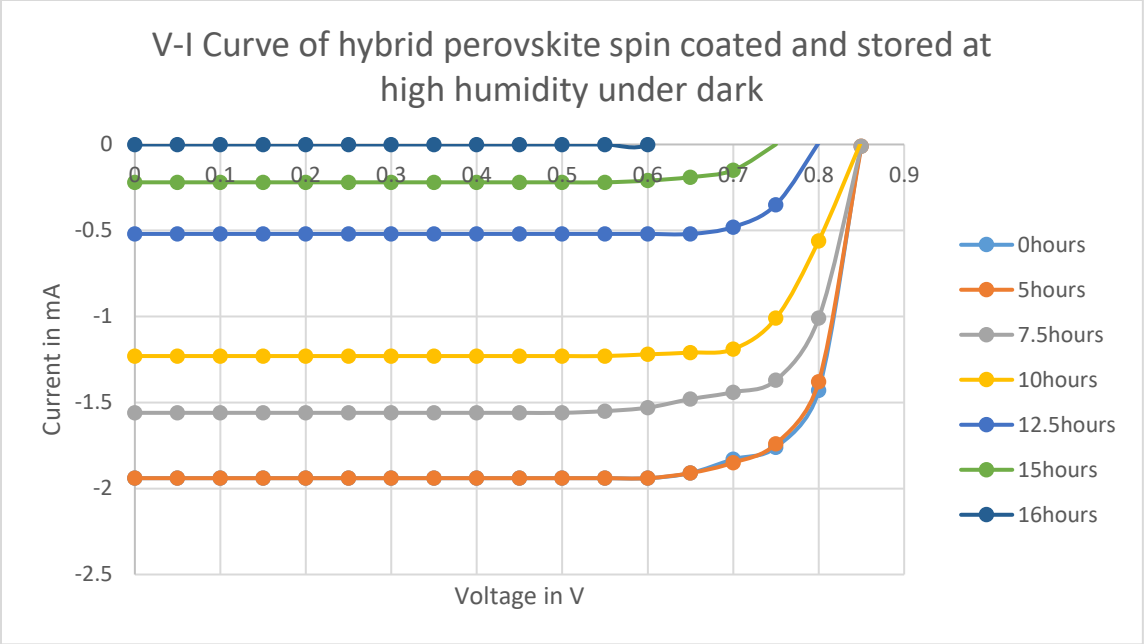


*Figure 53: I-V characteristic curve of hybrid perovskite solar cell spin coated and stored under dark in high humidity - Degradation Plot*

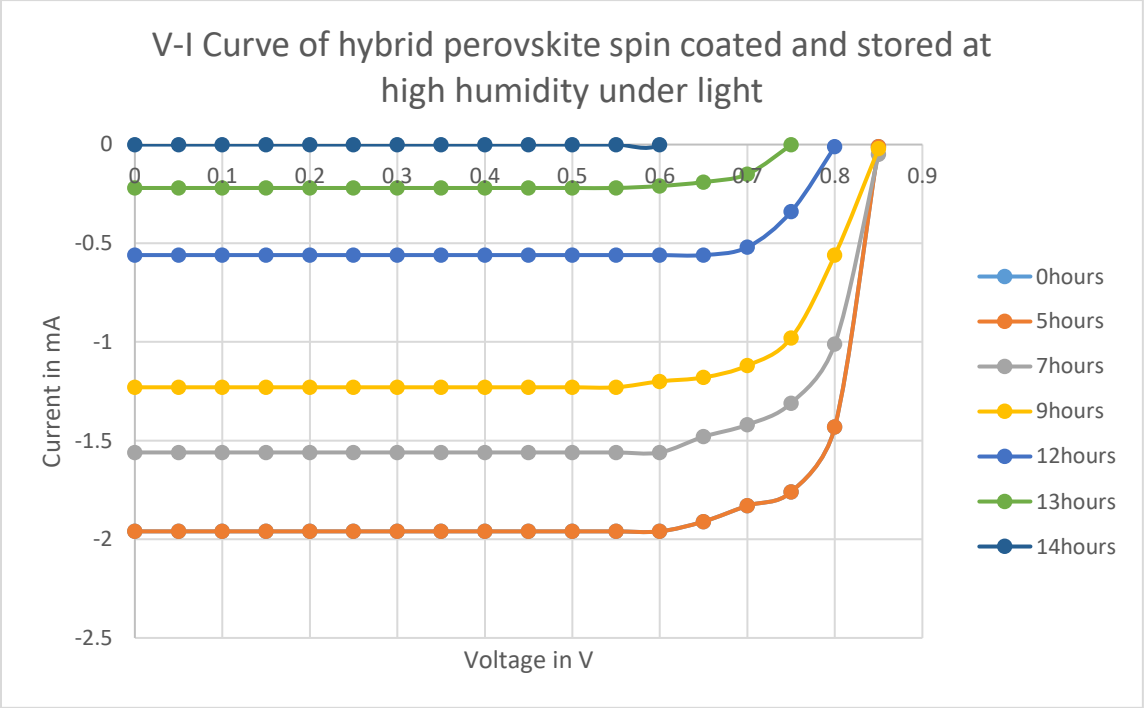


*Figure 54: I-V characteristic curve of hybrid perovskite solar cell spin coated and stored under light in high humidity - Degradation Plot*

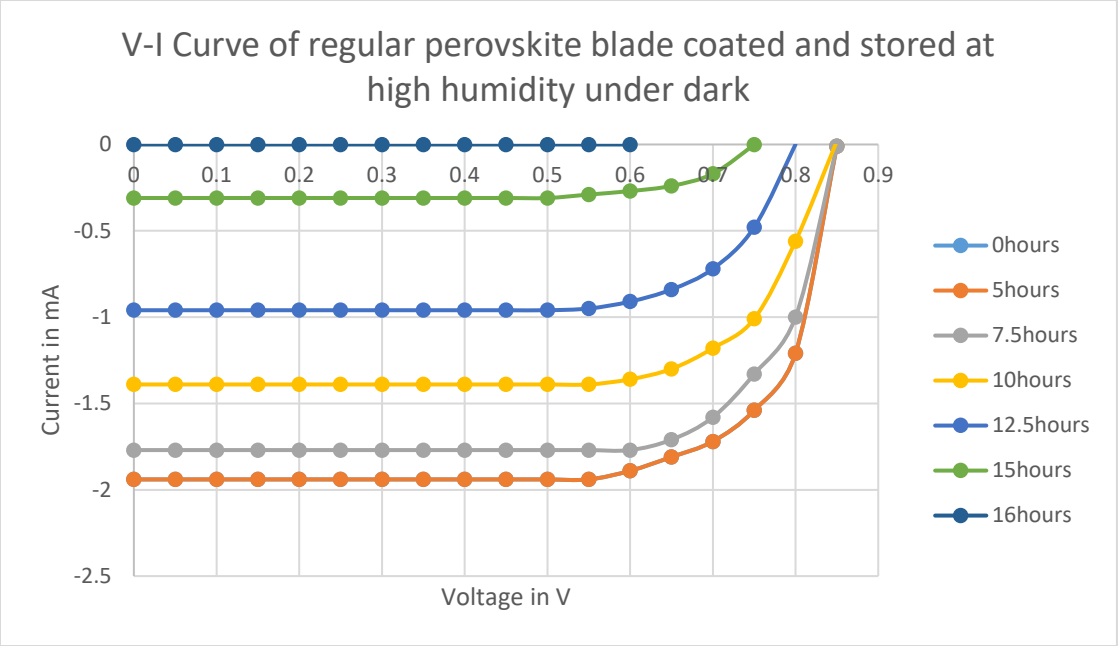


*Figure 55: I-V characteristic curve of regular perovskite solar cell blade coated and stored under dark in high humidity - Degradation Plot*

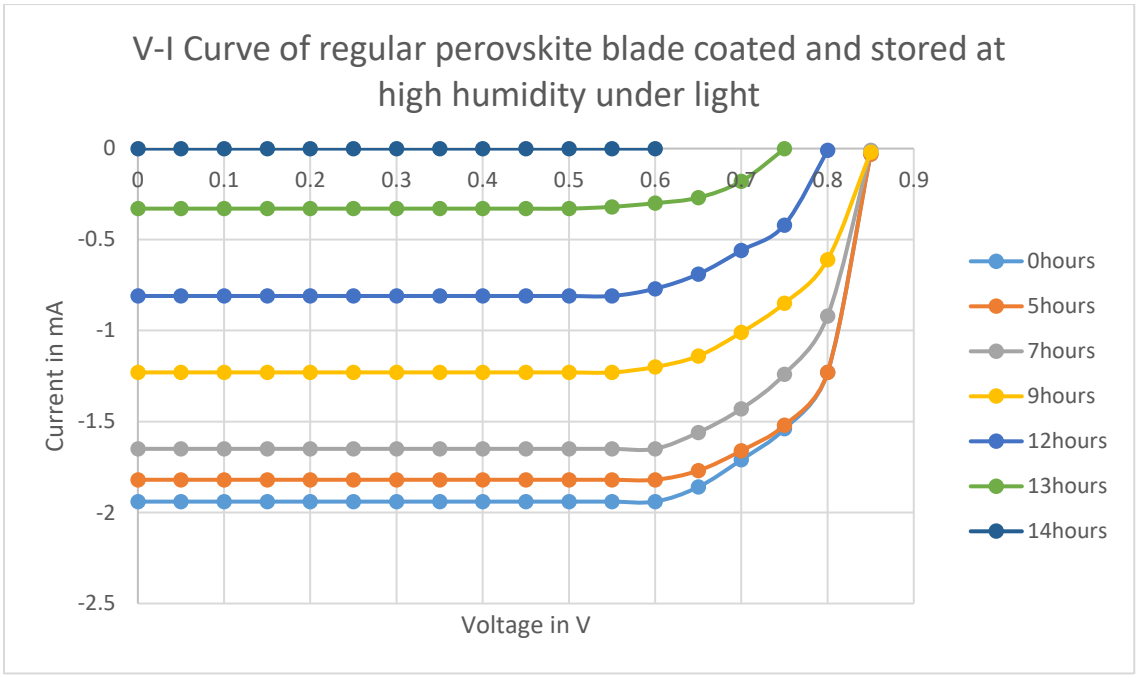


*Figure 56: I-V characteristic curve of regular perovskite solar cell blade coated and stored under light in high humidity - Degradation Plot*

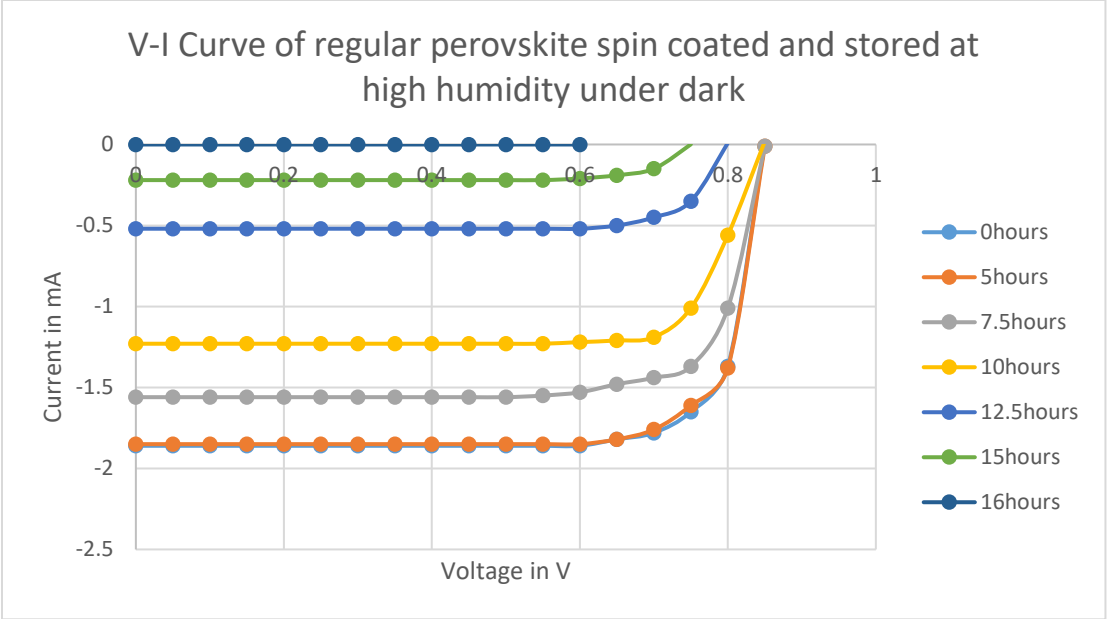


*Figure 57: I-V characteristic curve of regular perovskite solar cell spin coated and stored under dark in high humidity - Degradation Plot*

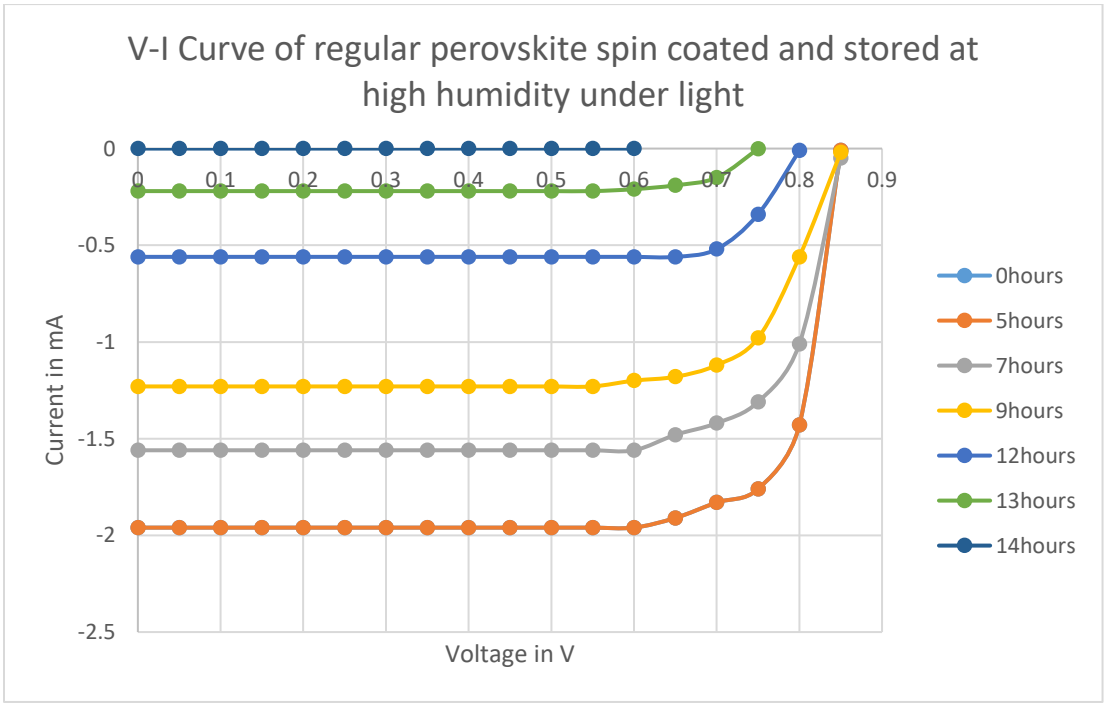


*Figure 58: I-V characteristic curve of regular perovskite solar cell spin coated and stored under light in high humidity - Degradation Plot*

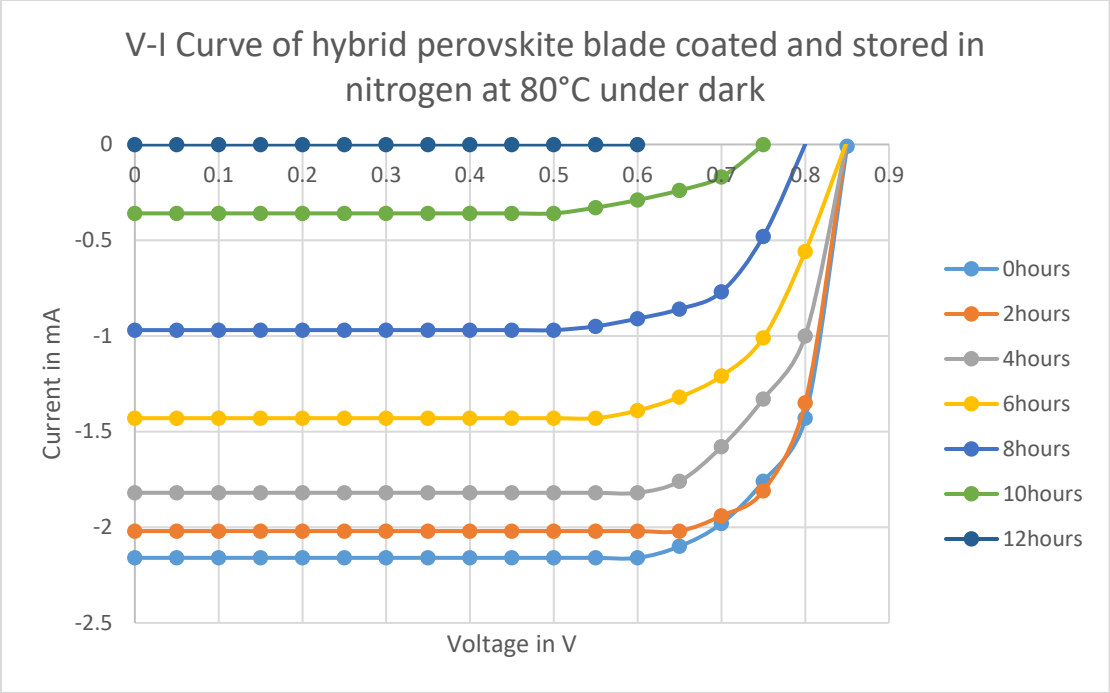


*Figure 59: I-V characteristic curve of hybrid perovskite solar cell blade coated and stored under dark in nitrogen at 80°C - Degradation Plot*

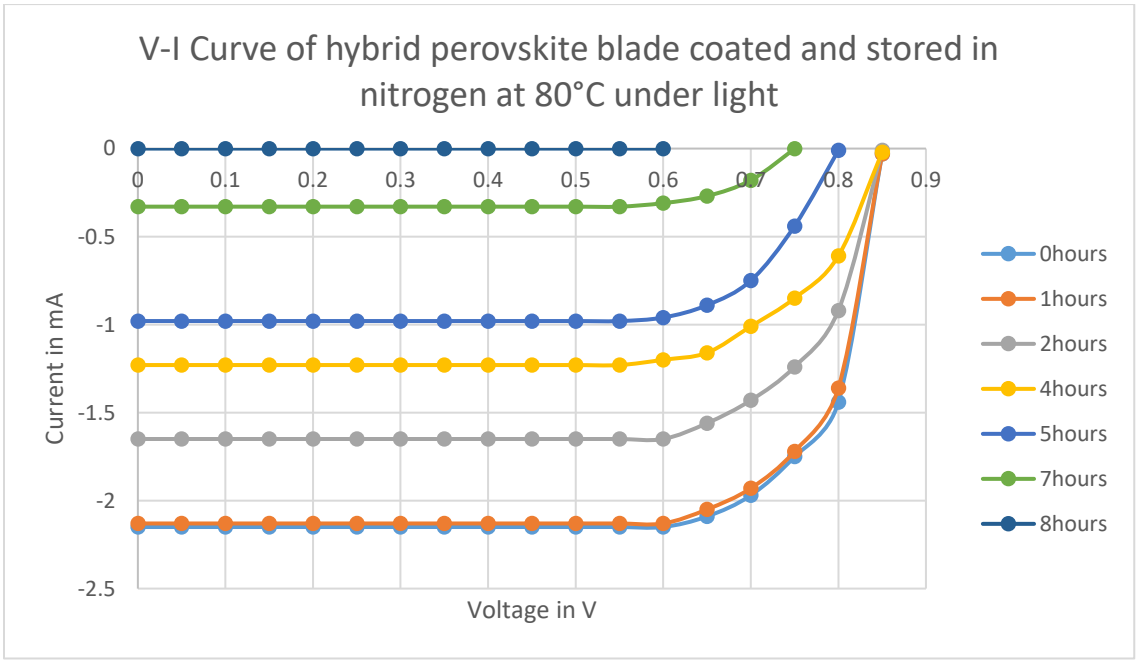


*Figure 60: I-V characteristic curve of hybrid perovskite solar cell blade coated and stored under light in nitrogen at 80°C - Degradation Plot*

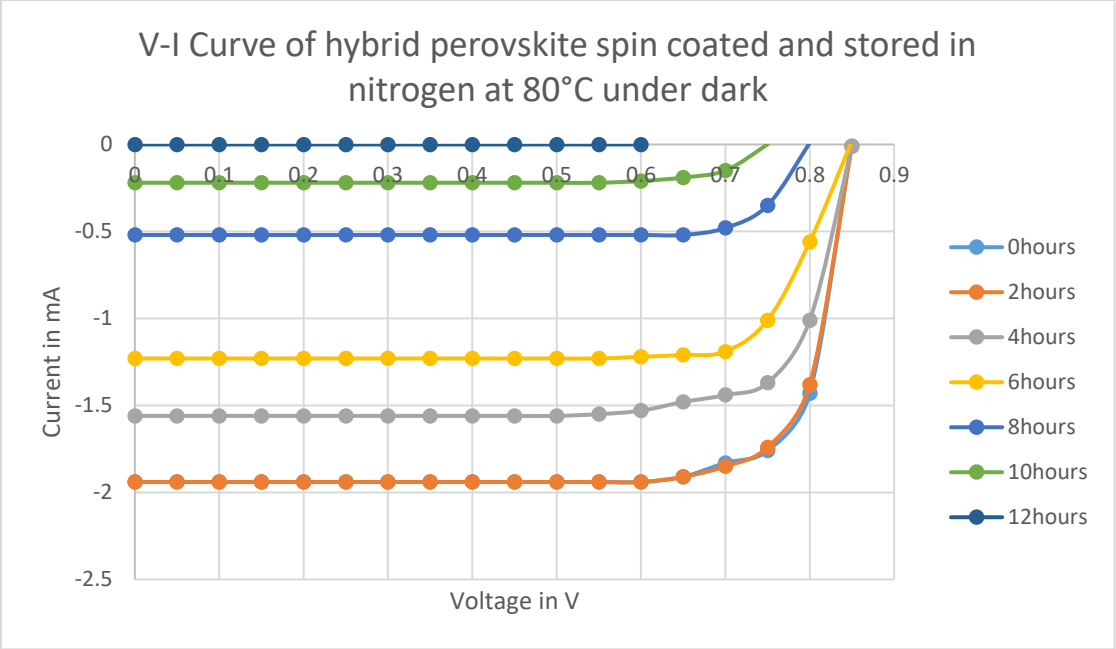


*Figure 61: I-V characteristic curve of hybrid perovskite solar cell spin coated and stored under dark in nitrogen at 80°C - Degradation Plot*

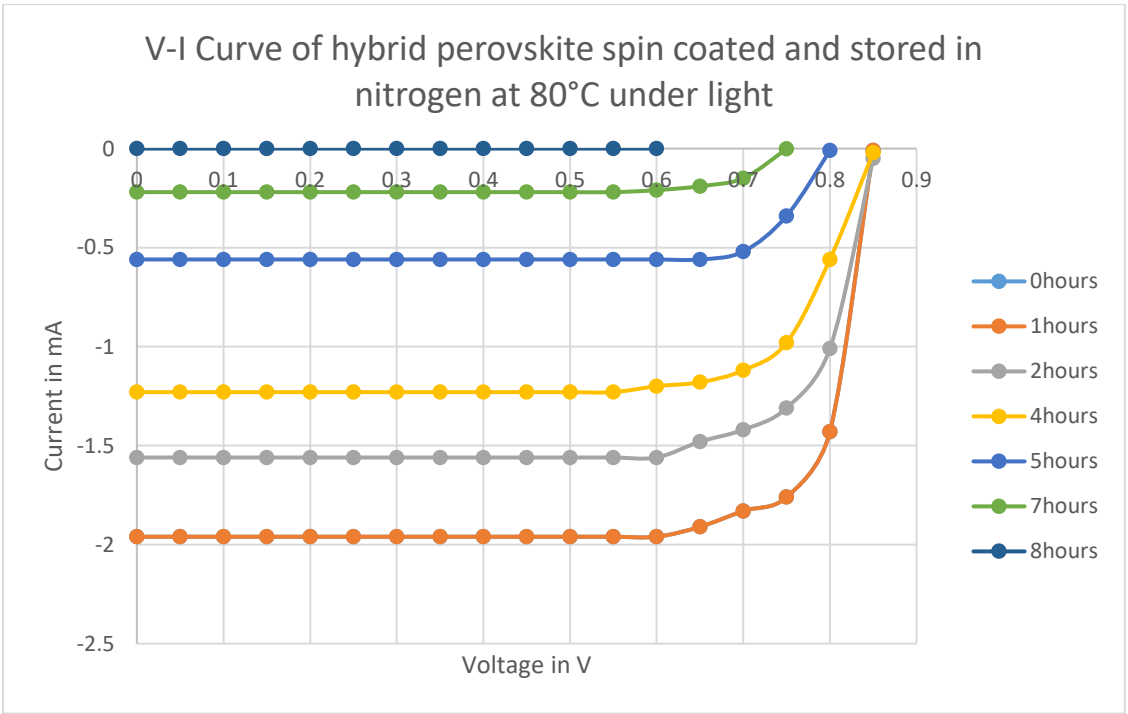


*Figure 62: I-V characteristic curve of hybrid perovskite solar cell spin coated and stored under light in nitrogen at 80°C - Degradation Plot*

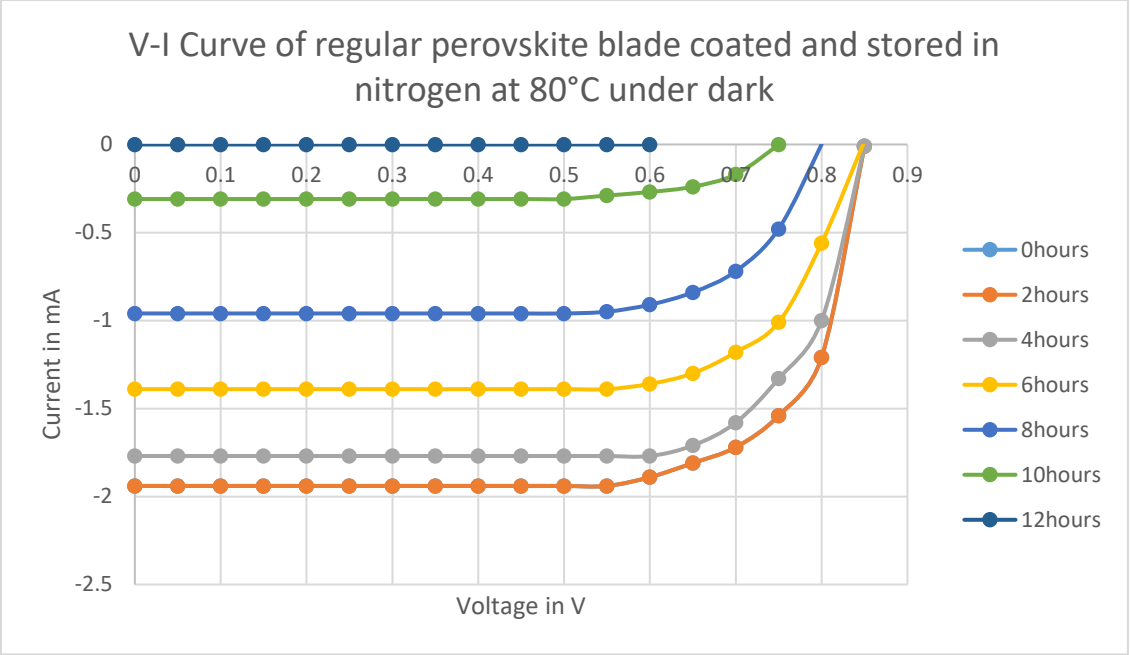


*Figure 63: I-V characteristic curve of regular perovskite solar cell blade coated and stored under dark in nitrogen at 80°C - Degradation Plot*

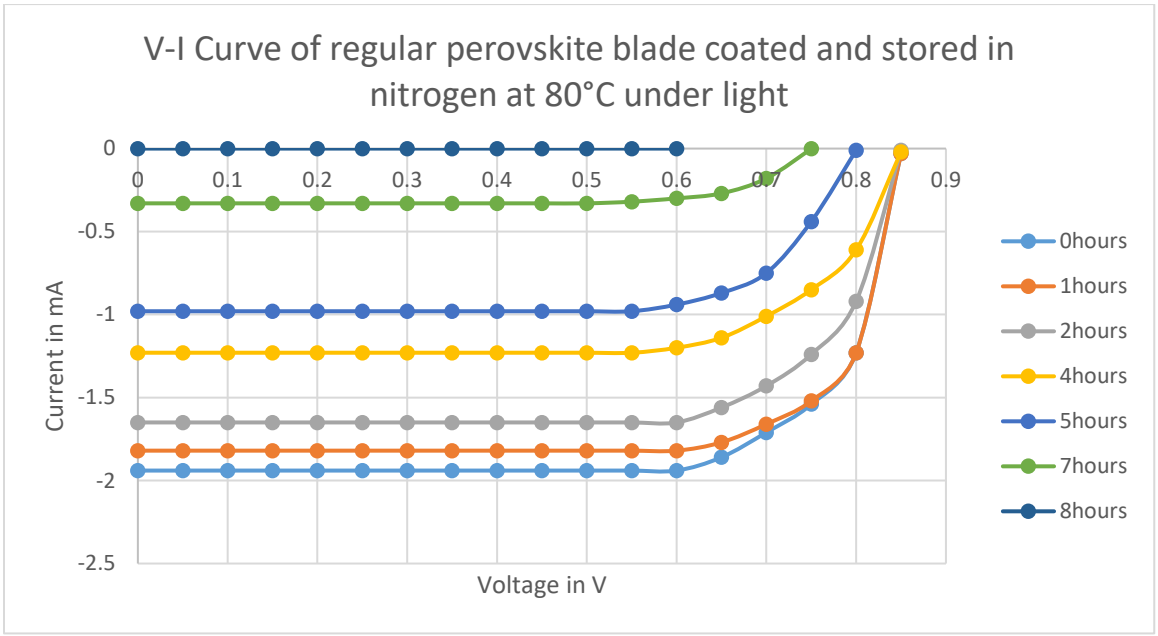


*Figure 64: I-V characteristic curve of regular perovskite solar cell blade coated and stored under light in nitrogen at 80°C - Degradation Plot*

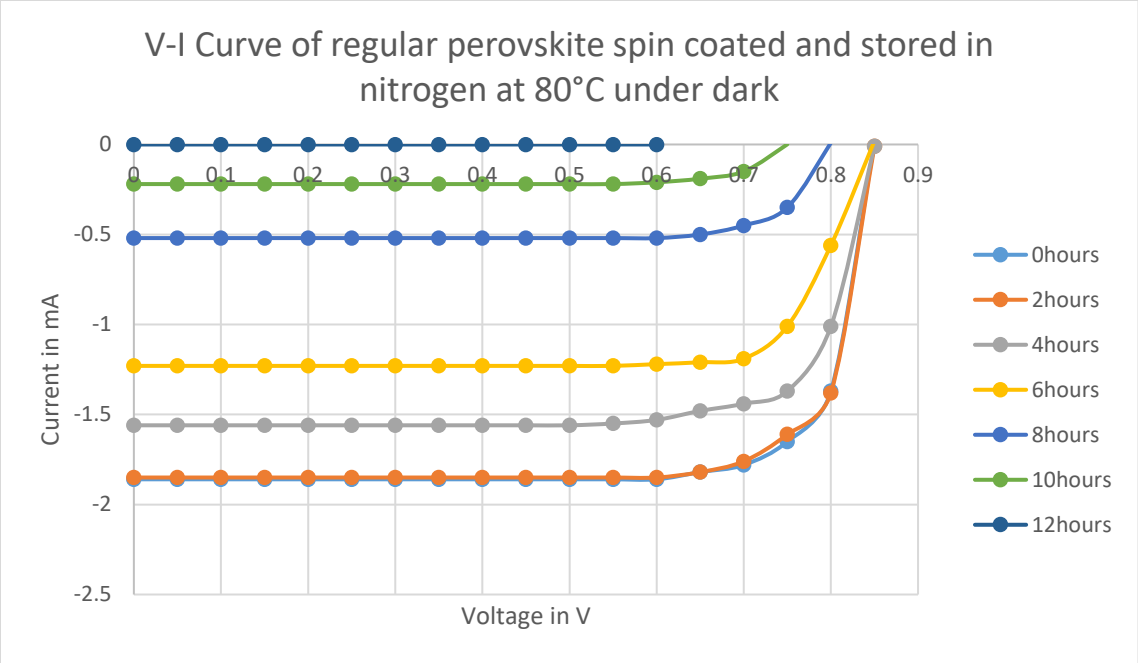


*Figure 65: I-V characteristic curve of regular perovskite solar cell spin coated and stored under dark in nitrogen at 80°C - Degradation Plot*

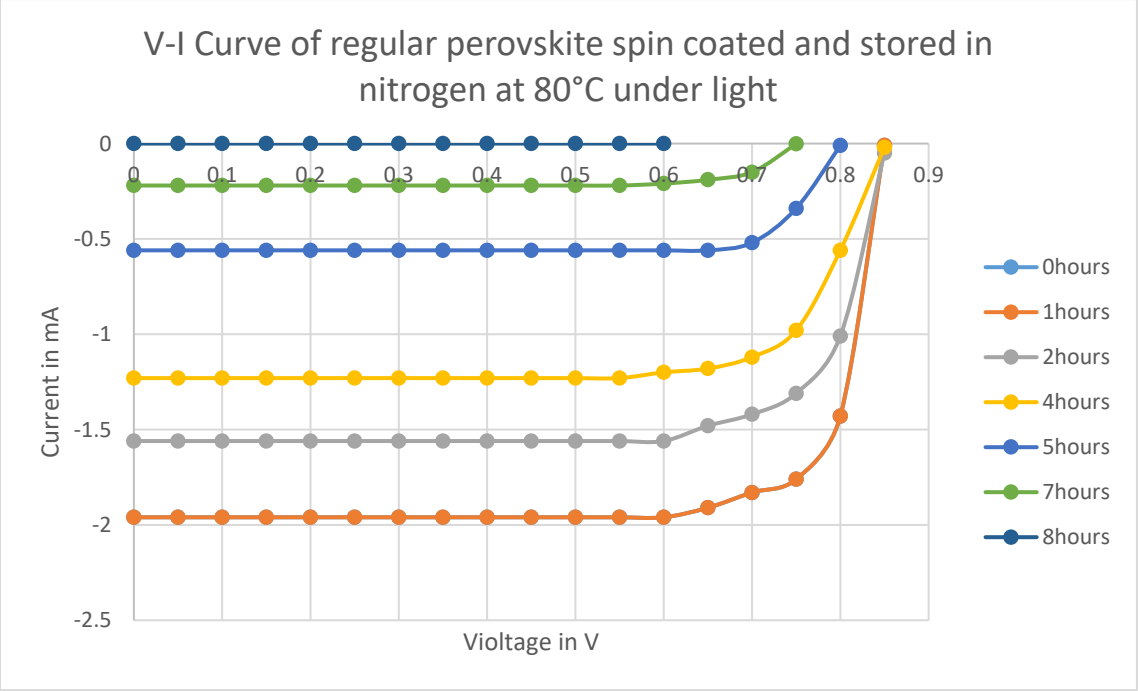


*Figure 66: I-V characteristic curve of regular perovskite solar cell spin coated and stored under light in nitrogen at 80°C - Degradation Plot*

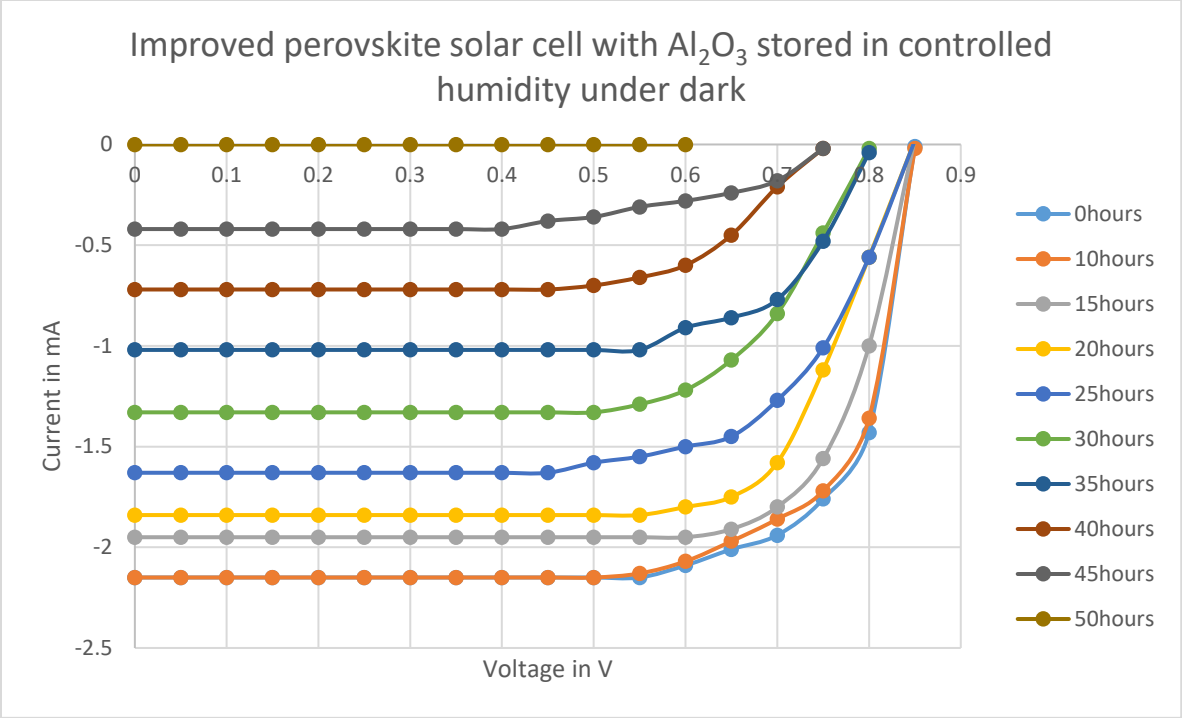


*Figure 67: I-V characteristic curve of improved perovskite solar cell with $Al_2O_3$ buffer layer and stored under dark in controlled humidity - Degradation Plot*

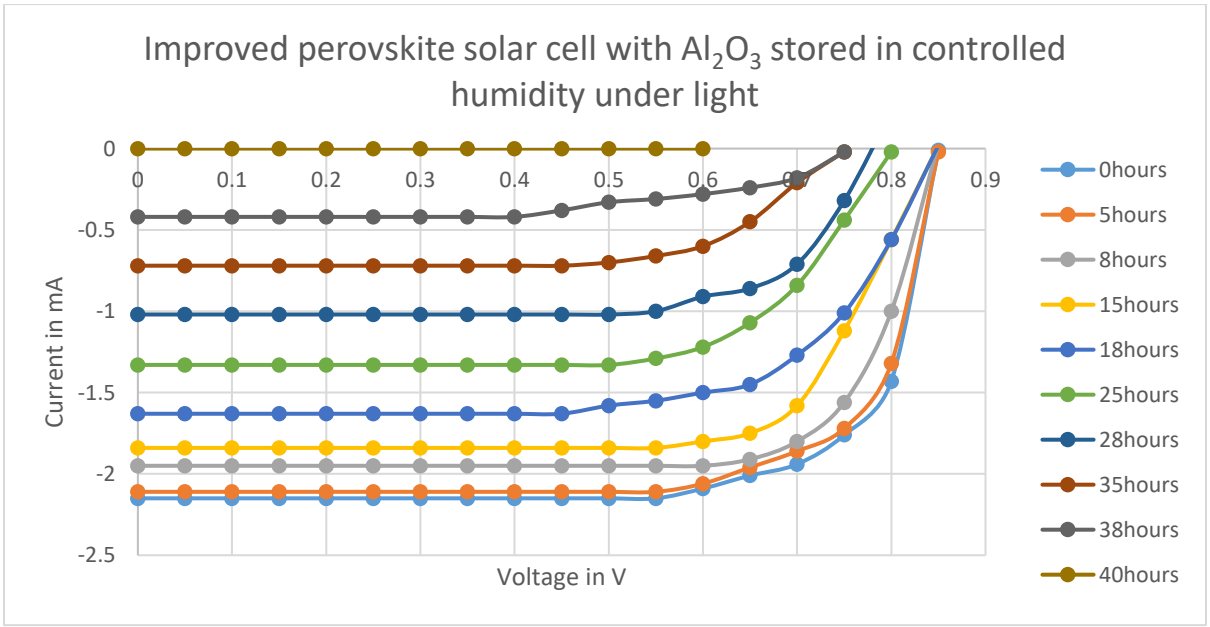


*Figure 68: I-V characteristic curve of improved perovskite solar cell with $Al_2O_3$ buffer layer and stored under light in controlled humidity - Degradation Plot*

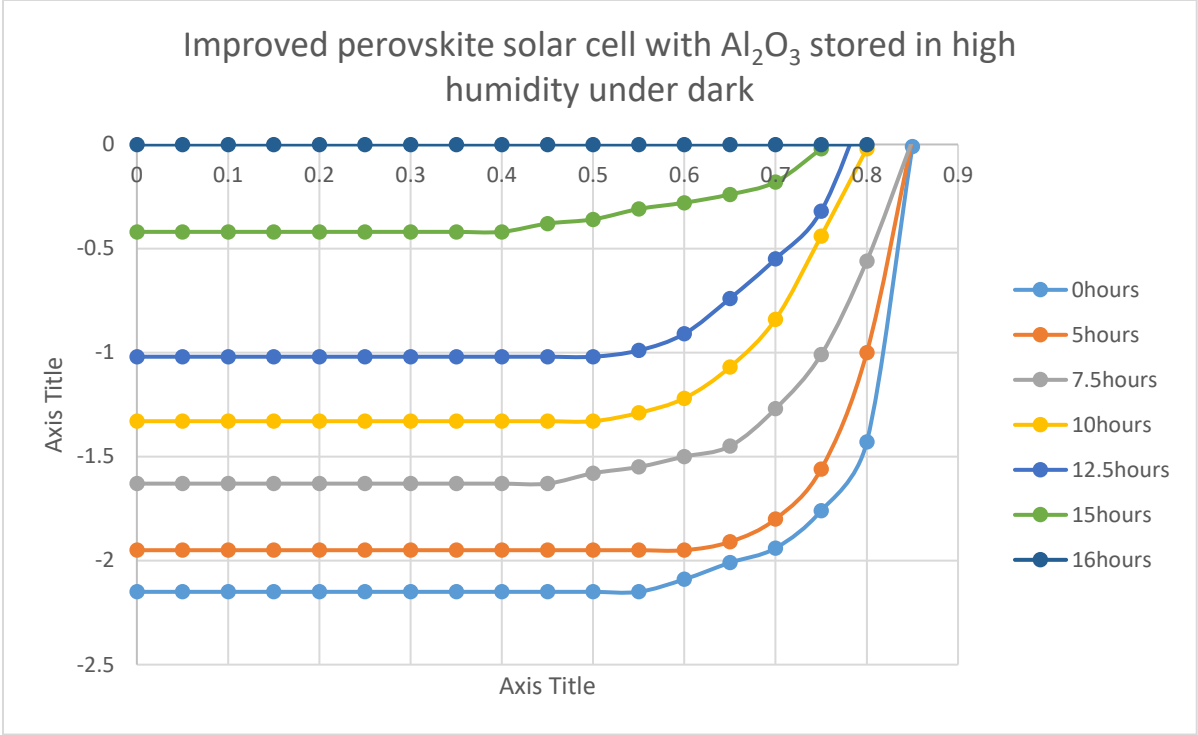


*Figure 69: I-V characteristic curve of improved perovskite solar cell with $Al_2O_3$ buffer layer and stored under dark in high humidity - Degradation Plot*

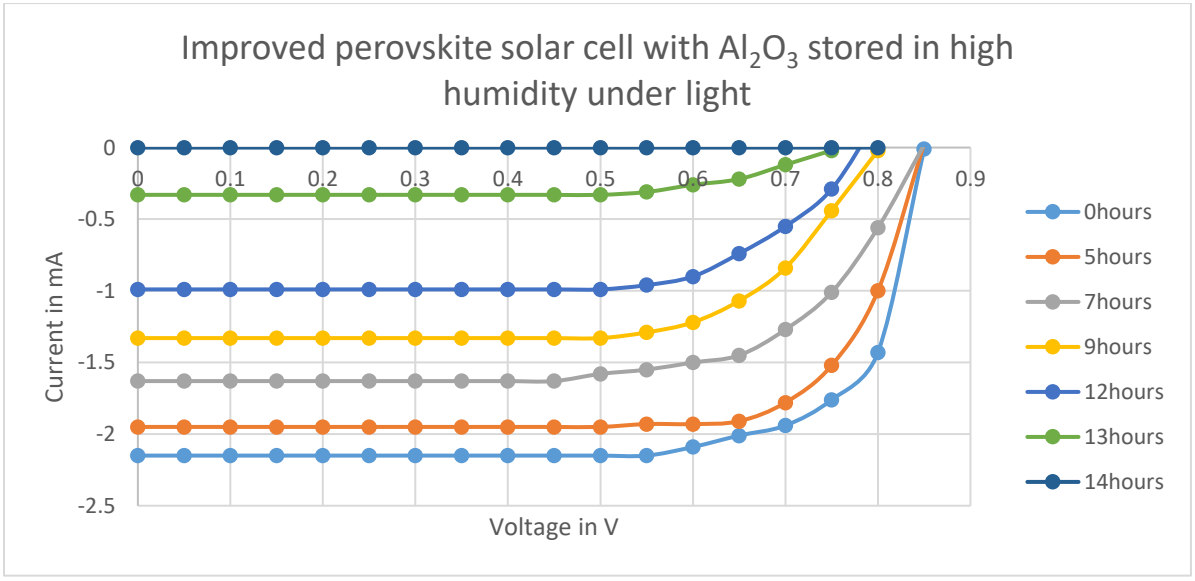


*Figure 70: I-V characteristic curve of improved perovskite solar cell with $Al_2O_3$ buffer layer and stored under light in high humidity - Degradation Plot*

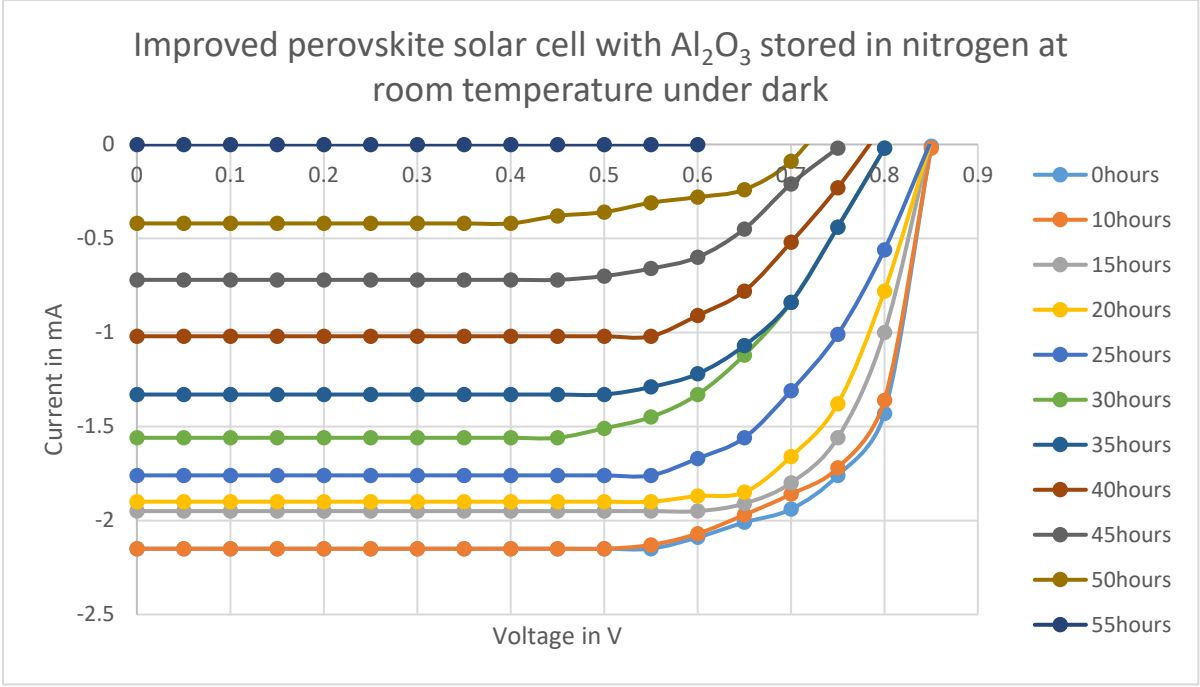


*Figure 71: I-V characteristic curve of improved perovskite solar cell with $Al_2O_3$ buffer layer and stored under dark in nitrogen at room temperature of 22°C- Degradation Plot*

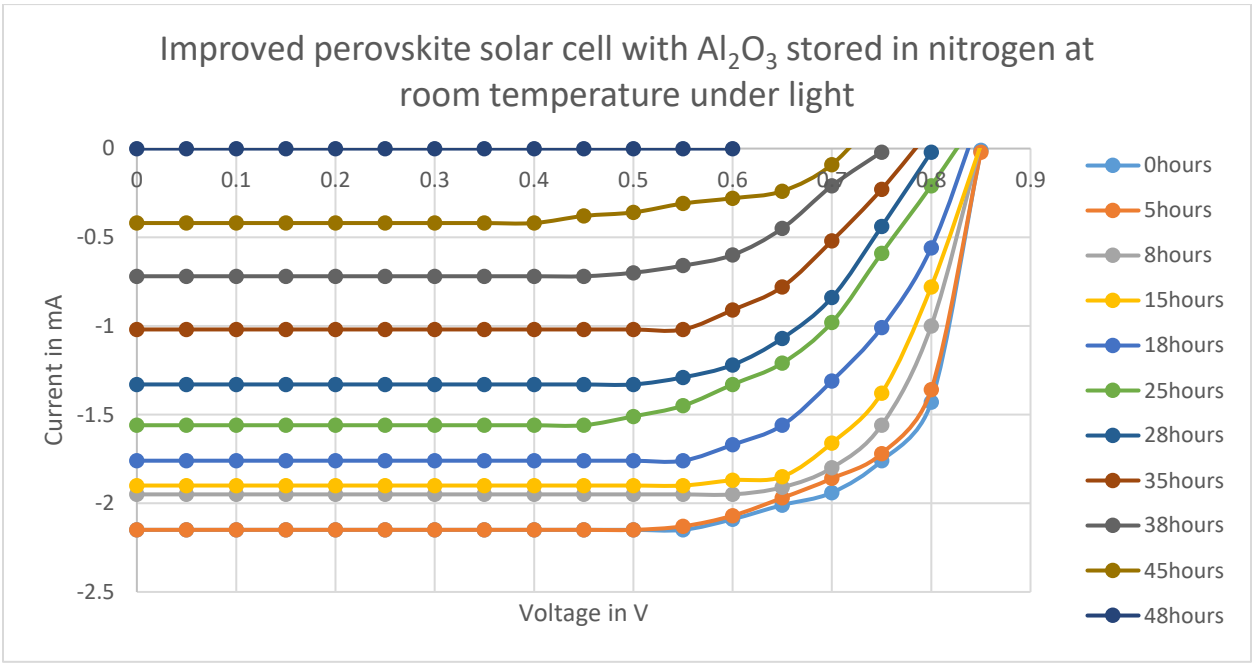


*Figure 72: I-V characteristic curve of improved perovskite solar cell with $Al_2O_3$ buffer layer and stored under light in nitrogen at room temperature- Degradation Plot*

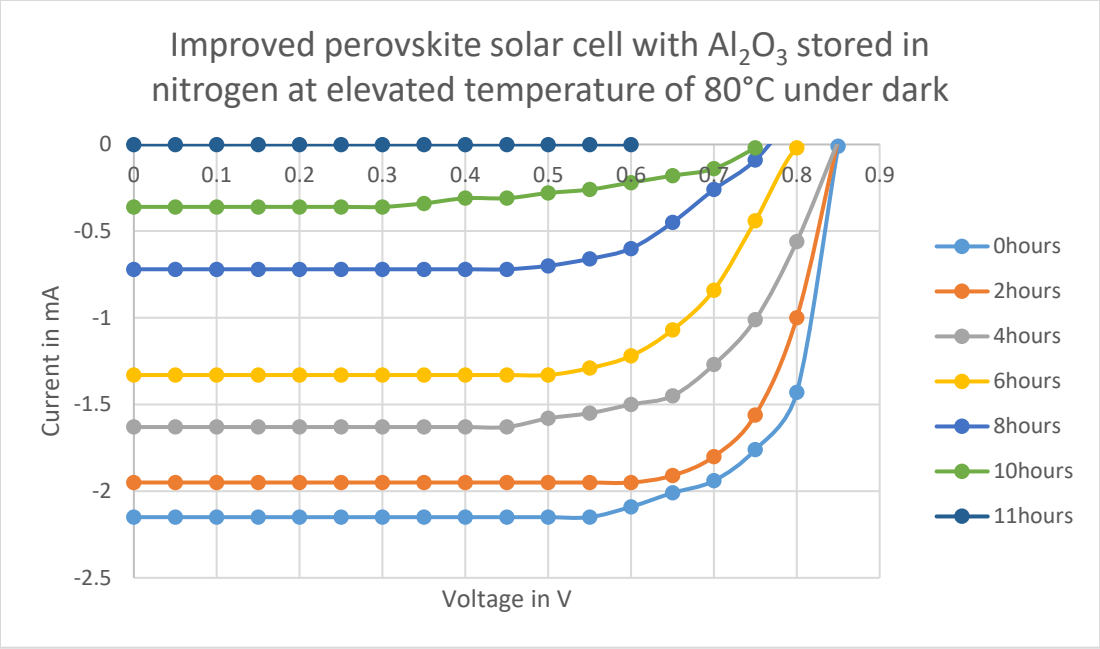


*Figure 73: I-V characteristic curve of improved perovskite solar cell with $Al_2O_3$ buffer layer and stored under dark in nitrogen at elevated temperature of 80°C temperature- Degradation Plot*

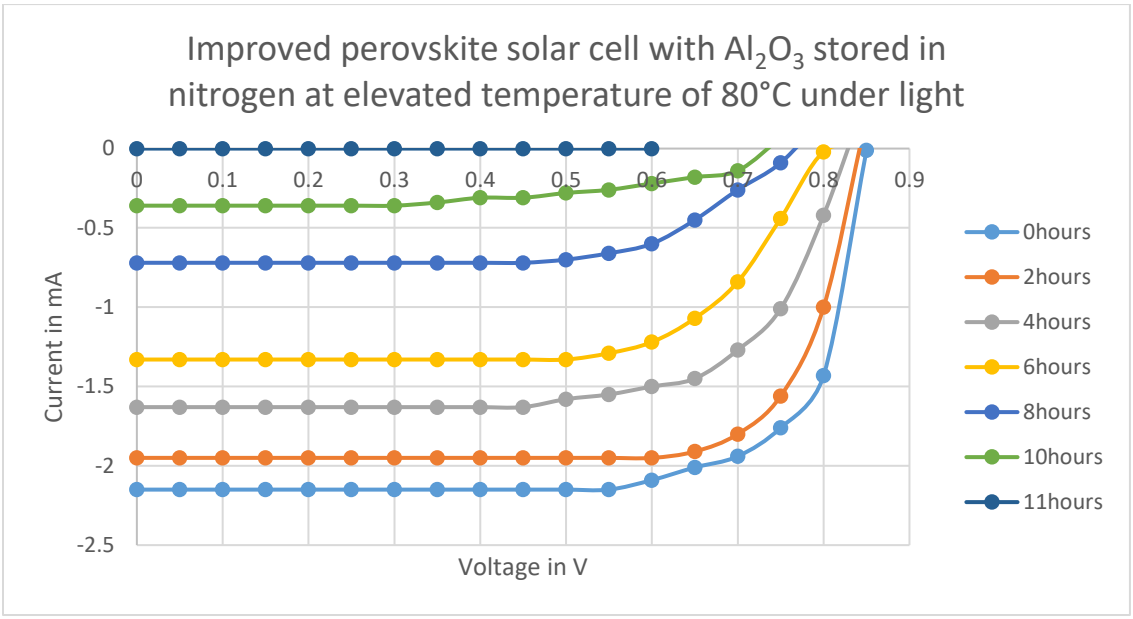


*Figure 74: I-V characteristic curve of improved perovskite solar cell with $Al_2O_3$ buffer layer and stored under light in nitrogen at elevated temperature of 80°C temperature- Degradation Plot*

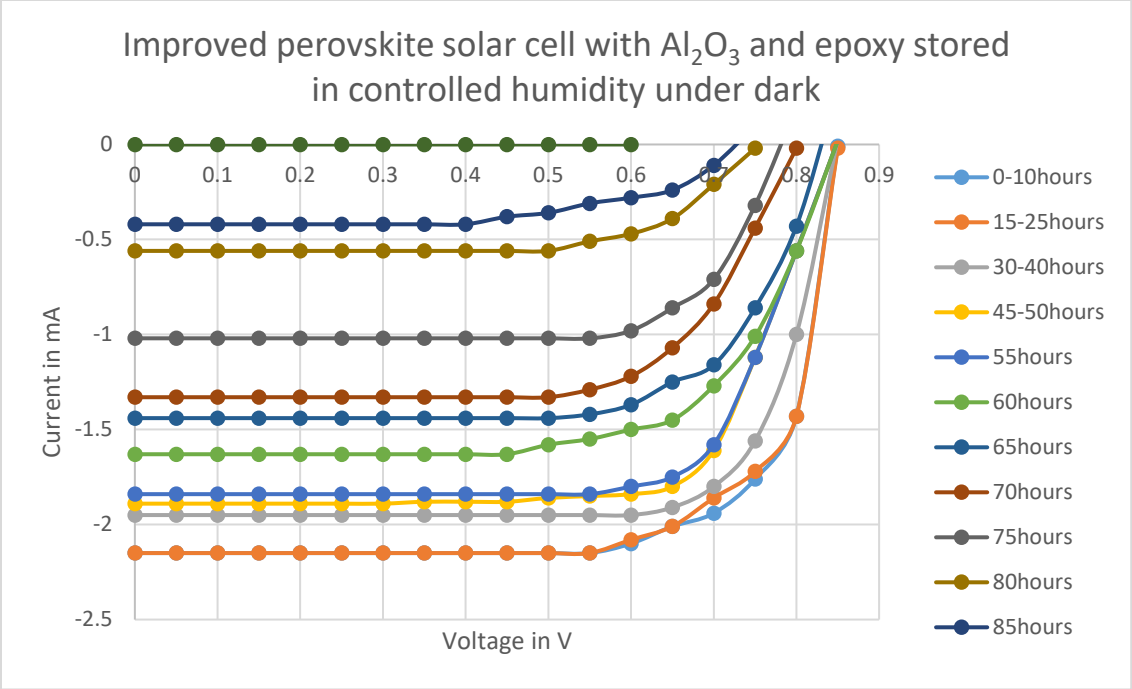


*Figure 75: I-V characteristic curve of improved perovskite solar cell with $Al_2O_3$ buffer layer + epoxy and stored under dark in controlled humidity- Degradation Plot*

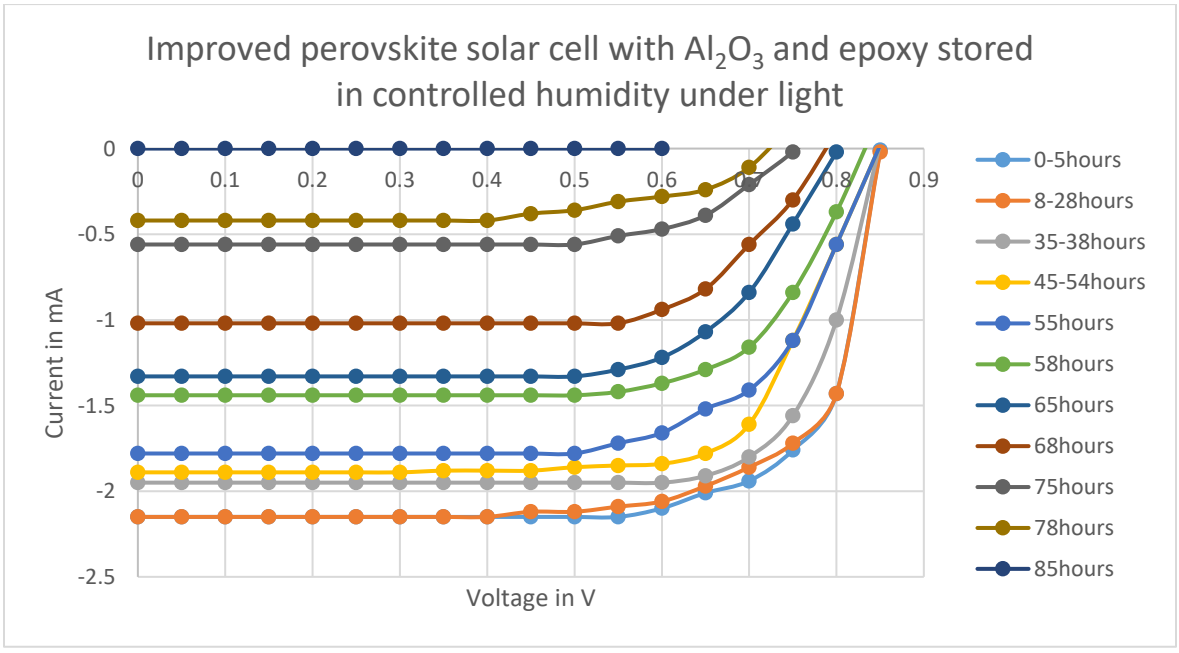


*Figure 76: I-V characteristic curve of improved perovskite solar cell with $Al_2O_3$ buffer layer + epoxy and stored under light in controlled humidity- Degradation Plot*

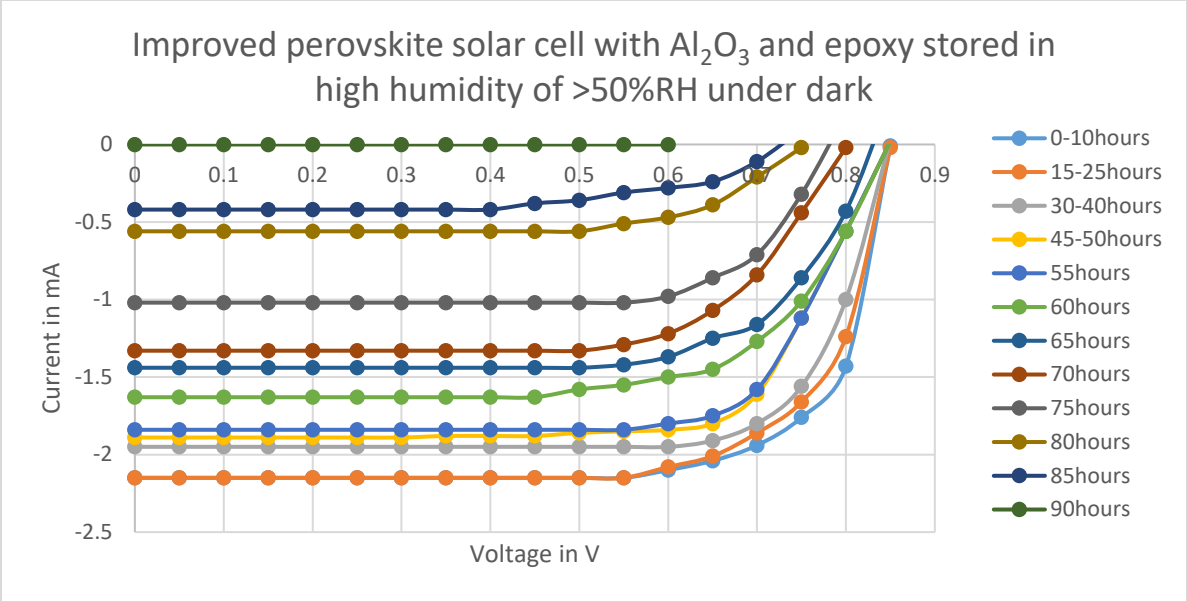


*Figure 77: I-V characteristic curve of improved perovskite solar cell with $Al_2O_3$ buffer layer + epoxy and stored under dark in high humidity (>50% RH)- Degradation Plot*

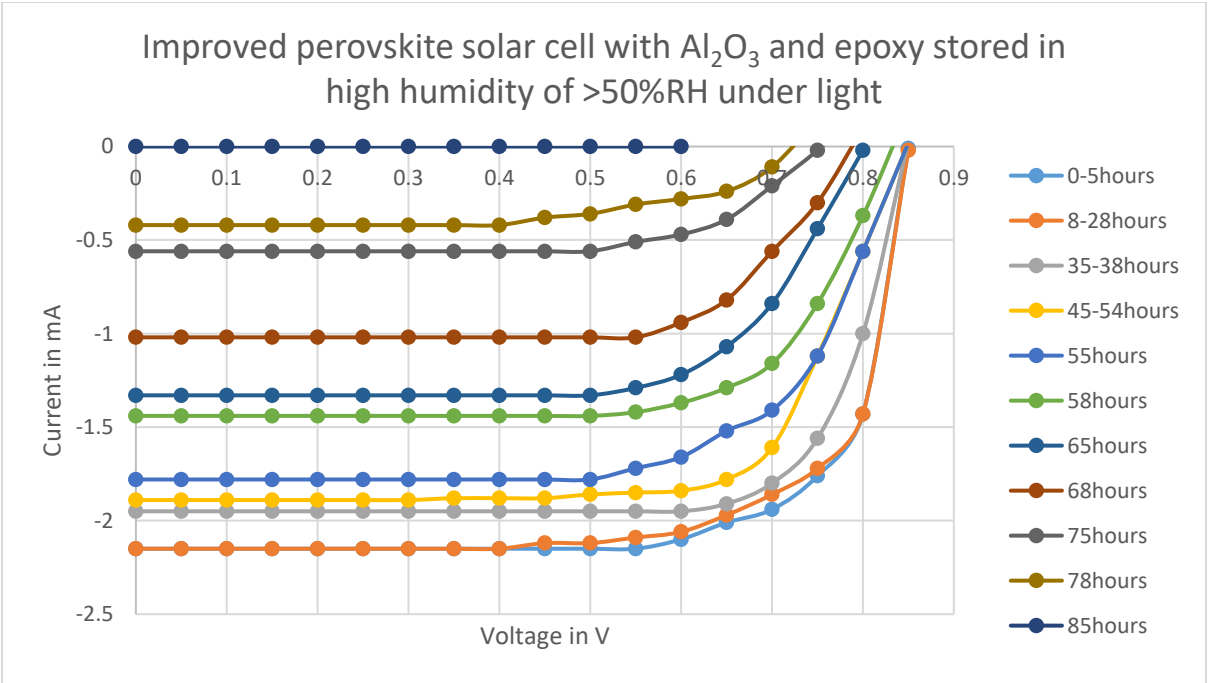


*Figure 78: I-V characteristic curve of improved perovskite solar cell with $Al_2O_3$ buffer layer + epoxy and stored under dark in high humidity (>50% RH)- Degradation Plot*

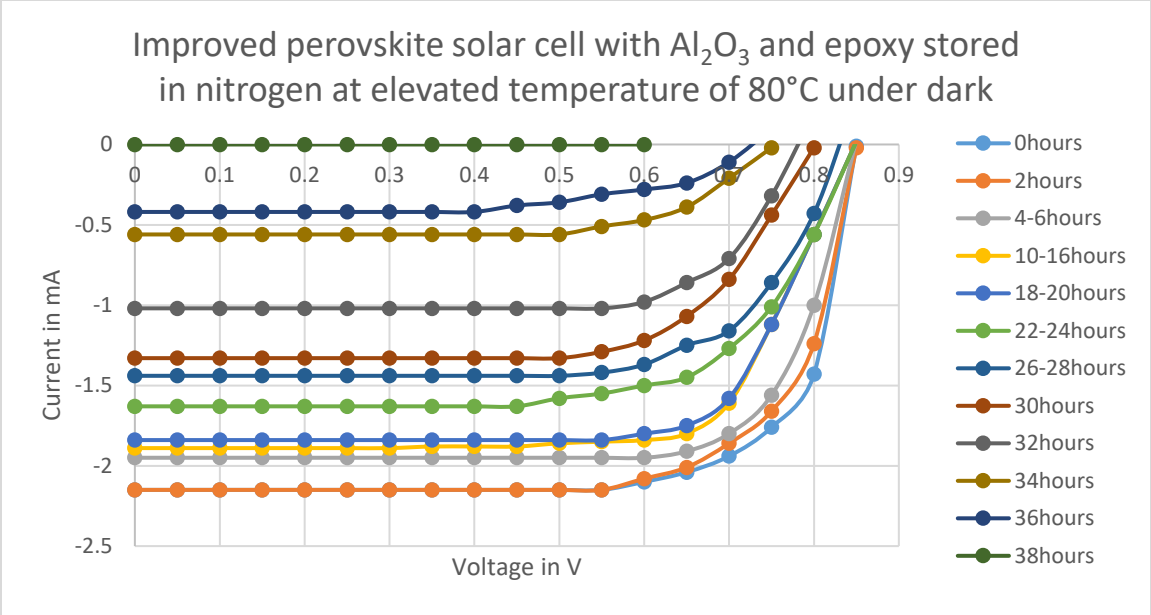


*Figure 79: I-V characteristic curve of improved perovskite solar cell with $Al_2O_3$ buffer layer + epoxy and stored under dark in nitrogen at elevated temperature of 80°C - Degradation Plot*

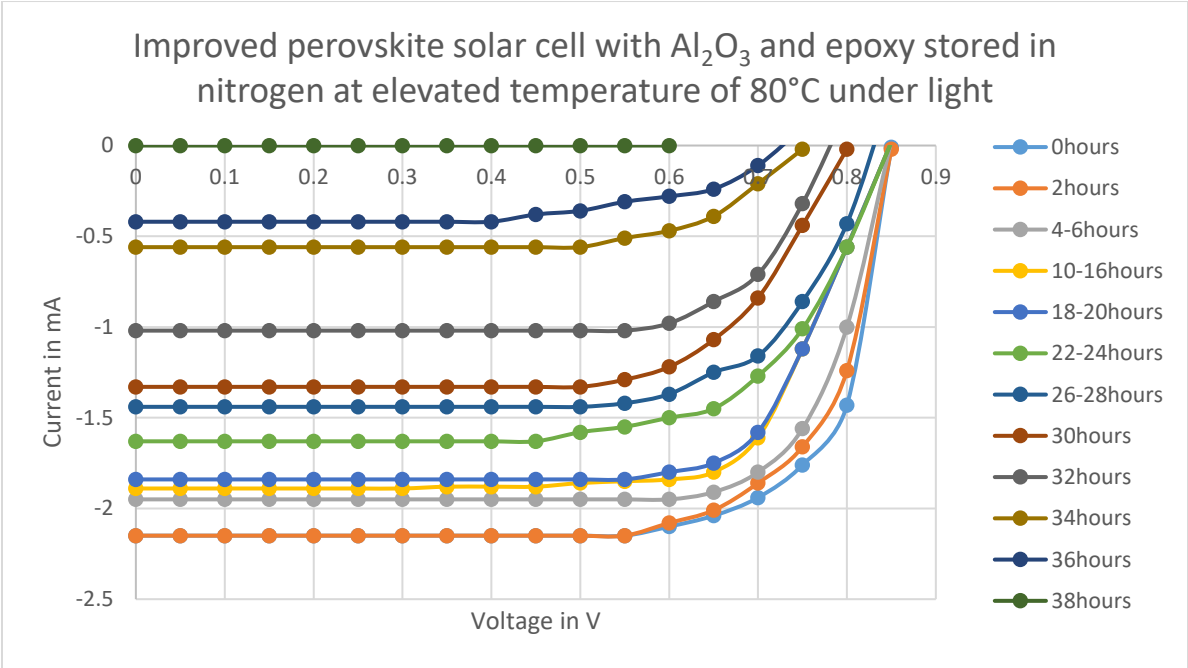


*Figure 80: I-V characteristic curve of improved perovskite solar cell with $Al_2O_3$ buffer layer + epoxy and stored under light in nitrogen at elevated temperature of 80°C - Degradation Plot*

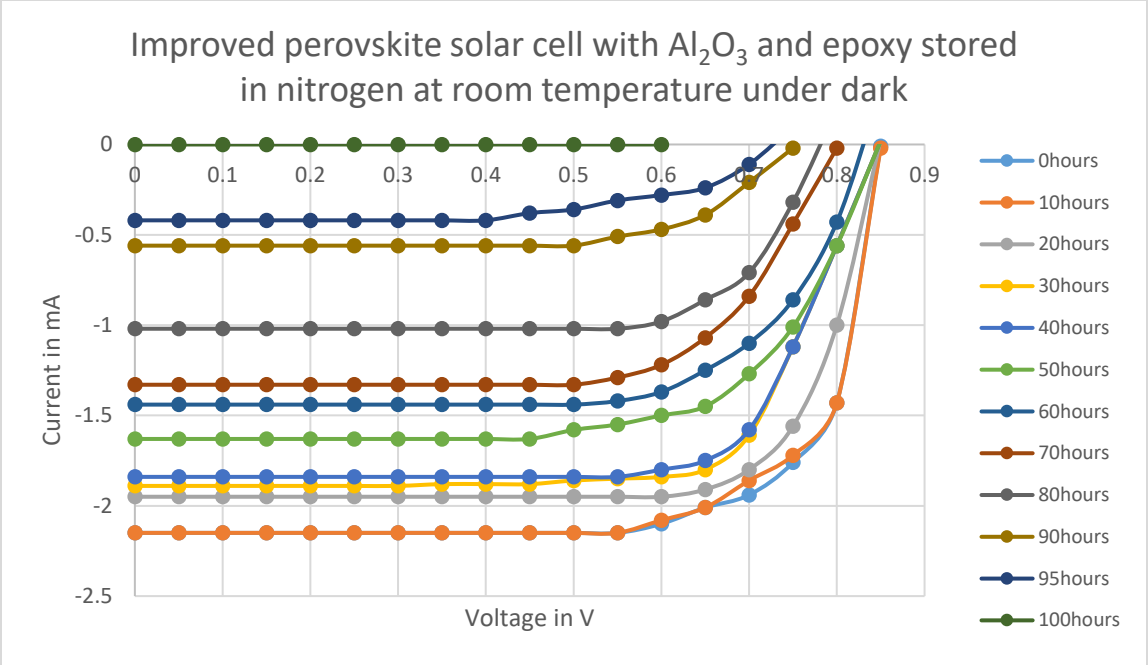


*Figure 81: I-V characteristic curve of improved perovskite solar cell with $Al_2O_3$ buffer layer + epoxy and stored under dark in nitrogen at room temperature of 22°C - Degradation Plot*

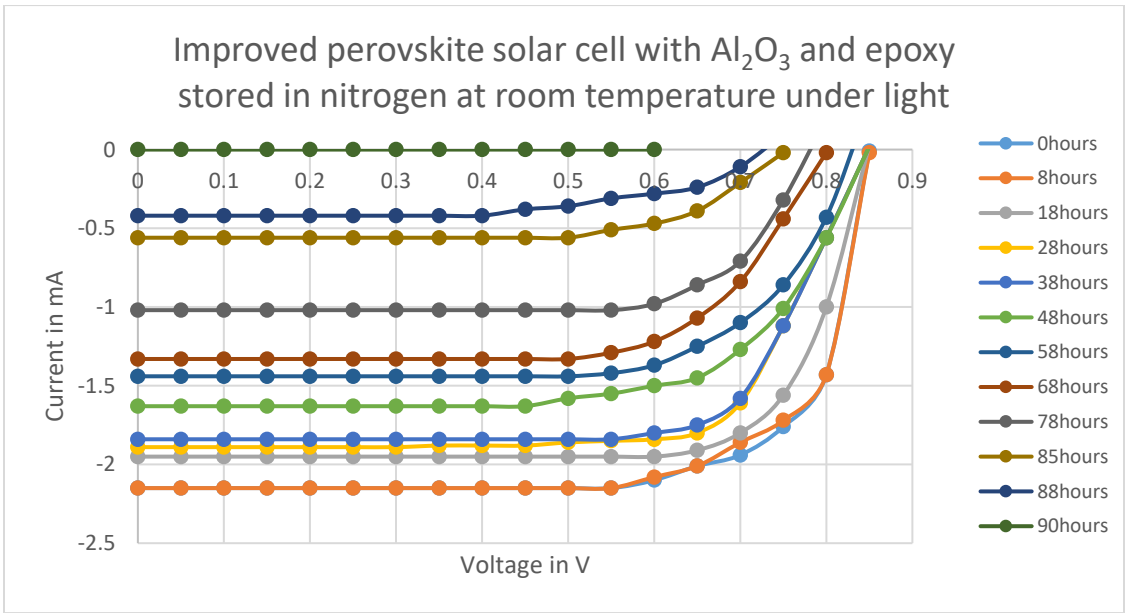


*Figure 82: I-V characteristic curve of improved perovskite solar cell with $Al_2O_3$ buffer layer + epoxy and stored under light in nitrogen at room temperature of 22°C - Degradation Plot*

**References**


1. N. Espinosa, M. Hösel, D. Angmo, F.C. Krebs, Solar cells with one-day energy payback for the factories of the future, Energy Environ. Sci. 5 (2012) 5117–5132.
2. Kojima, A., Teshima, K., Shirai, Y., Miyasaka, T., 2009. Organometal halide perovskites as visible-light sensitizers for photovoltaic cells. J. Am. Chem. Soc. 131 (17), 6050
3. Nam-Gyu Park, Perovskite solar cells: an emerging photovoltaic technology, materialstoday Volume 18, Issue 2, March 2015, Pages 65-72
4. H.J. Snaith, Perovskites: the emergence of a new era for low-cost, highefficiency solar cells, J. Phys. Chem. Lett. 4 (2013) 3623–3630.
5. Eperon, G.E., Burlakov, V.M., Docampo, P., Goriely, A., Snaith, H.J., 2014a. Morphological control for high performance, solution-processed planar heterojunction perovskite solar cells. Adv. Funct. Mater. 24 (1), 151–157.
6. Maria Antonietta Loi & Jan C. Hummelen, Hybrid solar cells- Perovskites under the Sun. Nature Materials, V 12, p1087-1089 (2013).
7. Gary Hodes, Perovskite-Based Solar Cells. Science magazine, Vol 342, p317-318 (2013).
8. Mitzi, D., Feild, C., Harrison, W. et al. Conducting tin halides with a layered organic-based perovskite structure. Nature 369, 467–469 (1994).
9. Jeong-Hyeok Im, Sang-Won Park, Nam-Gyu Park et al. 6.5% efficient perovskite quantum-dot-sensitized solar cell, Nanoscale, 2011,3, 4088-4093.
10. Burschka, J., Pellet, N., Moon, S. et al. Sequential deposition as a route to high-performance perovskite-sensitized solar cells. Nature 499, 316–319 (2013).

11. Bach, U., Lupo, D., Comte, et al. Solid-state dye-sensitized mesoporous TiO2 solar cells with high photon-to-electron conversion efficiencies. Nature 395, 583–585 (1998).
12. Kim, H., Lee, C., Im, J. et al. Lead Iodide Perovskite Sensitized All-Solid-State Submicron Thin Film Mesoscopic Solar Cell with Efficiency Exceeding 9%. Sci Rep 2, 591 (2012).
13. Niu, G., Guo, X., Wang, L., 2015. Review of recent progress in chemical stability of perovskite solar cells. J. Mater. Chem. A 3 (17), 8970–8980.
14. Leguy, A.M.A., Hu, Y., Campoy-Quiles, M., Alonso, M.I., Weber, O.J., Azarhoosh, P., van Schilfgaarde, M., Weller, M.T., Bein, T., Nelson, J., Docampo, P., Barnes, P.R.F., 2015. Reversible hydration of CH3- NH3PbI3 in films, single crystals, and solar cells. Chem. Mater.
15. Christians, J.A., Miranda Herrera, P.A., Kamat, P.V., 2015. Transformation of the excited state and photovoltaic efficiency of CH3NH3PbI3 perovskite upon controlled exposure to humidified air. J. Am. Chem. Soc. 137 (4), 1530–1538.
16. Leijtens, T., Eperon, G.E., Pathak, S., Abate, A., Lee, M.M., Snaith, H.J., 2013. Overcoming ultraviolet light instability of sensitized TiO(2) with meso-superstructured organometal tri-halide perovskite solar cells. Nat. Commun. 4, 2885.
17. Schoonman, J., 2015. Organic–inorganic lead halide perovskite solar cell materials: a possible stability problem. Chem. Phys. Lett. 619, 193–195.
18. S. Ito, S. Tanaka, K. Manabe, H. Nishino, Effects of Surface Blocking Layer of Sb2S3 on Nanocrystalline TiO2 for CH3NH3PbI3 Perovskite Solar Cells, J. Phys.C.hem. C. 118 (2014) 16995–17000.

19. B. Philippe, B.-W. Park, R. Lindblad, J. Oscarsson, S. Ahmadi, E.M.J. Johansson, H. Rensmo, Chemical and electronic structure characterization of lead halide perovskites and stability behavior under different exposures—a photoelectron spectroscopy investigation, Chem. Mater. 27 (2015) 1720–1731.
20. S.K. Pathak, A. Abate, P. Ruckdeschel, B. Roose, K.C. Gödel, Y. Vaynzof, A. Santhala, S.-I. Watanabe, D.J. Hollman, N. Noel, A. Sepe, U. Wiesner, R. Friend, H.J. Snaith, U. Steiner, Performance and stability enhancement of dye-sensitized and perovskite solar cells by Al doping of TiO2, Adv. Funct. Mater. 24 (2014) 6046–6055.
21. J. Yang, B.D. Siempelkamp, E. Mosconi, F. De Angelis, T.L. Kelly, Origin of the thermal instability in CH3NH3PbI3 thin films deposited on ZnO, Chem. Mater. 27 (2015) 4229–4236.
22. J. Song, E. Zheng, J. Bian, X.-F. Wang, W. Tian, Y. Sanehira, T. Miyasaka, Low temperature SnO2-based electron selective contact for efficient and stable perovskite solar cells, J. Mater. Chem. A 3 (2015) 10837–10844.
23. Y. Han, S. Meyer, Y. Dkhissi, K. Weber, J.M. Pringle, U. Bach, L. Spiccia, Y.- B. Cheng, Degradation observations of encapsulated planar CH3NH3PbI3 perovskite solar cells at high temperatures and humidity, J. Mater. Chem. A 3 (2015) 8139–8147.
24. S.N. Habisreutinger, T. Leijtens, G.E. Eperon, S.D. Stranks, R.J. Nicholas, H. J. Snaith, Carbon nanotube/polymer composites as a highly stable hole collection layer in perovskite solar cells, Nano Lett. 14 (2014) 5561–5568.

25. M. Zhang, M. Lyu, H. Yu, J.H. Yun, Q. Wang, L. Wang, Stable and low-cost mesoscopic CH3NH3PbI2 Br perovskite solar cells by using a thin poly(3- hexylthiophene) layer as a hole transporter, Chemistry 21 (2015) 434–439.
26. J.H. Kim, P.W. Liang, S.T. Williams, N. Cho, C.C. Chueh, M.S. Glaz, D.S. Ginger, A.K. Jen, High-performance and environmentally stable planar heterojunction perovskite solar cells based on a solution-processed copper-doped nickel oxide hole-transporting layer, Adv. Mater. 27 (2015) 695–701.
27. J. Liu, Y. Wu, C. Qin, X. Yang, T. Yasuda, A. Islam, K. Zhang, W. Peng, W. Chen, L. Han, A dopant-free hole-transporting material for efficient and stable perovskite solar cells, Energy Environ. Sci. 7 (2014) 2963–2967.
28. Y. Kato, L.K. Ono, M.V. Lee, S. Wang, S.R. Raga, Y. Qi, Silver iodide formation in methyl ammonium lead iodide perovskite solar cells with silver top electrodes, Adv. Mater. Interfaces 2 (2015) 1500195.
29. S. Guarnera, A. Abate, W. Zhang, J.M. Foster, G. Richardson, A. Petrozza, H. J. Snaith, Improving the long-term stability of perovskite solar cells with a porous Al2O3 buffer layer, J. Phys. Chem. Lett. 6 (2015) 432–437.
30. Cai, Molang, Yongzhen Wu, Han Chen, Xudong Yang, Yinghuai Qiang, and Liyuan Han. “Cost-Performance Analysis of Perovskite Solar Modules.” Advanced Science 4, no. 1 (2017): 1600269.
31. Mahboobeh Shahbazi, Hongxia Wang, 2015. Progress in research on the stability of organometal perovskite solar cells. Solar Energy, Volume 123, January 2016, Pages 74-87

32. Dian Wang, Matthew Wright, Naveen Kumar Elumalai, Ashraf Uddin. Stability of perovskite solar cells. Solar Energy Materials and Solar Cells Volume 147, April 2016, Pages 255-275

33. Olyaeefar, Babak, Sohrab Ahmadi-Kandjani, and Asghar Asgari. "Bulk and Interface Recombination in Planar Lead Halide Perovskite Solar Cells: A Drift-Diffusion Study." *Physica E: Low-Dimensional Systems and Nanostructures* 94 (October 1, 2017): 118–22.

34. P. Pistor, J. Borchert, W. Fränzel, R. Csuk, R. Scheer, Monitoring the phase formation of coevaporated lead halide perovskite thin films by in situ X-ray diffraction, J. Phys. Chem. Lett. 5 (2014) 3308–3312.

35. J. Yang, B.D. Siempelkamp, E. Mosconi, F. De Angelis, T.L. Kelly, Origin of the thermal instability in $CH_3NH_3PbI_3$ thin films deposited on ZnO, Chem. Mater. 27 (2015) 4229–4236.

36. Kim, Hui-Seon, Chang-Ryul Lee, Jeong-Hyeok Im, Ki-Beom Lee, Thomas Moehl, Arianna Marchioro, Soo-Jin Moon, et al. "Lead Iodide Perovskite Sensitized All-Solid-State Submicron Thin Film Mesoscopic Solar Cell with Efficiency Exceeding 9%." *Scientific Reports* 2, no. 1 (August 21, 2012): 1–7.

37. Li, Bairu, Tonggang Jiu, Chaoyang Kuang, Sushuang Ma, Qiushan Chen, Xiaodong Li, and Junfeng Fang. "Chlorobenzene Vapor Assistant Annealing Method for Fabricating High Quality Perovskite Films." *Organic Electronics* 34 (July 1, 2016): 97–103.

38. "Best Research-Cell Efficiency Chart." Accessed February 11, 2020. https://www.nrel.gov/pv/cell-efficiency.html.

39. Lee, Sang-Won, Seongtak Kim, Soohyun Bae, Kyungjin Cho, Taewon Chung, Laura E. Mundt, Seunghun Lee, et al. “UV Degradation and Recovery of Perovskite Solar Cells.” *Scientific Reports* 6, no. 1 (December 2, 2016): 1–10.
40. Niu, Guangda, Wenzhe Li, Jiangwei Li, Xingyao Liang, and Liduo Wang. “Enhancement of Thermal Stability for Perovskite Solar Cells through Cesium Doping.” *RSC Advances* 7, no. 28 (March 17, 2017): 17473–79.